Elaboration et étude de nouveaux matériaux d'électrodes: les "Nano-Crystallite-Insertion-Materials"

Sang-Do Han

N° d'ordre : 1061

THESE

PRESENTEE A

L'UNIVERSITE BORDEAUX I

ECOLE DOCTORALE DES SCIENCES CHIMIQUES

Par Sang-Do HAN

POUR OBTENIR LE GRADE DE

DOCTEUR

SPECIALITE : **SCIENCES DES MATERIAUX**

Elaboration et étude de nouveaux matériaux d'électrodes :les
<< Nano-Crystallite-Insertion-Materials>> (NCIMs)

Soutenue le : .17 février 1994

Après avis de MM.	**L. COT**	**Professeur**	**Université de Grenoble I**	**Rapporteurs**
	D. DEROO	**Professeur**	**Université de Montpellier II**	

Devant la Commision d'examen formée de :

MM.	**J. ETOURNEAU**	**Professeur**	**Examinateurs**
	M. KENNARD	**Docteur Nordwest University USA**	
	G.CAMPET	**Directeur de Recherches au CNRS**	
	J. C. LASSEGUES	**Directeur de Recherches au CNRS**	
	J. PORTIER	**Directeur de Recherches au CNRS**	
	J. SALARDENNE	**Professeur**	

-1994-

Je dédie cette thèse

A mes parents,

A ma chère épouse, Kui - Hwa,

A ma fille, Kyong - Jin,

A mon fils, Dong - Jin,

A mes frères et soeurs,

A tous ceux qui me sont chers.

REMERCIEMENTS

Ce travail a été réalisé au Laboratoire de Chimie du Solide du CNRS de l'Université de Bordeaux I.

Je tiens à remercier Monsieur le Professeur Jean ETOURNEAU, directeur du Laboratoire, pour l'intérêt qu'il a porté à mon travail et l'honneur qu'il me fait de présider le Jury.

Monsieur Louis COT, Professeur à l'Université de Montpellier II, m'a fait profiter de ses compétences en électrochimie au cours de ce travail qu'il a bien voulu juger. Qu'il trouve ici l'expression de ma respectueuse reconnaissance.

Monsieur Daniel DEROO, Professeur à l'Université de Grenoble, m'a fait le grand honneur de bien vouloir être rapporteur et de participer au Jury de cette thèse. Je le remercie très sincèrement.

Jean SALARDENNE, professeur à l'Université de Bordeaux I, a bien voulu me faire l'honneur de juger ce travail. Je lui exprime ici ma vive gratitude.

Tous mes remerciements s'adressent aussi à Monsieur Josik PORTIER, Directeur de recherche au CNRS, pour ses conseils et son soutien amical qu'il m'a porté et pour avoir accepté de porter un jugement sur ce travail.

Monsieur Mark KENNARD, Docteur de Chimie de l'Université de Nordwest aux USA, a suivi mon travail et a participé à mon Jury de thèse. Je lui exprime toute ma profonde reconnaissance.

Monsieur Jean-Claude LASSEGUES, Directeur de Recherche au CNRS, a dirigé ce travail m'a fait bénéficier de sa grande compétence dans le domaine des polymères. Qu'il accepte l'expression de ma sincère gratitude pour ses conseils éclairés et son amicale bienveillance.

Je remercie particulièrement mon directeur de thèse Monsieur Guy CAMPET, Directeur de Recherche au CNRS, pour l'intérêt permanent qu'il a montré pour ce sujet et pour sa gentillesse tout au long de ces heures de travail. Il m'a fait bénéficier de sa grande compétence dans le domaine de l'électrochimie.

Je me dois d'associer à l'aboutissement de ce travail plusieurs chercheurs avec qui nous avons collaboré:

- Monsieur Claude DELMAS, Directeur de Recherche au CNRS, pour ses conseils et sa contribution à mon travail;

- Monsieur Roger SALMON, Professeur à l'Université de Bordeaux I, pour son aide lors de la mesure de BET sur la poudre.

Ma gratitude va également à Monsieur Jean-Jacques VIDEAU, chargé de Recherche au CNRS et à Monsieur Etienne DUGUET, Maître de Conférence, pour leur aide et leur amicale collaboration durant ce travail.

Je ne saurais oublier de remercier Messieurs Louis RABARDEL et Joël VILLOT pour leur collaboration dans le domaine des mesures thermiques, Louis TRUT et Jean-Pierre CAZORLA pour les mesures de diffraction X, Emile MARQUESTAUT pour sa contribution aux mesures de la conductivité.

Mes remerciements s'adressents à mes collègues; WANG Ai-Gao, HUANG Sui-Yang, WEN Shi-Jie, XU Yue, Corinne MARCEL, Jean-François GERVAIS, Hélène GUENGARD, Didier CAMINO, Eric HARFMANN, SEUNG Do-Young, JUNG Duk-Young, HAN Kyoo-Seung, KIM Bai-Yong, SHIN Yu-Ju.

Je remercie enfin tous les membres du LCS , chercheurs, ingénieurs, techniciens, administratifs et étudiants pour leur esprit d'entraide et leur sympathie.

SOMMAIRE

CHAPITRE I.

CHAPITRE II.

LES NANO-CRYSTALLITE-INSERTION-MATERIALS (NCIMs): ces matériaux qui permettent le greffage réversible des ions Li^+ à la surface des cristallites.

Application aux oxydes: SnO_2, TiO_2 et WO_3 à l'état de poudres nanoscopiques.

CHAPITRE III.

CHAPITRE IV.

CHAPITRE V.

N° d'ordre : 1061

Chapitre I

INTRODUCTION GENERALE

I.1. ETAT DE L'ART

L'insécurité croissante, source de conflits, que l'Homme a lui-même engendrée parce qu'il a perdu ses racines, pousse celui-ci à se rapprocher de son environnement. Cela peut expliquer la renaissance de l'écologie humaine et l'éclosion de la "vague verte".

C'est ainsi que les nations industrialisées sont désormais pleinement conscientes qu'elles devront, dans les années à venir, faire le choix de nouvelles sources d'énergie en remplacement des combustibles fossiles. Il n'est guère besoin de rappeler maintenant que l'utilisation immodérée des composés hydro-carbonés (charbon, pétrole) se traduit, au-delà de la pollution localisée des villes, par une augmentation du taux de gaz carbonique dans toute l'atmosphère. A long terme, cela engendrera, engendre déjà, une perturbation des équilibres climatiques.

Quelles que soient les options retenues : solaire (le cas "idéal" dit-on, certes ! mais il faudra accepter de payer provisoirement le prix élevé du kW/h) ou nucléaire, l'énergie électrique restera le vecteur privilégié. Il est donc indispensable de disposer de moyens de stockages à grande échelle de cette électricité. Au niveau de la production d'abord, pour pouvoir gérer au mieux le parc énergétique, en l'adaptant aux besoins de la consommation, mais aussi pour les transports routiers. La voiture électrique semble en effet sur le point de "décoller" : selon la législation américaine, à partir de l'an 2000, au moins 10 % des voitures vendues en Californie devront être totalement non polluantes ; les pouvoirs publics français emboîtent le pas puisqu'ils ont récemment lancé le programme VPE (Véhicule Propre et Econome) qui associe PSA et Renault (1 200 millions de francs sur 8 ans). A la clé, la mise au point de véhicules urbains "tout électrique" et des modèles "hybrides" utilisables également sur route, les batteries étant alors relayées par un moteur Diesel ou une turbine à gaz.

Toutefois, le principal problème reste les performances des batteries actuelles.

Actuellement, il faut en effet 200 kg de batteries au cadmium nickel contre 10 litres de carburant pour obtenir sensiblement le même travail moteur. Les batteries Ni-Cd actuellement sur le marché[1] ont une énergie spécifique d'environ

[1]Selon le "Japan Industrial Journal", du 14 septembre 1992, la société Hitachi Maxell va prochainement introduire sur le marché une pile nickel-hydrogène ayant une capacité de stockage 24 fois supérieure à celle des piles nickel-cadmium (prix de vente deux fois plus élevé). La pile est

70 Wh/kg ; elles sont supérieures à celles de l'accumulateur au plomb, le plus répandu (40Wh/kg).
Elles sont malgré tout très insuffisantes pour l'application envisagée : en effet, un véhicule électrique exige des accumulateurs des performances bien supérieures, de l'ordre de 300 Wh/kg. De plus, cette énergie doit pouvoir être emmagasinée ou restituée dans un délai court, de l'ordre de deux heures, ce qui se traduit par une puissance spécifique nécessaire de 150 W/kg.

Un troisième point mérite d'être souligné : il s'agit de la durée de vie de la batterie qui doit évidemment être élevée (>> 1 000 cycles de charge-décharge).

Pour atteindre les chiffres d'énergie et puissance spécifiques précités (respectivement 300 Wh/kg et 150 W/kg), il faut utiliser des réactions correspondant à une grande variation de l'enthaphie libre pour des masses les plus faibles possibles. De telles réactions sont irréalisables dans les milieux aqueux utilisés pour les générateurs précités (Ni-Cd ou Ni-H_2).

Au début des années 70, Delmas, Rouxel et Armand [1-3] proposaient l'utilisation des composés d'intercalation des ions Li^+ comme matériaux d'électrodes dans des générateurs rechargeables à haute densité d'énergie. Depuis, de nombreuses études ont montré la validité de ce concept [4]. Nous rappellerons [1] qu'une structure dite "hôte d'intercalation", <H>, correspond à un solide capable d'intercaler un ion alcalin, tel que Li^+, pour former le composé <Li_xH> sans destruction du réseau de départ.

On peut utiliser ces matériaux dans deux types de générateurs secondaires au lithium à haute densité d'énergie : les générateurs dits "simple effet" et "double effet" ou "rocking chair" [1-3].

i) <u>Les générateurs "simple effet"</u>

$$\ominus \ \langle Li \rangle \ / \ Li^+ \ / \ \langle Li_xH \rangle \ \oplus$$

[4: Thèse J. M. Chabagno]

lithium métallique	électrolyte conducteur des ions Li^+	Composé d'intercalation (tel que : $Li_xNi_{1-y}Co_yO_2$) [5-6]

produite à partir d'un nouvel alliage de nickel qui contient du zirconium et du vanadium qui doivent emmagasiner de l'hydrogène.

La chaîne électrochimique permet la transformation de l'énergie chimique de la réaction d'intercalation :

$$x(Li^+ + e^-) + \langle H \rangle = \langle Li_xH \rangle$$

sous forme électrique en découplant le trajet des ions de celui des électrons.

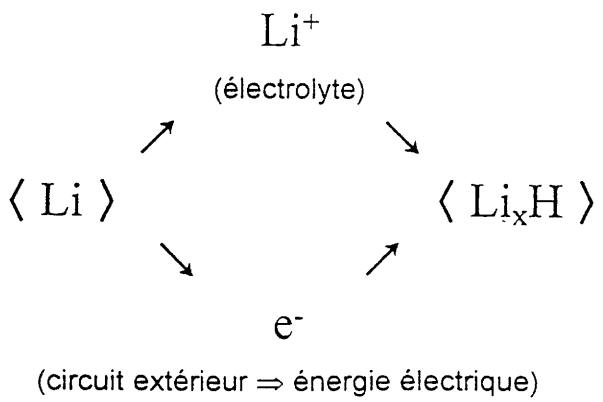

Remarquons que ces types de batteries rechargeables au lithium ne sont pas encore commercialisées : ces dernières sont en effet dangereuses du fait de la croissance dendritique du lithium métallique à l'interface lithium/électrolyte liquide lors de la recharge. Les dendrites augmentent la réacticité du lithium et peuvent occasionner des courts-circuits entraînant l'explosion de la batterie.

Il y a deux façons de contourner le problème. La première consiste à utiliser un électrolyte solide (polymère conducteurs d'ions lithium) avec lequel le lithium est moins réactif [7]. C'est la voie actuellement développée par Hydro-Québec au Canada et Yuasa Battery au Japon. La deuxième consiste à remplacer le lithium métallique par un composé d'insertion du lithium, ce qui conduit au système dit "rocking-chair" schématisé ci-dessous.

ii) <u>Les générateurs "rocking chair" ou à "double effet"</u>

$$\ominus \ \langle Li_xH_1 \rangle \ / \ Li^+ \ / \ \langle Li_yH_2 \rangle \ \oplus$$

Ils récupèrent la différence d'énergie liée à l'intercalation du lithium dans deux structures "hôte" différentes $<H_1>$ et $<H_2>$. La différence de potentiel chimique du lithium dans les deux structures détermine le potentiel de la batterie, ce qui entraîne une contrainte dans le choix des matériaux [8-10] (fig.I.1).

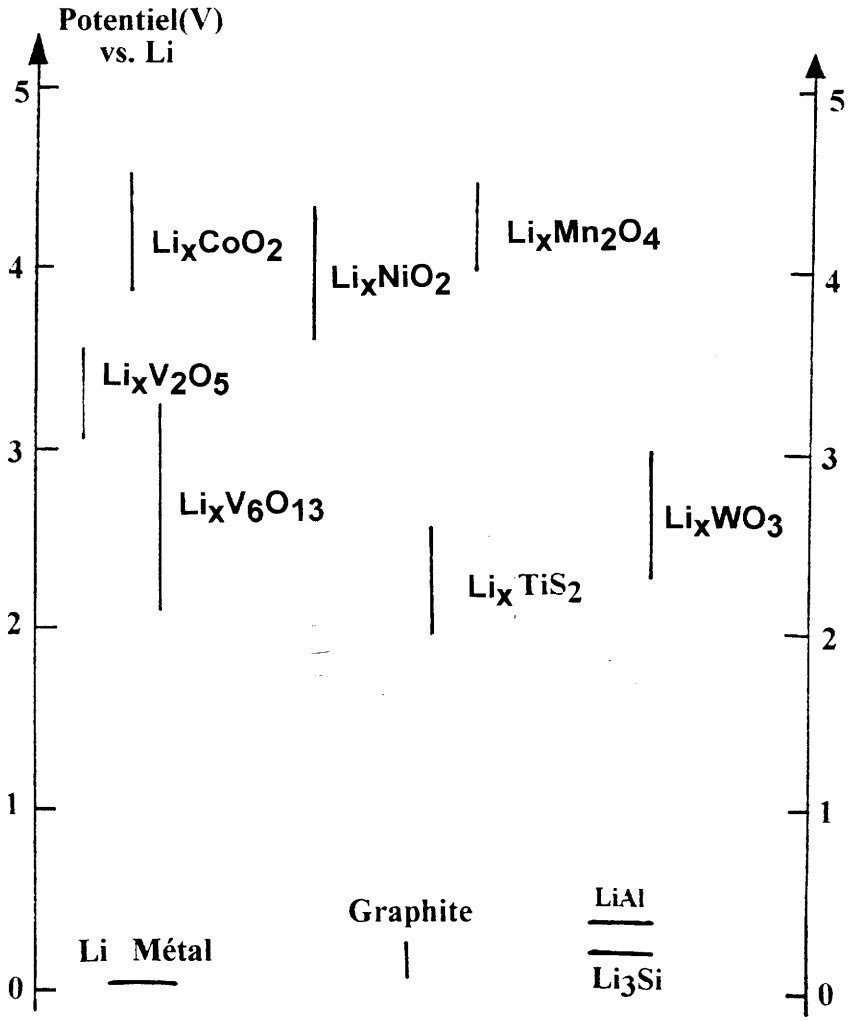

Fig. I. 1. Comparaison des potentiels d'équilibre des différents matériaux d'électrode.

Les batteries "rocking-chair" sont donc en compétition ; d'une part avec les batteries nickel hydrure métallique, qui remplaceraient les batteries nickel-cadmium et d'autre part avec les "batteries tout solide" au lithium métallique. Cette voie est développée par Sony Energytec, Sanyo et Matsushita au Japon, Moli Energy au Canada et Bellcore aux USA.

I.2. DEMARCHE SUIVIE

Un de nos objectifs est, compte tenu des remarques précédentes, la réalisation et l'étude de matériaux d'électrodes pour générateurs secondaires fonctionnant avec les ions Li^+.

Les applications visées sont à plus ou moins long terme. Elles concernent les véhicules électriques et, au-delà, une vision futuriste mais réaliste : le stockage de l'énergie à grande échelle (batteries rechargées dans des centrales solaires).

Ces générateurs seraient donc "idéalement" :

(i) à haute densité d'énergie (>> 300 Wh/kg)
(ii) à forte puissance spécifique (>> 150 W /kg)
(iii) à taux de cyclabilité élevé (> 1 000 cycles)
(iIV) sans "risque" pour l'utilisateur et de volume aussi réduit que possible.

Afin de satisfaire ces exigences, ils devraient combiner les avantages des générateurs "rocking-chair", évoqués précédemment, avec ceux des super-capacités[2] [11], et finalement être à "armature polymère" [3-7].

L'approche que nous avons adoptée est dans cette optique. Elle découlait en fait de travaux antérieurs, effectués conjointement aux LCS, LEMME et GRL sur les dispositifs électrochromes[3] : les dispositifs étudiés (fig.I.3) fonctionnaient précisément avec les ions Li^+ et possédaient à la fois la puissance spécifique et le taux de cyclabilité élevés des supercapacités, mais aussi la forte énergie spécifique des batteries rocking-chair [12-17].

---

[2]Le principe de fonctionnement des supercapacités est illustré sur la figure I.2.
[3]Le principe de fonctionnement des dispositifs électrochromes est illustré sur la figure I.3.
(LEMME : Laboratoire d'Etude des Matériaux pour la Micro-Electrique-Univ. Bordeaux I.
GRL : Groupement de Recherches de Lacq de la Société Elf - 64 - Artix).

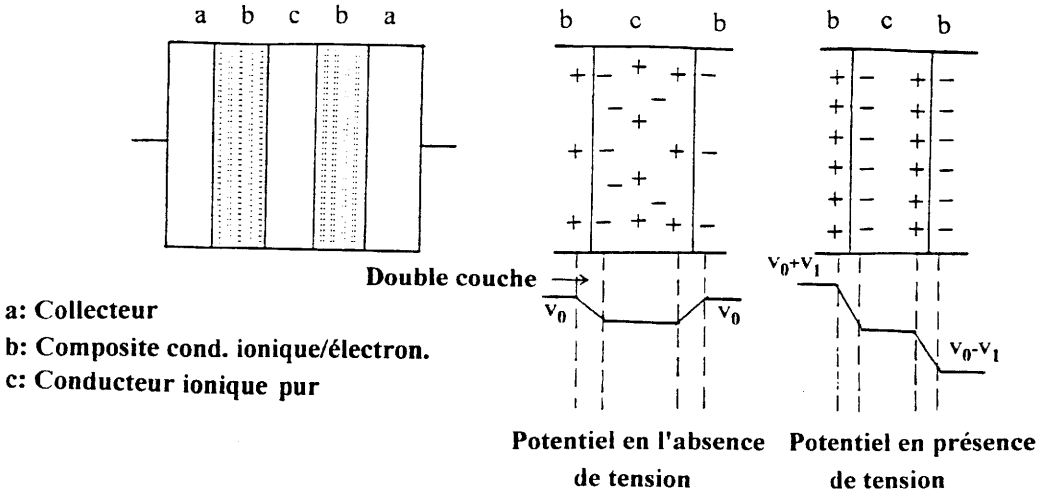

Fig. I. 2. Schémas de principe d'un supercondensateur utilisant des particules de carbon activé comme électrode.

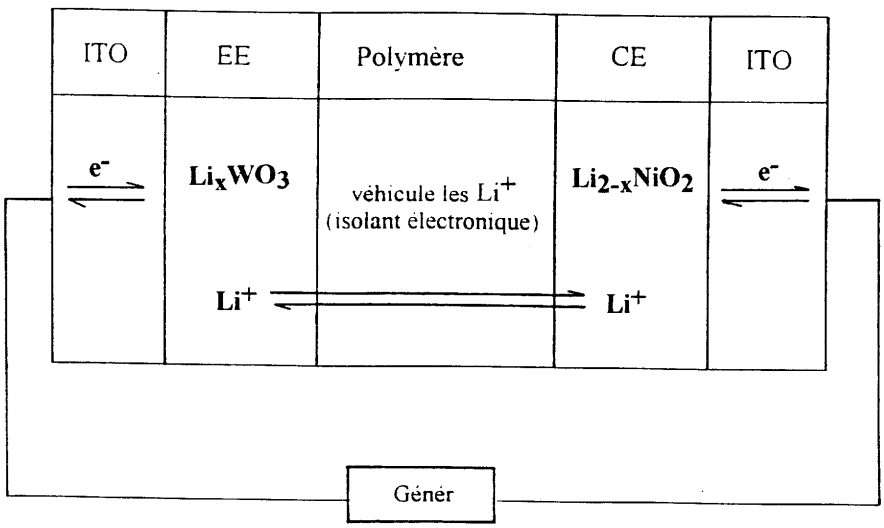

$Li_xWO_3 \rightleftharpoons xe^- + xLi^+ + WO_3$ (*bleu* → *transparent*)

$Li_{2-x}NiO_2 + xe^- + xLi \rightleftharpoons Li_2NiO_2$ (*orangé* → *transparent*)

Fig. I. 3. Dispositif électrochrome symétrique, dit "rocking-chair" utilisant respectivement WO_3 et $Li_{2-x}NiO_2$ comme électrode électrochrome(EE) et contre électrode(CE). La contre électrode $Li_{2-x}NiO_2(0\leq x\leq 1)$ avait été proposée pour la premiére fois aux LCS, LEMME et GRL(groupe ELF) depuis 1989, ITO symbolise In_2O_3 dopé par Sn^{4+} [18].

En effet, il avait été mis en évidence une gamme étendue de matériaux d'électrodes, baptisés NCIMs ("Nano-Crystallite-Insertion Materials"), et qui, sous forme de films minces, étaient capables de (dés)insérer réversiblement les ions Li^+ ($n_{cycles} > 10^5$; $Q > 10^3 C.cm^{-3}$; $t_{cycle} = 1'$), [12-17]. Les matériaux font intervenir les défauts existants à la surface ou au voisinage de la surface de cristallites et agissant comme centres de (de)greffage des ions Li^+ . Dans ces conditions, **pour obtenir des taux élevés de lithium inséré, il suffit donc d'avoir un "système nanoscopique" pour disposer d'une surface électrochimiquement active très importante**.

Une question se posait alors: l'approche est-elle la même lorsque les NCIMs se présentent non plus sous forme de films mais à l'état de poudre ?
Afin d'y répondre nous avons, dans un premier temps (**chapitre II**), réalisé et étudié des électrodes à base de poudres d'oxydes très finement divisés ; leur conductivité électrique est assurée par du noir de carbone intimement mélangé à l'oxyde de départ. Il convenait, en particulier, de différencier les processus d'intercalation, intervenant au coeur des cristallites, des mécanismes de "greffage" intervenant à leur surface.
A cette fin, nous avons considéré trois NCIMs : Li_xWO_3 (bronze cubique), Li_xTiO_2 (anatase) et Li_xSnO_2 (rutile). Ils se différencient par le fait que la structure interne des cristallites est plus ou moins adaptée à l'intercalation des ions Li^+, selon qu'elle présente des tunnels tri, bi, ou monodimensionnels (fig.I.4).

Les concepts développés dans le chapitre précédent ont été étendus, dans le **chapitre III**, à des **matériaux d'électrodes hybrides** de caractère organique-inorganique ($NCIM_S$ encapsulés dans des groupements organiques pour éviter leur agglomération en particules de taille trop importantes...). Si l'objectif d'ordre pratique était, ici, d'élaborer des électrodes à armature polymère pour des générateurs électrochimiques "souples et peu encombrants", nous souhaitions surtout que l'étude abordée dans ce chapitre III permette l'essor d'une nouvelle classe de matériaux hybrides.

Le **chapitre IV** se démarque quelque peu de notre stratégie principale puisque les **systèmes électrochromes** sont ici concernés. Il s'agissait en fait de compléter les études antérieures sur les systèmes électrochromes, évoqués plus haut (fig.I.3).
Le chapitre IV est ainsi consacré, en partie, à l'étude des propriétés électrochimichromiques de $NCIM_S$ déposés en couches minces. Les matériaux

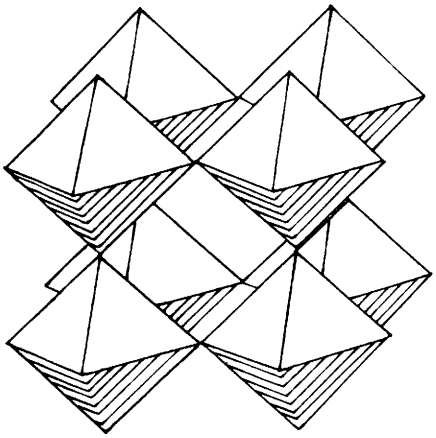

à tunnels tridimensionnels (Li_xWO_3)

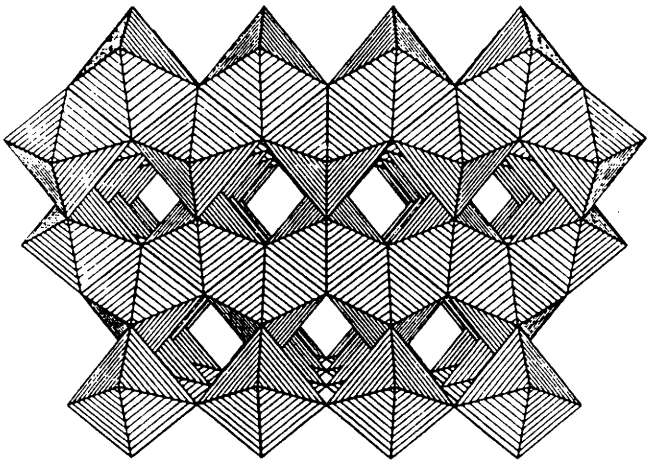

à tunnels bidimensionnels (Li_xTiO_2)

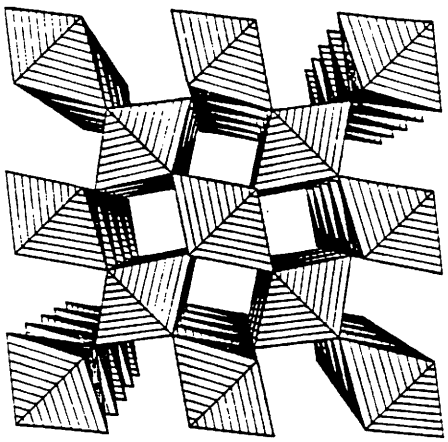

à tunnels monodimensionnels (Li_xSnO_2)

Fig. I. 4. Structures (Li_xWO_3, Li_xTiO_2 et Li_xSnO_2).

d'électrodes considérés jusqu'ici aux LCS, LEMME et GRL étaient déposés par pulvérisation cathodique [12-17]. Nous avons, au cours de ce travail, utilisé la voie sol-gel, plus facile à mettre en oeuvre que la pulvérisation cathodique.
En effet, la préparation de gels d'oxydes minéraux à partir de précurseurs alcoxydes est maintenant une technique largement répandue pour la mise en forme de divers types de matériaux parmi lesquels on peut citer : les poudres céramiques, les fibres... C'est ainsi que nous avons élaboré par spin coating des contre électrodes pour vitrages électrochromes de Fe_2O_3, ayant une taille moyenne de cristallite de 100 Å. Le sol consistait en une solution de pentanédionate de Fe(III) légèrement hydrolysée.

(L'ensemble de ce travail a donné lieu à 7 publications que nous avons reportées dans les chapitres suivants).

Chapitre II

Les $NCIM_s$

(Nano - Crystallite - Insertion - Materials) :

ces matériaux qui permettent le greffage réversible des ions Li^+ à la surface des cristallites.

Application aux oxydes : $Sn O_2$, TiO_2 et WO_3 à l'état de poudres nanoscopiques

II. 1. INTRODUCTION

L'étude que nous entreprenons résulte des travaux antérieurs sur les systèmes électrochromes, réalisés par les chercheurs du LCS, LEMME et GRL, (chap. I). Constatant qu'il n'existait pas de CE (Li^+) suffisamment performante, les chercheurs avaient mis au point dès 1989 une contre électrode Li_{2-x} NiO_2 (fig.I.3), déposée en couche mince et fonctionnant sur un principe nouveau. Une approche "surfacique" avait, en effet, été adoptée : fabrication de films, tels que Li_{2-x} NiO_2, à texture nano-cristalline, intercalant réversiblement les ions Li^+ au coeur des cristallites mais aussi fixant réversiblement ces cations à la surface des cristallites via les défauts de surface.

Une gamme étendue de matériaux d'électrodes à base d'oxydes d'éléments à valence mixte avait ainsi été proposée. Outre Li_{2-x} NiO_2, citons par exemple $Li_xMn_2O_3$, Li_xCrO_2, $Li_xFe_2O_3$, Li_xSrTiO_3.....[12-17]. Tous ces matériaux étaient donc déposés en couches minces; ils ont été par la suite symbolisés par NCIMs (Nano-Crystallite-Insertion-Materials).

L'approche "surfacique" précédente devrait également être vérifiée lorsque les oxydes nanoscopiques se présentent non plus sous forme de films minces, mais à l'état de poudre. Ils constitueraient, alors, une alternative intéressante aux matériaux d'intercalation, de structure lamellaire ou à tunnel, utilisés jusqu'ici dans les générateurs secondaires au lithium.

C'est ainsi que ce chapitre sera consacré à l'étude de $NCIM_s$ à l'état de poudre[1]. Nous y reporterons les résultats les plus significatifs. Ceux-ci sont extraits des trois publications jointes à la fin du chapitre.
Nous n'omettrons pas également de mettre en lumière les difficultés rencontrées; citons la principale : comment prévenir l'agglomération des nanocristallites en particules de taille trop élevée, souvent supérieure au μm ?

[1] *Les techniques expérimentales utilisées sont reportée dans les publication jointes.*

II.1.1. SYNTHESE ET CARACTERISATION DE NCIMs A L'ETAT DE POUDRE

II.1.1.1. Généralités

Compte tenu des remarques précédentes, on conçoit que les électrodes devront être élaborées suivant le principe utilisé pour les super condensateurs (fig. I.2) : il suffit de remplacer, en partie, les charbons actifs utilisés dans les super capacités par des NCIMs. Rappelons qu'une difficulté devra alors être surmontée dans la mesure du possible : il s'agira d'éviter l'agglomération des nanocristallites en particules de taille trop importante nuisant aux cinétiques des réactions électrochimiques (⇒ affaissement de la puissance spécifique).

La préparation de petite cristallite d'oxyde est classiquement réalisée par les méthodes de chimie douce mettant en oeuvre l'hydrolyse de précurseurs [19]. Toutefois, la taille des particules reste, généralement, trop importante. Afin de résoudre ce problème[2], nous avons mis au point une **nouvelle méthode** de préparation des NCIMs sous forme de poudre (§ II.2). Cette méthode consiste à préparer un complexe polymère sel à partir de solutions, dans un solvant aprotique, d'un sel inorganique et d'un polymère présentant des sites basiques où se fixent les cations. Un gel polymérique (et non colloïdal) est ensuite formé. L'hydrolyse ménagée puis la pyrolyse à basse température conduit effectivement à de fines particules de taille généralement inférieure au μm.

Nous avons utilisé cette méthode pour la préparation de WO_3, SnO_2 et TiO_2 (le choix de ces matériaux a été justifié au chap. I).

II.1.1.2. Application à WO_3, SnO_2 et TiO_2

a. Préparation de WO_3

Nous avons mélangé un précurseur à base de tungstène, en l'occurrence WCl_6 (99,9 %, Aldrich) avec un précurseur polymère : le polyoxyde d'éthylène

---

[2] *Le prolème n'a été ici que partiellement résolu (voir § II. 2). Une solution plus avantageuse sera présentée au chapitre III.*

(POE, Aldrich, $M_W = 5.10^5$) dans la proportion $[-CH_2-CH_2-O-]/W = 8$: les concentrations sont exprimées par le rapport du nombre de motifs monomères par atome de tungstène.
Le mélange a ensuite été dissous dans l'acétonitrile et agité à température ambiante jusqu'à homogénéisation. L'évaporation du solvant (étuve à 60° C pendant une nuit) a conduit à l'obtention d'un "complexe polymére gel " (fig. II.1).

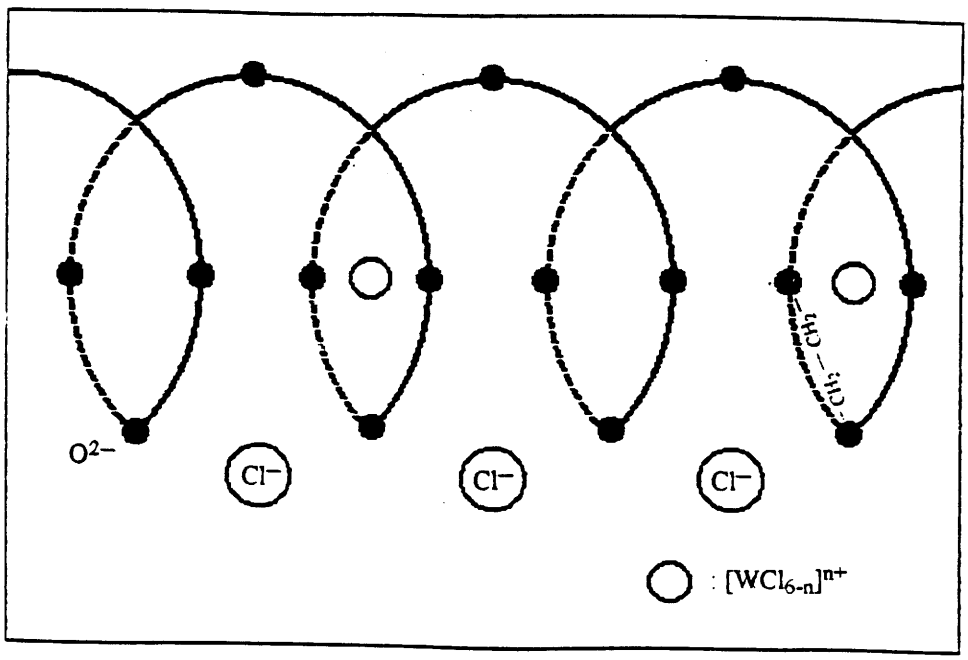

Fig. II.1.1. Structure probable du "complexe polymére gel".

Pour obtenir des poudres de WO_3 avec des cristallites de taille donnée, le "gel" a été pyrolysé selon le profil de température suivant :

- montée en température : 1° C/min.
- palier de 2 heures à la température de pyrolyse, Tp.
- descente en température : 1° C/min.

Le choix du polyoxyde d'éthylène s'explique en raison du pouvoir solvatant des polyéthers vis à vis des cations en général. En effet, il dispose de sites basiques ou de fonctions chimiques, où se fixent les cations et ils sont donc capables de dissocier le sel en ions libres. La méthode repose sur une réaction de complexation par solvatation, entre les cations et les atomes d'oxygène des unités éthoxy pouvant appartenir à plusieurs chaînes macromoléculaires. Cette complexation maintient les cations à longue distance (figure II.1.1) et ralentit, de ce fait, la croissance des grains due au chauffage.

b. Préparation de SnO_2 et TiO_2

La méthode de synthèse des poudres nanoscopiques de SnO_2 et TiO_2 est analogue à la précédente avec comme précurseurs de départ $(POE)_8$ $SnCl_4.5H_2O$ dans l'acétonitrile et $(POE)_8$ $TiCL_4$ dans le pentanol.

c. Caractérisation des NCIMs

Rappelons que les techniques de caractérisation utilisées ont été reportées dans les publications jointes (mesure des surfaces spécifiques et distribution des pores par la méthode BET, caractérisations par spectroscopie infrarouge et diffraction des rayons-X, variations de masse suivies par analyse thermogravimétrique...).

L'ensemble des résultats obtenus sont évidemment reportés dans les publications jointes. Nous retiendrons, notamment, que les nanocristallites ($D < 70$ Å : fig. II.1.2), s'agglomèrent pour former des particules de taille souvent inférieure à 1 µm (fig. II.1.3). Cependant, ces dernières sont parfois agglomérées en **"mini - fibres"**, (fig. II.1.3 et II.1.4), **qui sont, très vraisemblablement les "empreintes" de longues fibres amorphes** présentes dans le gel avant pyrolyse (fig. II.1.5).

II.1.1.3. Remarques

Les voies sol-gel plus classiques ont également été utilisées pour la préparation des poudres, ne serait-ce que dans le cadre d'une étude comparative (§II.2).

Nous avons également examiné l'influence du pH du gel sur les propriétés des poudres obtenues après calcination de celui-ci. Nous avons ainsi montré qu'une corrélation étroite existerait entre la taille des cristallites et le pH du gel. Un modèle rendant compte de cette évolution a été proposé (§II.3).

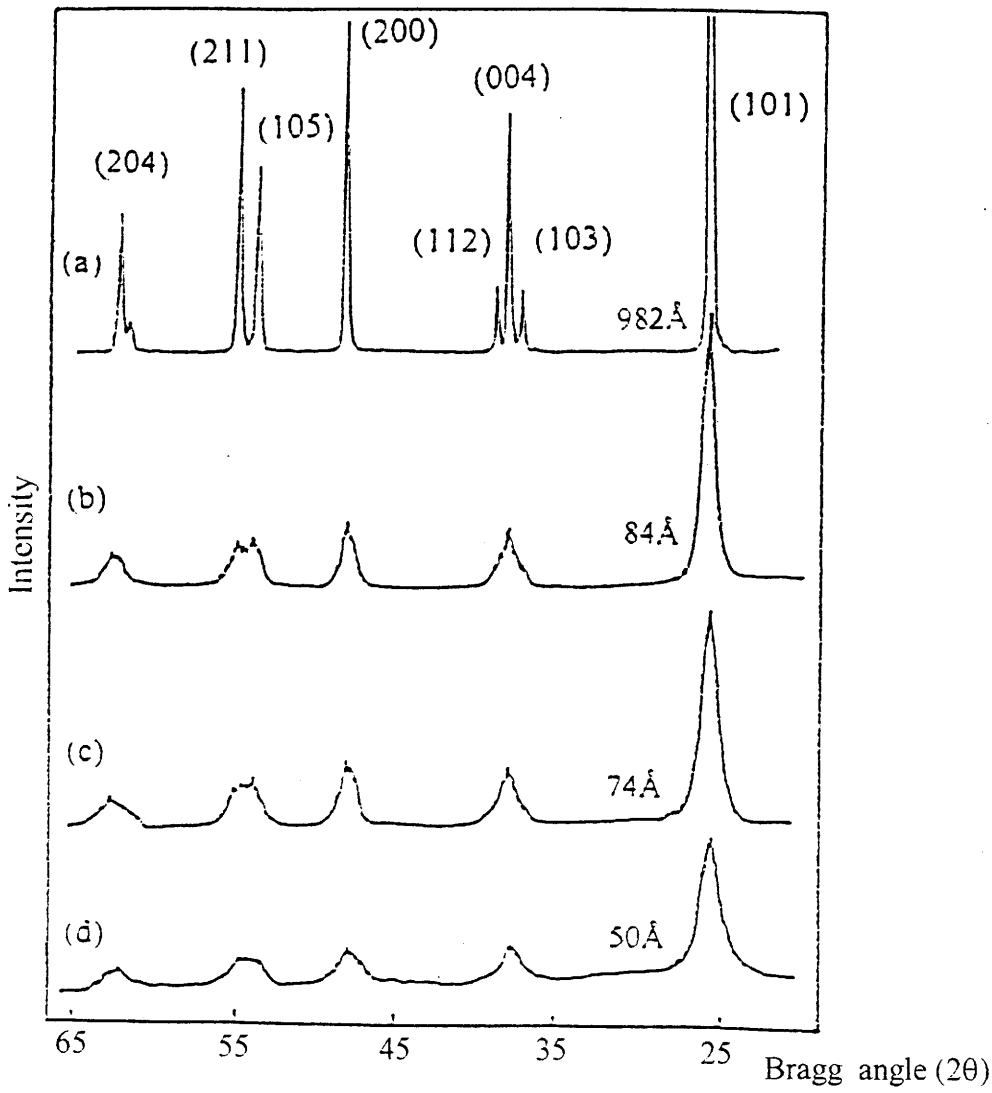

Fig. II. 1.2. Comparaison des spectres de diffraction X de TiO_2 (anatase) commercial (a) et TiO_2-NCIMs obtenus par pyrolyse du "gel polymérique" $(POE)_8TiCl_4$ à 550C° (b), 450°C (c), 350°C (d). La taille moyenne des cristallites est reportée en Å (±6Å).

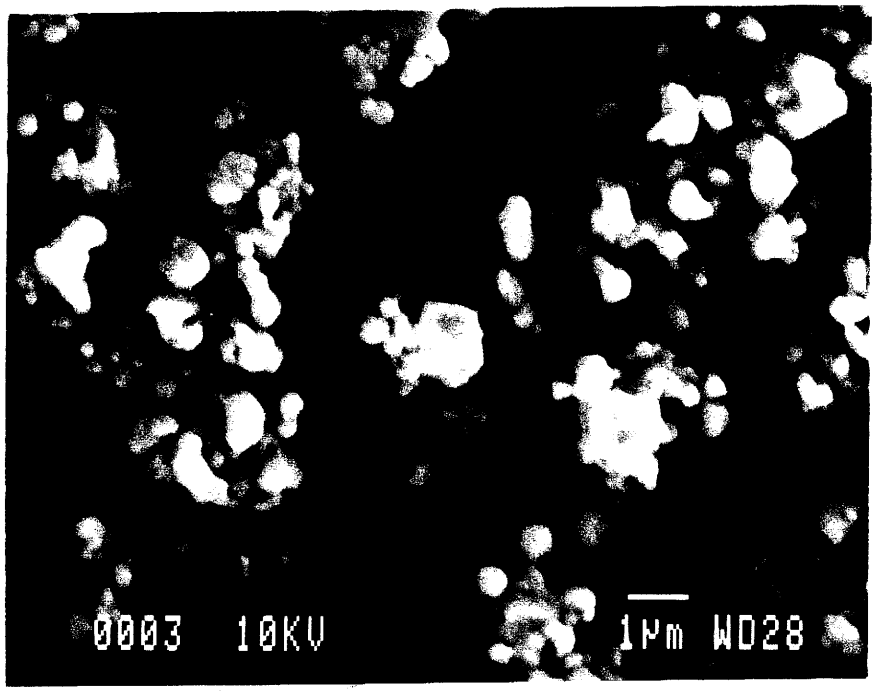

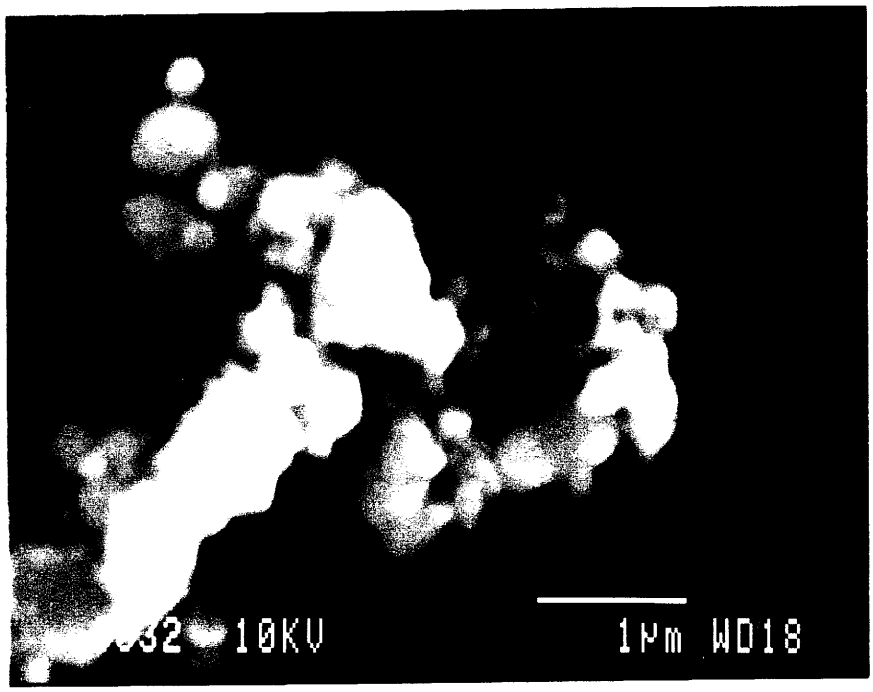

Fig. II.1. 3, 4. Clichés de TiO_2 - NCIM obtenus par pyrolyse à 450°C du "gel-polymérique" $(POE)_8TiCl_4$.

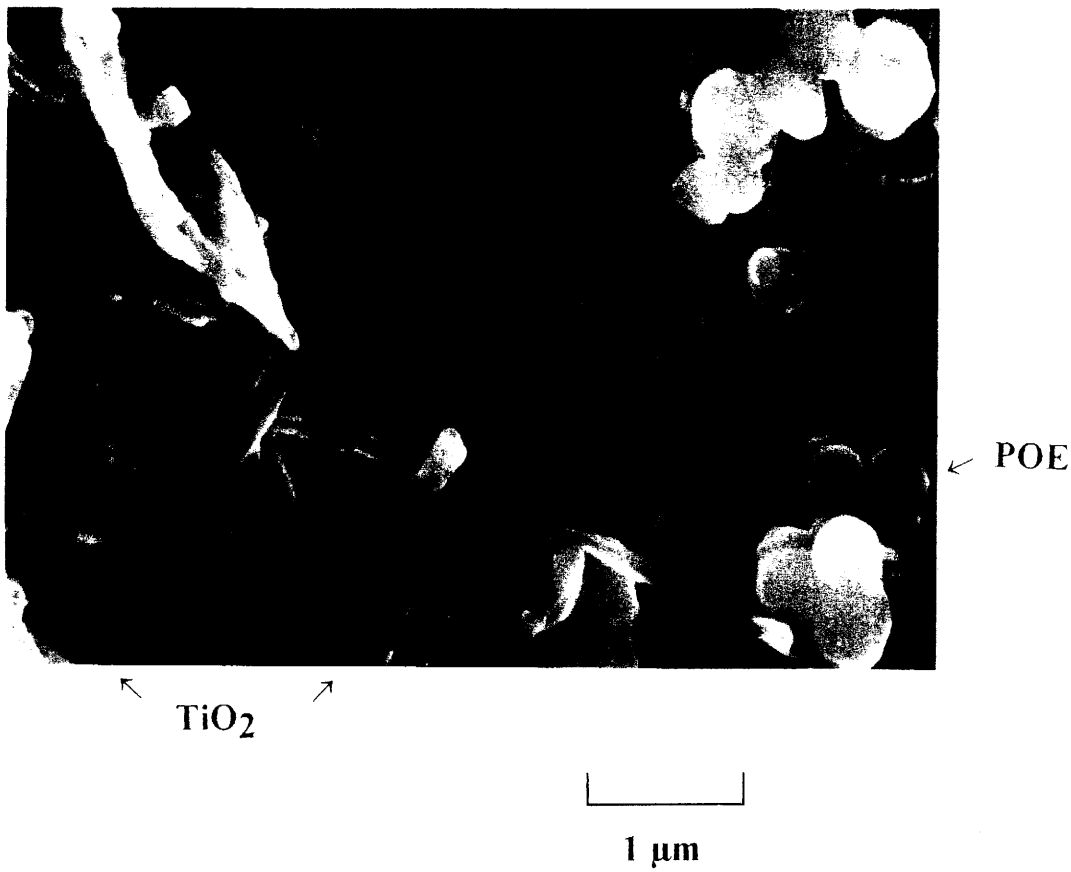

Fig. II.1.5. Clichés du "gel-polymérique" $(POE)_8TiCl_4$ aprés hyrolyse à l'air.

II.1.2. UTILISATION DE "L'OUTIL ELECTROCHIMIQUE" POUR DIFFERENCIER LES PHENOMENES DE COEUR (processus d'intercalation au coeur des cristallites) DES PHENOMENES DE SURFACE (processus de greffage)

En accord avec le modèle proposé pour les films nanocristallins (Chap. I, [12 - 17]), il apparaît que, dans le cas des poudres également, les textures constituées des grains les plus fins permettent un taux d'insertion en ions Li^+ maximal (§II.2). A titre d'exemple, la figure II.1.6 illustre les courbes de décharge des cellules $Li/LiCF_3SO_3/Li_x\ WO_3$: le taux de lithium inséré dans le domaine 1.5 - 3.2 V est supérieur à1.5 lithium par atome de tungstène pour WO_3-NCIM(59Å) alors qu'il n'est que de 0.19 pour le matériau le plus cristallisé (WO_3 - Aldrich).[1]

D'après les travaux antérieurs (et "extérieurs" aux nôtres) un tel résultat s'interprétait de la façon suivante : en augmentant la surface spécifique, on diminue le temps de transit des ions Li^+ depuis la surface jusqu'au coeur des cristallites; corrélativement x croît lorsque la taille des grains diminue. En effet, plus le grain est gros, plus l'équilibre est difficile à atteindre au cours de l'intercalation : le pourtour du grain sera surintercalé par rapport au coeur et le potentiel observé sera celui de la phase la plus conductrice formée à l'extérieur. On constate effectivement, à partir des mesures de l'évolution en fonction du temps du potentiel en circuit ouvert (OCV), que l'électrode est d'autant plus loin de l'équilibre thermodynamique qu'elle est constituée de gros cristallites.

Néanmoins, cette vision des choses n'est que partielle : selon la littérature, la composition $Li_1\ WO_3$ correspond à un remplissage complet des tunnels ; le fait d'obtenir un taux supérieur à 1 laisse présumer un autre processus que nous allons présenter ci-dessous.

A cette fin, nous avons étudié l'évolution du potentiel d'équilibre (OCV) en fonction du taux d'insertion, x, pour WO_3 - NCIM et WO_3 commercial (fig. II.1. 7). Précisons que chaque OCV est mesuré après avoir laissé "relaxer" la cellule en circuit ouvert pendant 5 à 10 jours, c'est-à-dire jusqu'à ce que l'équilibre thermodynamique soit, à priori, atteint.

---

1. Ces résultats sont à rapprocher de ceux de Boccoli et al.: les auteurs suggèrent (sans le démontrer clairement), qu'après "amorphisation" de l'oxyde de tungstène, des taux de lithium "anormalement élevés" peuvent être insérés[20].

L'évolution des courbes reportées sur la fig. II.1.7 s'interprète logiquement comme suit. Des états d'énergie localisés au sein de la bande interdite existent dans les NCIMs,(fig. II.1.8),[12 - 17]. Leur concentration diminue lorsque la taille, D, des cristallites augmente, comme cela est le cas lorsque l'on passe de WO_3-NCIM à WO_3 commercial (fig. II.1.7). Etant donné que ce sont les derniers niveaux électroniques occupés qui fixent l'énergie de Fermi et donc le potentiel OCV, on conçoit que pour de faibles valeurs de x ($x<0,15$), le potentiel est d'autant plus anodique que D est faible. Par contre, pour des taux en lithium supérieurs à 0,15, une inversion des potentiels est observée (fig. II.1.7). Les électrons injectés au cours de la décharge, pour $x>0,15$ sont maintenant délocalisés dans la bande de conduction ; à ce moment là, intervient le processus d'intercalation au sein de la structure. On sait en effet que la largeur de bande interdite augmente lorsque la taille des cristallites diminue [19]. Le bord de bande de conduction est donc plus élevé dans le matériau "amorphe" (au sens nanocristallin du terme) et par conséquent le potentiel sera plus cathodique pour $x > 0,15$ (fig. II.1. 7).

Ainsi interviendrait, dans un premier temps, et ce pour de faibles taux en lithium, le processus de greffage en surface puis, dans un second temps, le processus d'intercalation lié à l'existence de tunnels tridimensionnels.

Des résultats similaires, non reportés ici par souci de clarté, ont été obtenus avec les autres oxydes SnO_2 (§II.2) et TiO_2.[1] Les valeurs relativement faibles des potentiels mesurés dans le cas de TiO_2 (fig. II.1.9), s'expliquent par la faible affinité électronique du couple rédox Ti^{3+}/Ti^{4+}. Ils rendent possible l'**utilisation de TiO_2 - NCIM en tant qu'électrode négative dans des dispositifs "rocking - chair"**.

---

1. Lorsque l'on considéde des électrodes ayant une structure lamellaire parfaitement adaptée à l'intercalation des ions Li^+, comme Li_xNiO_2, il n'est apparemment par nécessaire de dimimuer la taille des cristallites pour accroitre les performances des électrodes[21]. Cependant nos concepts faisant intervenir l'aspect "surfacique" sont tout à fait valables dans le cas des matériaux d'électrodes édudiés ici, qui présentent des structures à tunnel pour lesquelles l'intercalation des ions lithium est plus difficile.

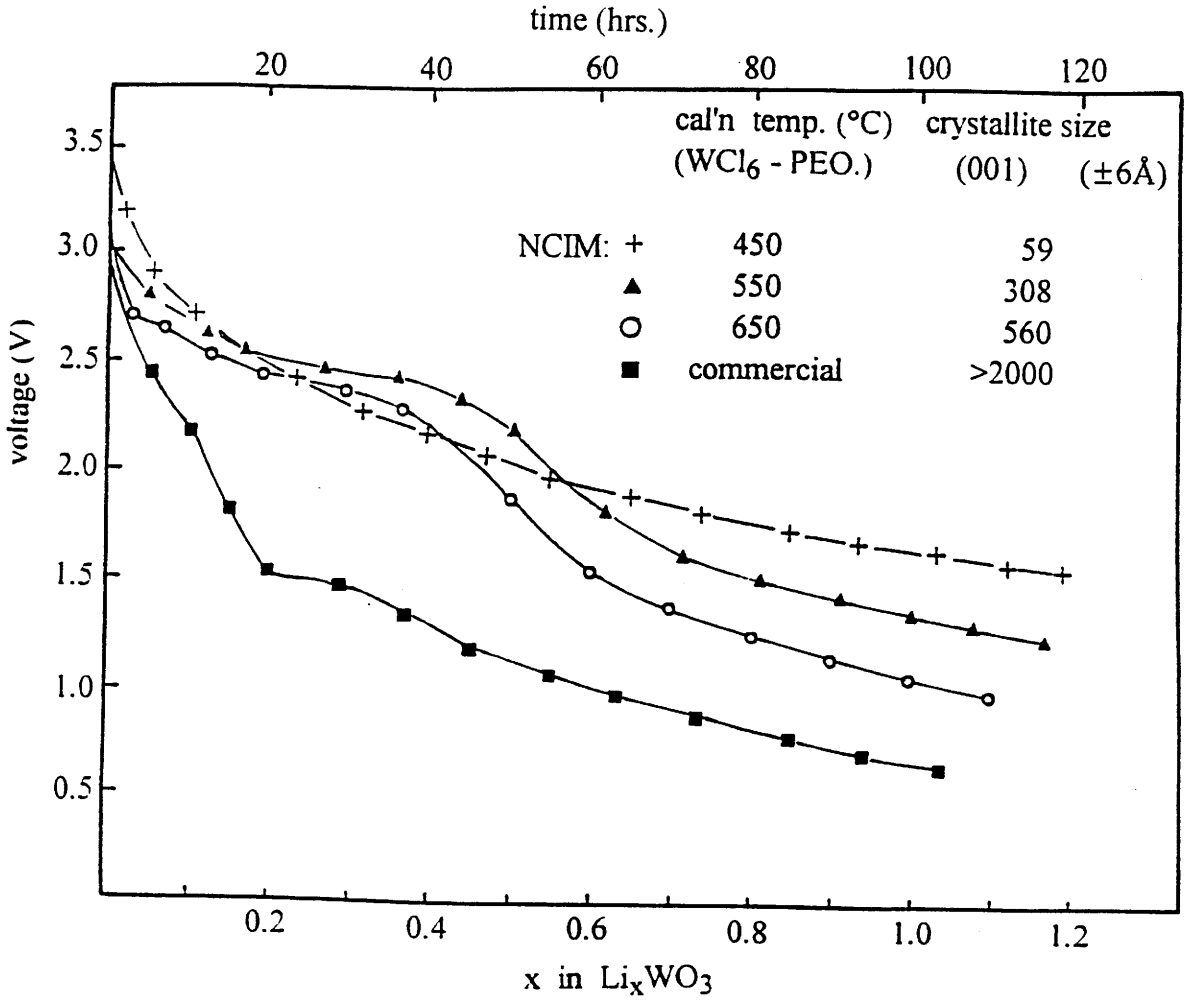

Fig. II. 1. 6 Discharge curves for Li / $LiCF_3SO_3$ / Li_xWO_3 cells using the various WO_3 powders having different crystallite size.

I = 50μA/cm², m (WO_3) = 42mg, m(C) = 8mg.

Remark: For information, the charge - discharge curve for the most efficient sample, i.e. having the smallest crystallite size (59Å) have been reported on fig. III. 4, p.100.

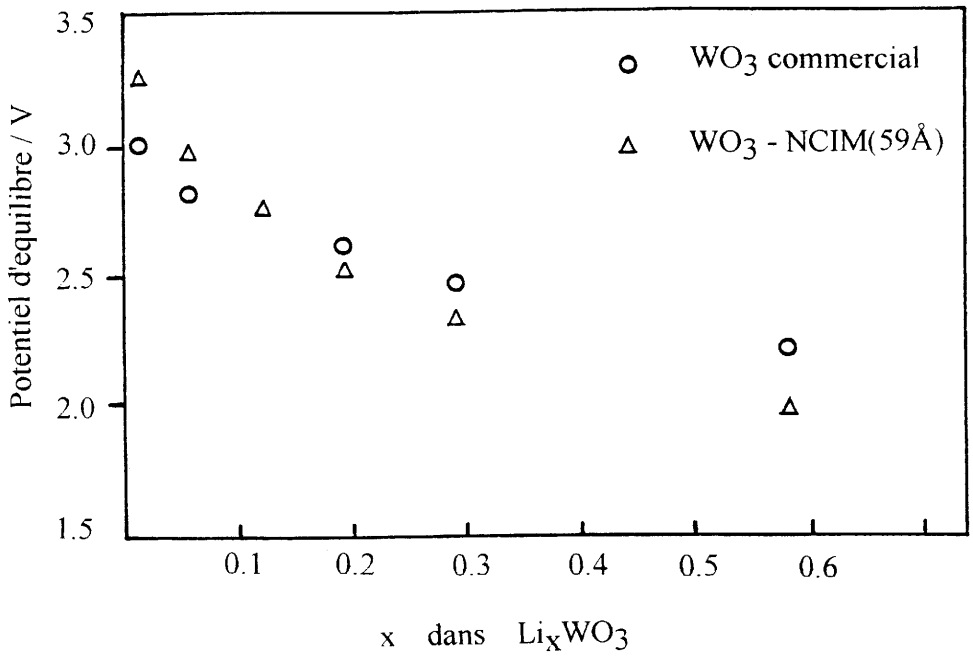

Fig.II.1.7. Evolution du potentiel d'équilibre en fonction du taux d'insertion des cellules Li / $LiCF_3SO_3$ / Li_xWO_3.

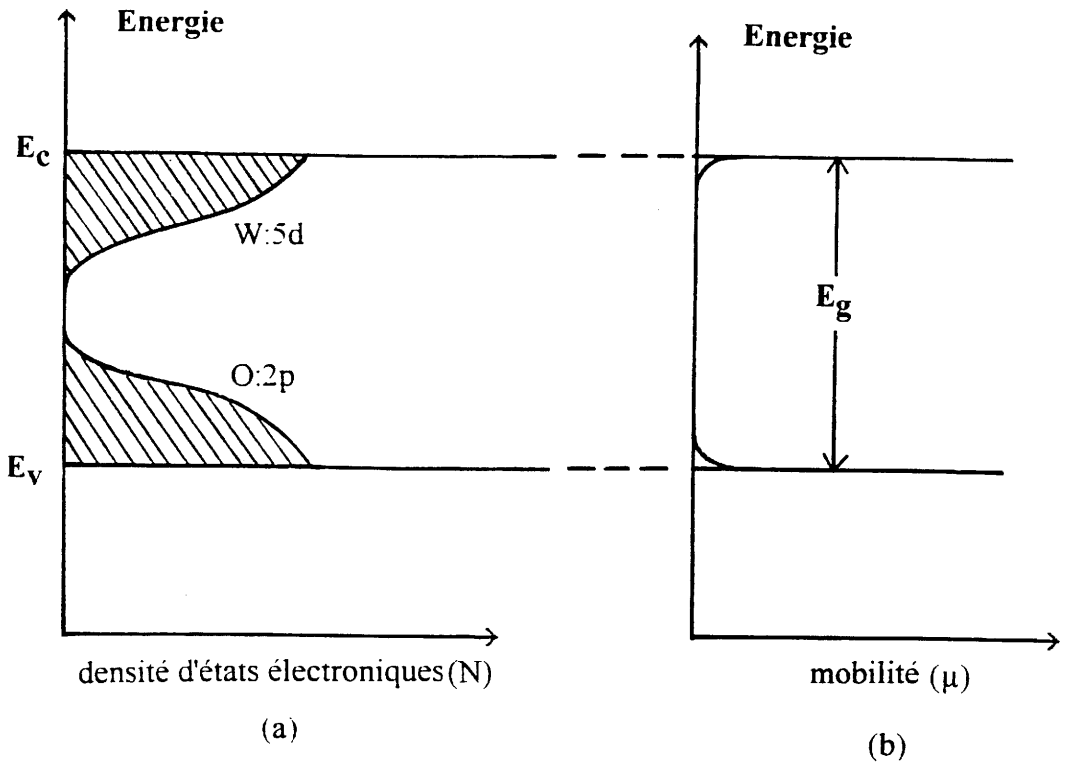

Fig. II. 1.8. Modèle Mott-CFO pour un semi-conducteur "amorphe" tel que WO_3-NCIM
(a) Etats localisés (aires hachurées)
(b) Gap de mobilité (T>O K)

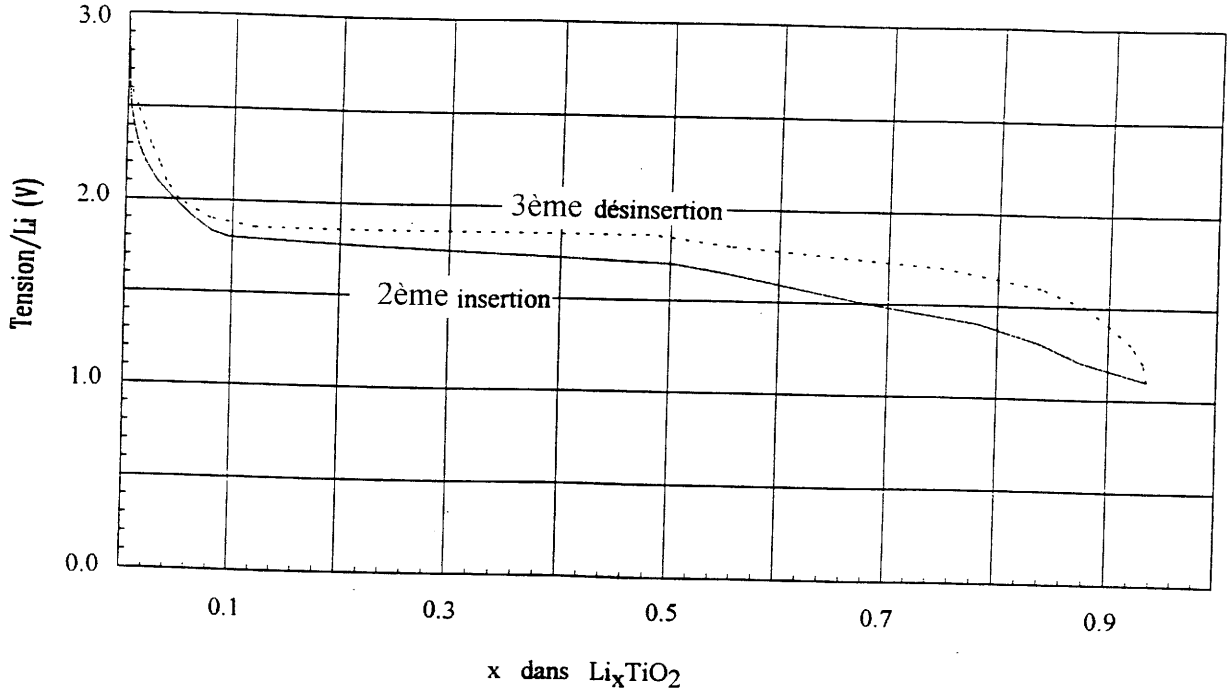

Fig. II.1.9. Courbes de cyclage électrochimique des batteries $Li/LiCFSO_3/Li_xTiO_2$, mettant en évidence l'excellente réversibilité insertion - désinsertion de l'électrode.

$I = 40\mu A/cm^2$; masse de TiO_2 = 20mg; masse de noir de carbone = 3mg; taille moyenne des cristallitees (évaluée par TEM. et diffraction X) ≅ 50Å; taille moyenne des particules (estimée par SEM.) ≅1μm.

Les taux de lithium que l'on peut insérer réversiblement correspond à x= 0.95.

C'est à notre connaissance la première fois qu'une telle réversibilité est observée sur des poudres de TiO_2, bien que la composition $LiTiO_2$ ait déja été reportée [22]. Au delà de x = 0.95 les ions lithium peuvent toujours être insérés, mais (hélas) irréversiblement. Des tests de cyclage à long terme sont actuellement effectués dans le groupe de C. Delmas.

REFERENCES

1. C. Delmas, Thèse de Doctorat d'Etat. Univ. Bordeaux (1976).

2. Rouxel, dans Levy (ed.), Physics and Chemistry of Layered Materials, Vol. VI, Reidel, Dordrecht (1979).

3. Armand dans "Fast ion transport in solids", North Holland Pub. Co. Ed. Van Gool (1972).

4. Voir par exemple :
   - M. Armand, Thése de Doctorat d'Etat, Univ. de Grenoble (1978).
   - J. M. Chabagno, Thése de Docteur - Ingénieur, Univ. de Grenoble (1980).
   - C. Delmas, J. Braconnier, A. Maazaz and P. Hagenmuller, Rev. Chem. Miner., 19, 343 (1982).
   - Mizushima, P.C. Jones, P.J. Wiseman et J.B. Goodenough, Solid State Ion., 3-4, 171 (1986).
   - Molenda, Solid State Ion., 21, 263 (1986).
   - Miyazaki, S. Kikkawa et M. Koizumi, Synth. Met., 6, 211 (1983).

5. C. Delmas et I. Saadoune, Solid State Ion.; in press

6. C. Delmas, I. Saadoune et A. Rougier, J. Power Sources, in press.

7. Armand, "Materials for advanced batteries", D.W. Murphy, J. Broadhead et B.C.H. Cteele (Editeur), Academic Press, New York (1980).

8. Dipiekro, M. Patriarca et B. Scrosaki, J. Power Sources, 8, 289 (1982).

9. Tarascon, J.Electochem. Soc., 132, 2089 (1985).

10. Fauteux et A. Kokslang, J. of Appl. Electrochem., 23, 1 (1983).

11. Société Matsuchita, J. Electron. Eng., 25, 80 (1988).

12. J-P. Couput, G. Campet, J.M. Chabagno, M. Bourrel, D. Muller, R. Garrié. C. Delmas, B. Morel, J. Portier and J. Salardenne. *Int. Appl. Publ. under PCT. Int. Pat. Class GO2F 1701, FO1 G9/00, C 23C 14/34, WO 91/01510,* 1989.

13. G. Campet, J. Portier and S. J. Wen, J. *Active Passive Electron. Compon.* 14 (4) 225 (1992).

14. G. Campet and J. Portier, J. *Active Passive Electron. Compon.* 14 (4) 219 (1992).

15. G. Campet, B. Morel, M; Bourrel, J.M. Chabagno, D. Ferry, R. Gorie, C. Quet, C. Geoffroy, J. Videau, J. Portier, C. Delmas and J. Salardenne, *Mater. Sci. Eng., B8* (1989) 303.

16. B. Morel, *Doctoral Thesis*, University of Bordeaux I, 1991.

17. M.Barloux, J.M. Tarascon anf F.K. Shokoohi, J. *Solid State Chem.*, 94 (1991) 185.

18. S. J. Wen, Doctoral Thesis, University of Bordeaux I, 1992.

19. P.E. Lippen et M. Lannoo, Phys. Rev. B, 39, 10935(1985)

20. M. Boccoli, F. Bonino, M. Lazzari et B. Rivolta, Solid State Ionics, 7,65(1982).

21. C. Delmas, private communication.

22. D. W. Murphy, Solid State Ionics, 9 & 10, 413 (1983).

II. 2. A NEW METHOD FOR THE PREPARATION OF FINE-GRAINED SnO_2 AND WO_3 POWDERS:

influence of the crystallite size on the electrochemical insertion of Li^+ in SnO_2 and WO_3 electrodes.

(publication)

Submitted to Materials Science and Engineering

A new method for the preparation of fine-grained SnO_2 and WO_3 powders: influence of the crystallite size on the electrochemical insertion of Li^+ in SnO_2 and WO_3 electrodes.

S.D. Han, G. Campet*, M.C.R. Shastry, J. Portier and C. Delmas
Laboratoire de Chimie du Solide du CNRS, Université Bordeaux I, 351 Cours de la Libération, 33405 Talence cedex, FRANCE.

J.C. Lassègues
Laboratoire de Spectroscopie Moléculaire et Cristalline, Université Bordeaux I, 351 Cours de la Libération, 33405 Talence cedex, FRANCE.

J.B. Goodenough
Center for Materials Science and Engineering, University of Texas, Austin TX 78712, USA.

ABSTRACT

We have proposed an unconventional method to obtain fine-grained SnO_2 and WO_3 powders. It deals with the well known polymerization method starting from the respective metallic halides of Sn and W with polyethylene oxide (PEO). With this method, metal-oxide powders possessing small crystallite sizes are obtained by appropriate pyrolysis of the polymer. In addition the powders are also free from water and hydroxyl group contaminations, which is an added advantage where the application of these materials to Li-batteries is concerned. We have also demonstrated that these powders show good ability to reversibly insert lithium ions in the $Li/Li^+/Li_xSnO_2$ (Li_xWO_3) cells.

---

* Author for correspondence

1. Introduction

Stannic oxide is an n-type semiconductor with a tetragonal rutile structure [1] and a large indirect band energy gap. It has attracted considerable attention due to the variety of applications related to its unique electrical, optical and catalytic properties. Among its applications, to mention only a few, are in transparent heaters for windshield defrosting, in anti- reflection coating for solar cells, as a transparent electrode for electrochromic devices, as a sensing material for combustible gas sensors, and as an electrocatalyst for organic oxidation [2-4]. In the last two applications mentioned above, a fine powder of SnO_2 is used. These powders have generally been obtained through two different methods: one involves the oxidation of elemental tin with acids (HNO_3, H_2SO_4 etc.) and the other utilizes the well-known sol-gel route. The sol-gel method involves the dispersion of stannic hydrate in aqueous ammonia to give a sol. The sol is later 'solidified' through stages of stiffening and polymerization to give a gel (gelation). The gel so obtained is thoroughly washed with distilled water, filtered, dried and finally heated to high temperatures to obtain the required material [5]. The sol-gel route has been found to give finer crystallites compared to the former method. However, samples free from water and hydroxyl groups are hardly achievable.

We propose here an unconventional and easy-to-carry-out method for the preparation of fine dry particles of SnO_2 and WO_3 powders. It uses the well known polymerization method starting from the respective halides $SnCl_4$ and WCl_6 with polyethylene oxide (PEO) [6]. The method has been shown to give not only very fine particles, obtained after eliminating the polymer by heating,but also particles free from water and OH group impurities.

These two sol-gel related methods are compared here; they are referred to as method 1 (for the conventional one) and method 2.

We also investigated the ability to insert reversibly lithium ions into the fine-grained SnO_2 and WO_3 powders in $Li/Li^+/Li_xSnO_2$ (WO_3) cells. We have reported elsewhere that electrodes based on fine-grained transition metal oxides ($Li_xFe_2O_3$, $Li_{2-x}NiO_2$ etc.) in the

form of thin films exhibit highly efficient electrochemical (de)insertion of Li^+ ions into lithium conducting electrolytes [7-9]. The materials were symbolized as NCIMs (nano-crystallite-insertion-materials). Indeed, by minimizing the crystallite size, we favour the formation of dangling and weak bonds at the surface and the rate of reversible lithium insertion. Since the previously studied NCIMs were based on transition metal oxides, we were more concerned in earliers publications in the cationic 'd' orbitals that were involved in the electrochemical processes [7-9]. In the case of SnO_2 based electrodes, it is the cationic 5s orbital that would be of concern. It is worthwhile to have an insight into the respective influences of 's' and 'd' orbitals on the electrochemical response. In this paper we report an investigation of NCIMs powders based on WO_3 prepared with method 2 and on SnO_2 prepared by both methods 1 and 2 for comparison.

2. Experimental

2.1 Sample preparation

a) Method 1

A colloidal stannic hydroxide was precipitated by the dropwise addition of an ammonium hydroxide (35%, Aldrich) to an aqueous solution of stannic chloride (99.99%, Aldrich) maintained at ~ 2°C in an ice-water bath. Residual impurities of ammonium hydroxide and ammonium chloride were removed by repeatedly washing using distilled water. The washing and filtering processes were repeated until the pH of the solution decreased to 7.5 (from an initial value of ~ 12.5). The as-obtained α- stannic acid gel was heated in dry air for 2h at different temperatures (150, 350 and 550°C) in order to get powdery samples with different crystallite sizes. The heating and cooling temperature rate (1°C/min) was controlled by an Eurotherm programmer. In the following the samples will be symbolized as 1-(150); 1-(350); 1-(550); "1" designates the method of preparation and the number within brackets represents the heat treatment temperature.

b) Method 2.

PEO (Aldrich, M. W. 500,000) was first added to acetonitrile. The solution was stirred at room temperature in an ultrasonic bath until a satisfactory homogeneity was achieved. $SnCl_4 \cdot 5H_2O$ or WCl_6 (99.99%, Aldrich) were then added to the solution in the proportion $[-CH_2-CH_2-O]/M = 8$, (M = Sn or W)]. Once a complete homogeneity of the 'sol' was achieved, the 'sol' was casted into a teflon mould. Evaporation of the solvent at about 40°C under a stream of dry air, gave a polymer film of typical thickness 100μm. Finally, fine-grained SnO_2 and WO_3 powders are obtained by eliminating the polymer with slow heating in dry oxygen. In order to get NCIMs with different crystallite sizes, the polymer films were heated up to 350°C, 450°C or 550°C and soaked for 2hrs at those temperatures.

The powdery SnO_2 and WO_3 samples are identified as 2-(350), 2-(450), 2-(550) and 2-(350)-W, 2-(450)-W, 2-(550)-W; as above, "2" designates the method of preparation and the number within brackets the temperature of heat treatment. The symbol 'W' identifies the tungsten oxide samples.

The experimental procedure involved in methods 1 and 2 are schematically illustrated in fig. 1, and the probable structures of the "polymerized" oxides (SnO_2 or WO_3) obtained in methods 1 and 2 are shown in figs. 2a and 2b respectively.

2. 2. Sample analysis

Thermogravimetric analyses (TGA) were performed in dry air between 22°C and about 600°C with a Setaram thermobalance. X-ray diffraction measurements were obtained with a Phillips PW 1050 spectrometer and CuK_α radiation. The average crystallite size, D, was calculated from the well known Scherrer's formula

$$D = 0.9 \lambda / \beta_{1/2} \cdot \cos\theta \qquad (1)$$

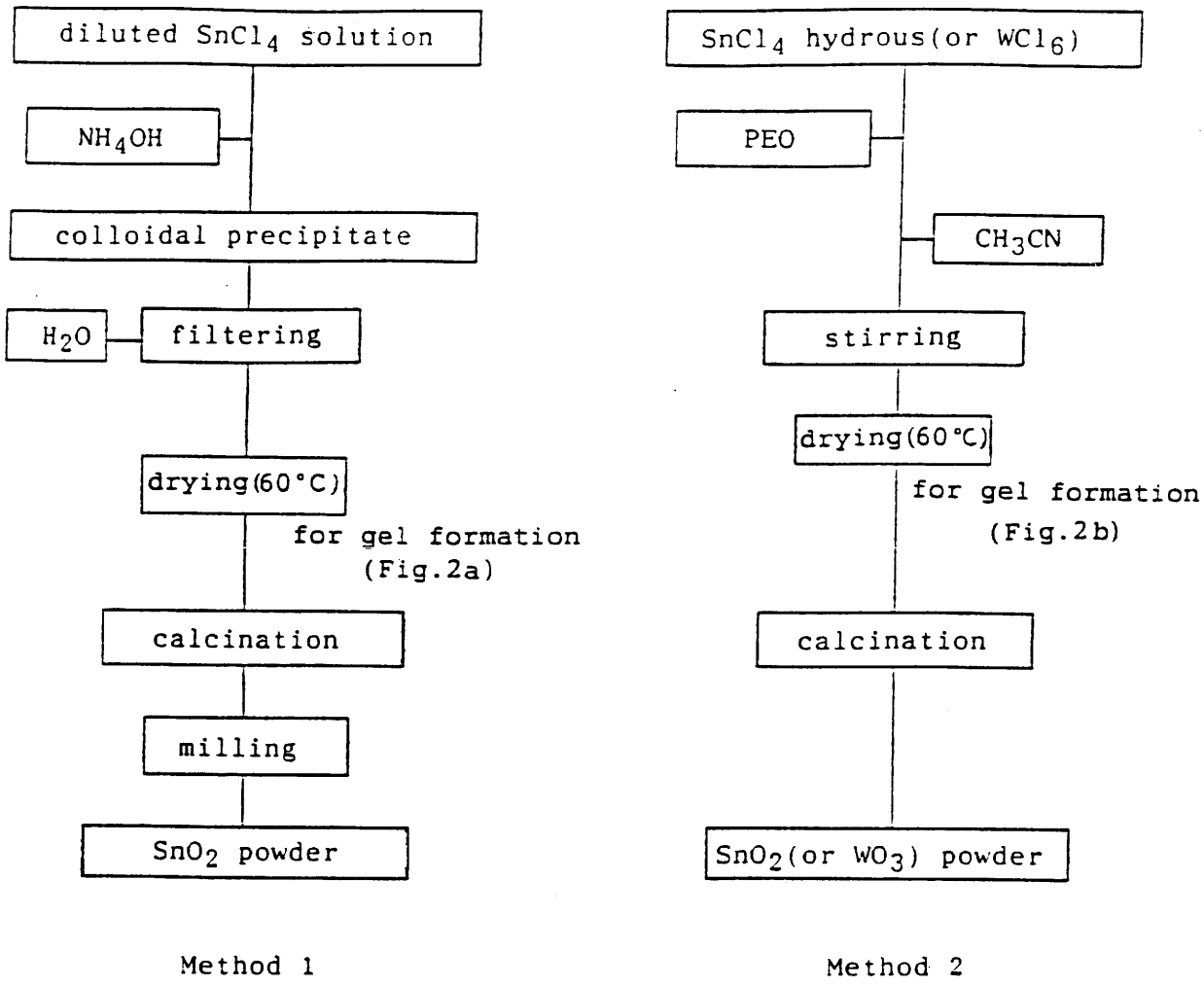

Fig. 1. Schematic diagrams of the steps involved in obtaining fine-grained SnO_2 and WO_3 powders.

$\beta_{1/2}$ is the corrected width of the main diffraction peak at half height, λ is the X-ray wavelength and θ the diffraction angle. The specific surface area of the samples was measured by the single point Brunauer Emnett and Teller (BET) method with a Micromeretics Accu Sorb 2100 E. The samples were outgassed at 180 °C for 5 hrs. The adsorbate gas was nitrogen. The IR spectra in the absorbance mode were recorded on a Perkin-Elmer 983G spectrometer between 4000 and 200cm^{-1} with an average resolution of 5 cm^{-1}. The experiments were performed on SnO_2 and WO_3 powders dispersed in Nujol and sandwiched between two cesium iodide disks. Conductivity experiments using the Van der Pauw four probe technique have been carried on using samples that were isostatically pressed at 5 tons/ cm^2 in a steel die of diameter 13 mm.

2.3. Electrochemical measurements

Electrochemical (de)insertion of lithium was realized in bottle-type cells having two electrodes. The cathode consisted of 35 mg of SnO_2 or WO_3 powder and 6 mg of carbon black (i.e. ~ 15w%). The cathode was prepared by intimately mixing the powders (previously outgassed at 180°C for 5 hrs) and pressing in the form of a disk in a 1.3 cm diameter stainless steel die. Lithium metal was used as both reference and anode. The electrolyte was a 1M $LiCF_3SO_3$-propylene carbonate solution impregnated into a glass filtre paper. The propylene carbonate (Aldrich 99+%) was further dried by fractional distillation under 4Å molecular sieves. The lithium triflate (Aldrich 97%) was kept under vacuum at 150°C during 72hrs.The experiments have been then carried out in an air-free and moisture-free glove box maintained under argon atmosphere.

3. Results and discussion

3-1 Sample composition

a) Samples 1-(150), 1-(350), 1-(550)

(a) method 1

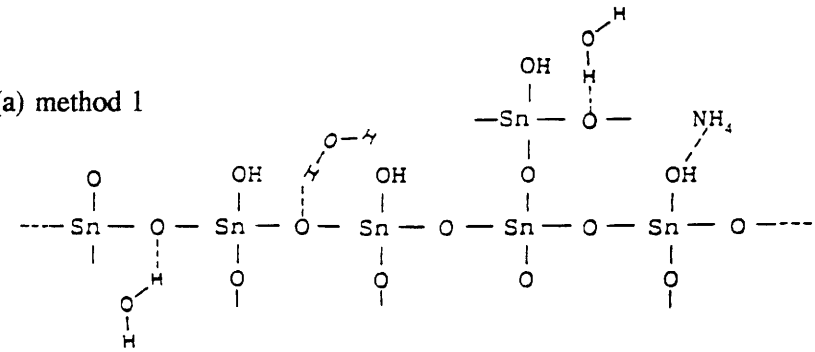

(b) method 2.

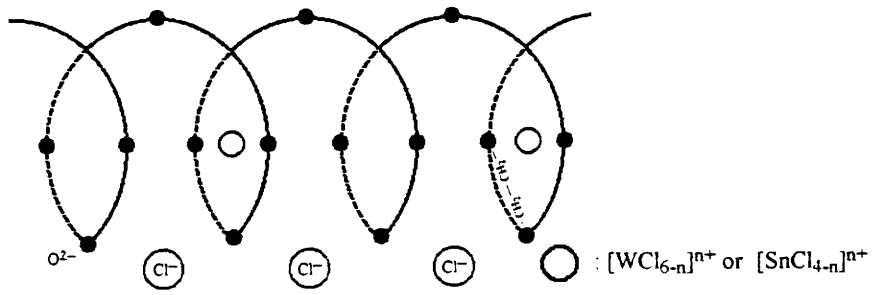

Fig. 2. Probable structures of the "polymerized oxides" obtained in methods 1 and 2 .

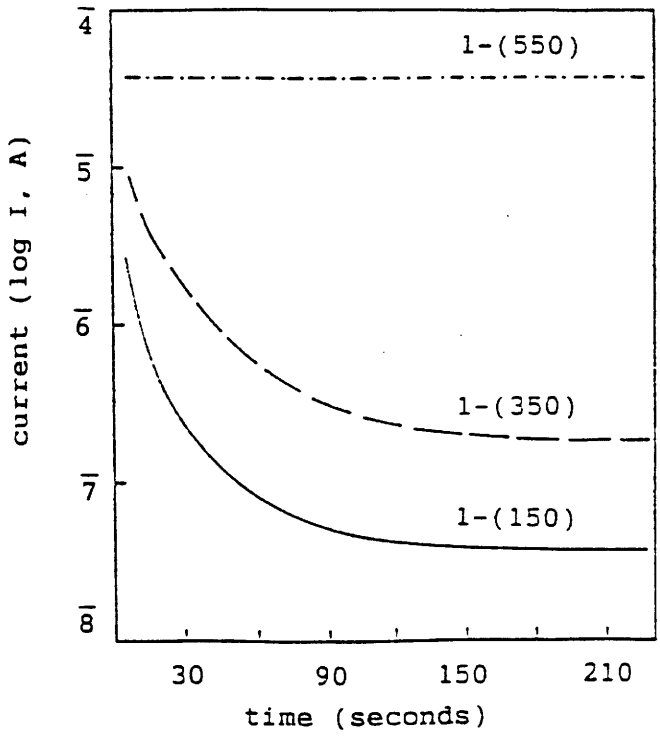

Fig. 3. Electrical current accross a disk of SnO_2 prepared employing method 1.

The d.c.electric current induced by an applied potential of 1 V accross a disk of SnO_2 (1mm thickness, 13mm diameter) is shown in fig.3 for electrodes that are blocking to ionic motion.

It is known that the presence of hydroxyl groups and adsorbed water in fine-grained SnO_2 powders favours protonic conductivity by means of a drift (and non-hopping) process [10, 11]. With blocking electrodes, the protonic conductivity causes the 'polarization effect' illustrated in fig. 3 for samples 1-(150) and 1-(350). It can be noted on the one hand that the measured current is time dependent in both of these cases suggesting an ionic (i.e. protonic) conductivity. On the other hand, the constancy of the current observed uniquely for sample 1-(550) shows an absence of ionic conductivity and hence of hydroxyl groups or adsorbed water. The occurrence of protonic conductivity in samples heated only up to 350°C has also been observed by others [12-15]. The higher total current observed for the sample 1-(550) is attributed to an increased electronic conductivity due to an increase in concentration of oxygen vacancies.

The presence of adsorbed water and hydroxyl groups in the samples 1-(150) and 1-(350) is also revealed in the IR spectra (fig. 4). Adsorbed water is best characterized by its deformation mode δ OH_2 occuring near 1620 cm^{-1}. This absorption band is only observed in sample 1-(150). The broad features between 3500 and 3100 cm^{-1}observed for samples 1-(150) and 1-(350) can involve stretching modes of water, hydroxyl groups. Traces of ammonium ions arising from the synthesis might also occur and contribute to the previous broad absorption (υ_1 and υ_2 modes of NH_4^+). However, nothing is detected around 1420cm^{-1}(υ_4 mode of NH^{4+}).

On the other hand, a weak and broad feature is observed at about 1200cm^{-1} in both 1-(150) and 1-(350) samples. It can be attributed to an hydroxyl bending mode. Therefore, for sample 1-(350) which presents no water absorption at 1620 cm^{-1}, it can be concluded that the protons are essentially involved in hydroxyl groups and the broad high frequency absorption reflects mainly the stretching vibrations of these hydroxyl groups.

Finally, sample 1-(550) exhibits neither water nor hydroxyl group vibrations.

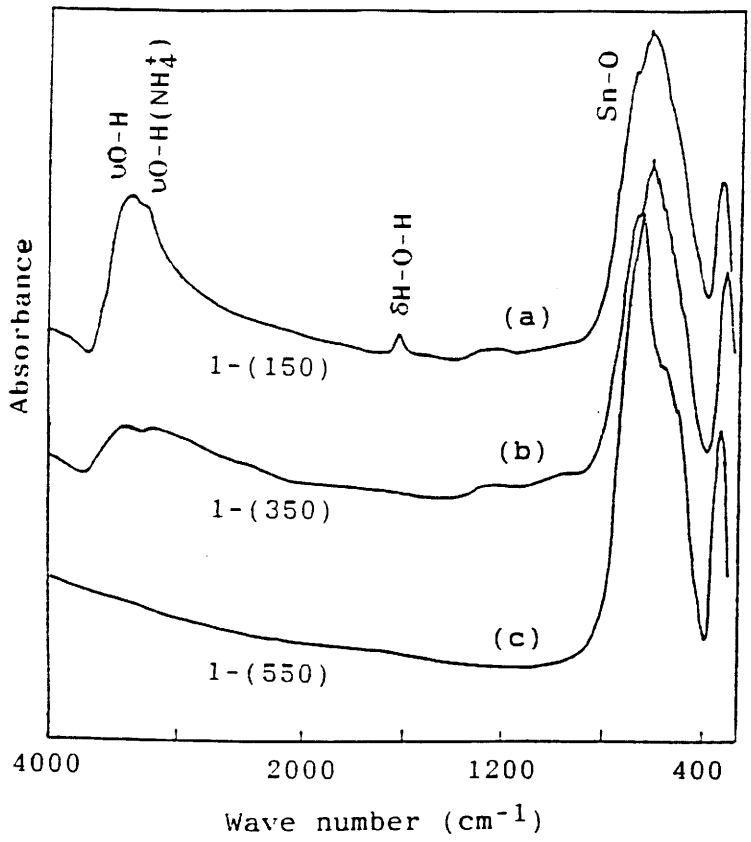

Fig. 4. IR absorption spectra of (a)1- (150), (b)1- (350) and (c) 1- (550) samples.

Even though a small amount of ammonia not detectable by IR spectroscopy might occur, the compositions deduced from TGA measurements (fig.5a) and reported in table I, have been estimated from the general formula SnO_2-nH_2O [16].

b) Samples 2-(350), 2-(450),2-(550); 2-(350)-W, 2-(450)-W and 2-(550)-W

As reported above the powdery SnO_2 and WO_3 samples result from the calcination of polymer-metal halide complexes (fig. 2b) at the required temperatures (350°C, 450°C, 550°C). The corresponding overall weight loss, as evidenced from TGA studies, is about 80%: it takes place in four stages as depicted in fig. 5b. The initial weight loss of ~12%, stage (i), is completed below ~100°C. It corresponds to the evaporation of the residual CH_3CN solvent. The stages (ii) and (iii) are completed between ~130 and 200°C and ~300°C respectively; they account for the emission of H_2O and HCl (~65%weight loss). The last step (iv) is completed at ~500°C, it corresponds to the departure of CO, CO_2 traces (~3% weight loss). Carbon traces remaining in samples 2-(350), 2-(450), 2-(350)-W and 2-(450)-W give them a dark coloration (table I). IR spectroscopy reveals no measurable traces of water and hydroxyl groups in all samples (table I); the IR spectra for these samples have been recorded in a manner mentioned earlier and a detailed report will be published elsewhere [17]. Consequently, the SnO_2 and WO_3 powders are likely to behave as the (quasi) water free and hydroxyl group free NCIMs whose electrochemical Li^+ (de)insertion efficiency has already been demonstrated by some of us [8, 9]. To prove the occurrence of the similarity in the behavior of the SnO_2 and WO_3 powders to those of the NCIMs, we have to examine first the crystalline structure and texture prior to any electrochemical investigation.

3-2. Crystalline structure and texture

X-ray diffraction measurements were carried out on all samples listed in table 1 in order to know the evolution of the crystallite size as a function of calcination temperature.

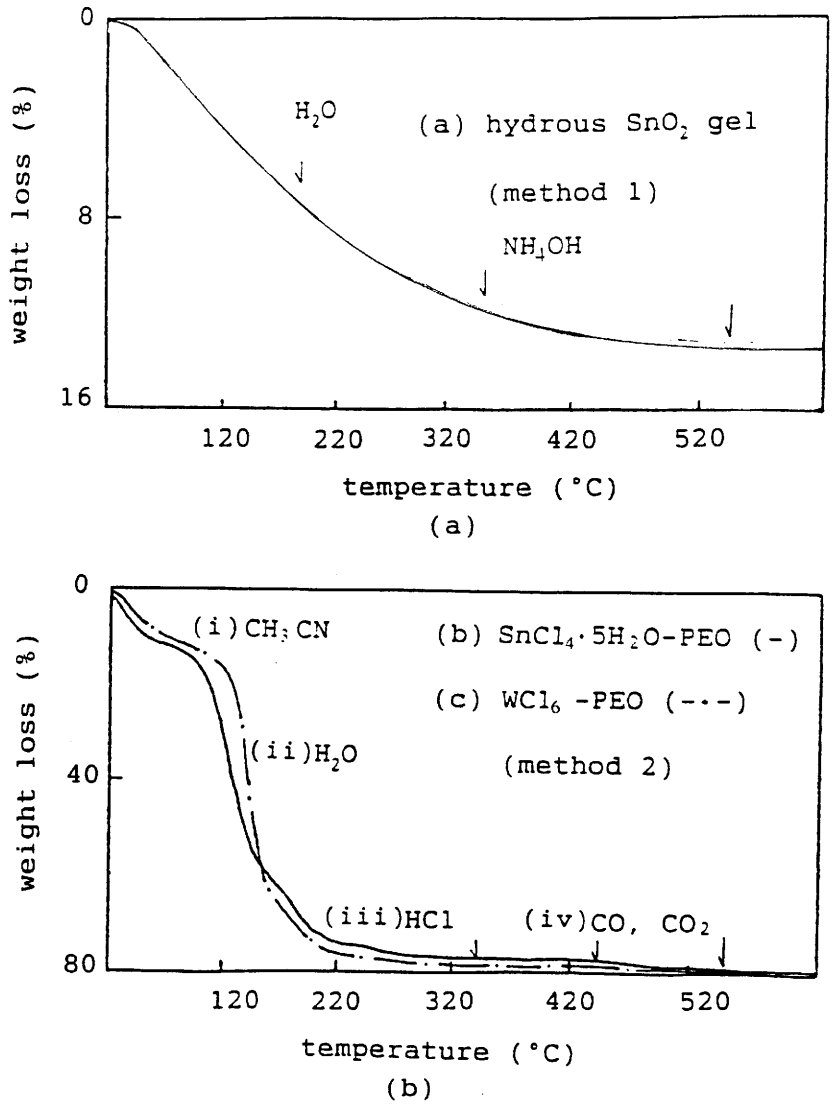

Fig. 5. TGA profiles of hydrated SnO_2 gel (a), $SnCl_4$. $5H_2O$-PEO and WCl_6-PEO (b), recorded in dry air with a heating rate of 1°C per minute.

For the sake of clarity, the diffractograms, which are the most representative of this evolution, are shown in fig. 6. The X-ray diffraction lines are very broad for 1-(350), 2-(450) and 2-(450)-W. However, their very presence indicates that they are nanocrystalline in nature rather than glasses. The main size, D, of the nanocrystallites, listed in table 2, were estimated by considering the diffraction broadening of the peaks corresponding to the (110) plane for tin oxide and to the (001) plane for tungsten oxide (§-II.2).

We compare in table 2 the specific surface areas of the SnO_2 powders 1-(550) and 2-(550) having rather similar crystallite size and being free from contamination by water and/or hydroxyl groups and carbon (originating from PEO). Most interestingly, a much higher BET surface area is formed for sample 2-(550). The structures of the gels shown in fig. 2 account for this difference in specific surface area, which is not only related to the crystallite size but also to the particle size. Indeed, the Sn or W ions (fig. 2) are strongly bound with the basic centers of the PEO due to the acidic character of W^{6+} and Sn^{4+} [21]. The metal ions are also separated by long distances (longer than those between Sn^{4+} ions as it occurs in fig. 2a). Consequently the PEO strongly restrains the growth of the crystalline phase of these oxides. The crystal and particle growths are promoted only when the organic part is almost eliminated (occurs above 450°C (fig. 5b)). As expected, the specific surface area increases as the crystallite size is reduced, from 2-(550) to 2-(450) on the one hand, and from 2-(550)-W to 2-(450)-W, on the other (table 2). Finally the low surface area values reported in table 2 for samples 2-(350) and 2-(350)-W are due to an incomplete elimination of the polymer at 350°C; the carbon contents are higher than 10% (table 1). It may be possible that the SnO_2 and WO_3 crystallites are bound together through O-C bonds; consequently very small surface areas are observed for 2-(350) and 2-(350)-W.

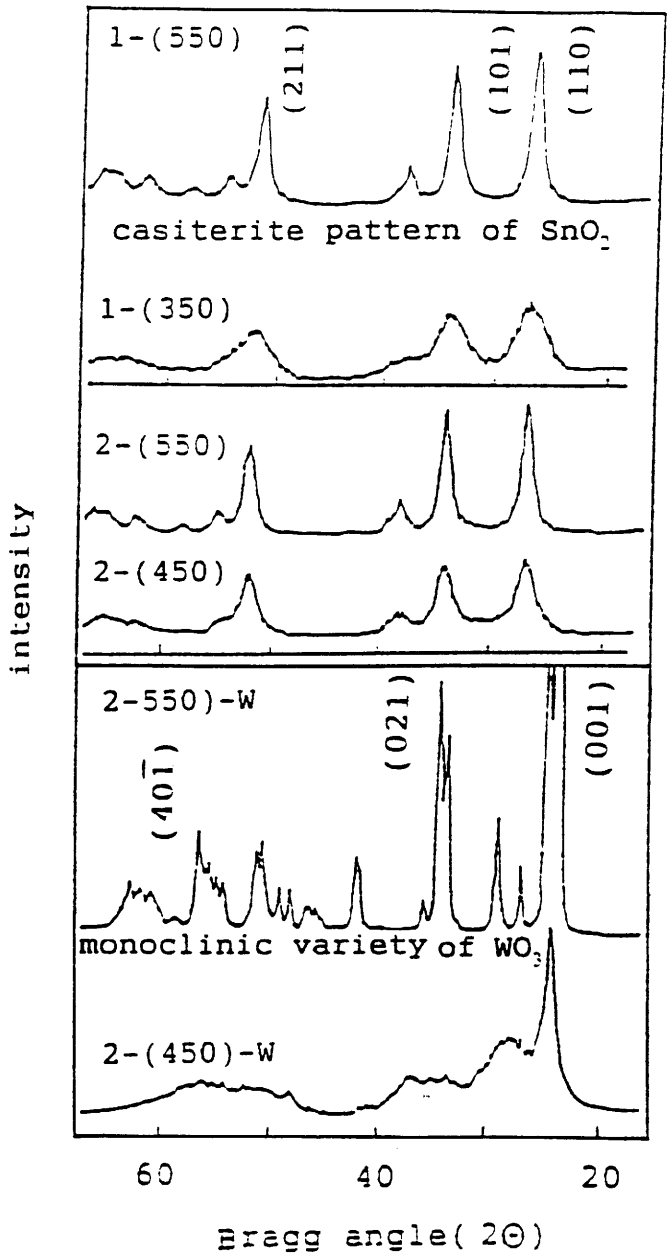

Fig. 6. X-ray diffractograms of some SnO_2 and WO_3 powders.

Table 1. Sample characteristics according to the preparation conditions.

Preparation procedure	Method 1			Method 2					
	SnO_2			SnO_2			WO_3		
Samples	1-150	1-350	1-550	2-350	2-450	2-550	2-350-W	2-450-W	2 550-W
'n' value in $SnO_2 \cdot nH_2O$ $WO_3 \cdot nH2O$	1.5	0.5	0.0	0.0	0.0	0.0	0.0	0.0	0.0
Content carbon(w/o)	0.0	0.0	0.0	~15	~5	0.0	~10	<5	0.0
Colour	white	pale yellow	pale yellow	black	brown	grey white	black	brown	pale green

Table 2. Evolution of the crystallite size and specific surface area with calcination temperature using both methods 1 and 2.

Samples	1-150	1-350	1-550	2-350	2-450	2-550	2-350-W	2-450-W	2-550-W
Crystallite (a) size (±6Å)	<20	30	75	<20	45	70	<30	60	308
(110) (b)	25	55	150	-	-	-	-	-	-
Surface (a) area (m^2/g)	122	148	39	16	104	75	16	38	25

(a) this study: *let us quote that the surface areas reported here are related to the particle size and pore volume (the accepted definition being that many crystallites make a particle).*

(b) from references 18-20.

3-3 Electrochemistry: influence of grain and particle sizes on the reversible electrochemical insertion of lithium in SnO_2 and WO_3 NCIM electrodes

Fig. 7 illustrates the reversible 10^{th} discharge curve of $Li/Li^+/Li_xSnO_2$ (a) and $Li/Li^+/Li_xWO_3$ (b) cells for the samples free from contamination by water, hydroxyl groups and residues of PEO (table 1). In agreement with our model [7-9], the highest rate of lithium insertion occurs for the NCIMs 2-450 and 2-450-W, which possess the highest specific surface area. Our results concerning WO_3 are also in agreement with Zhang [22] who shows that powdery Li_xWO_3 electrodes having surface areas of $4.3m^2/g$ and $12.2m^2/g$ reversibly insert $x = 0.28$ and $x = 0.48$ lithium, respectively, between 1.8 and 3.2 V vs Li. In our case, the rate of lithium reversibly inserted is higher ($x = 1.2$ for 2-(450)-W) because of the higher specific surface area. Within the same voltage range (fig.7), the amount of Li inserted is larger in the case of WO_3 compared to SnO_2 : it is indeed related to the electron affinity of the W^{6+}/W^{5+} couple which is larger (in absolute value) than that of the Sn^{4+}/Sn^{2+} couple [8, 21]. Fig. 8 illustrates the good cycling reversibility observed for 2-(450) and 2-(450)-W electrodes.

4. Conclusions

In this paper we have distinguished two methods of preparing fine-grained tin oxide powder. The method 2, to our knowledge, seems to be original and leads to SnO_2 powders free from water and/or hydroxyl groups and with small crystallite and grain sizes. Method 2 also has been used to prepare powdery WO_3 samples having the finest crystallites. Related to the fine-grained texture of the samples, we have shown that they are able to sustain long-term electrochemical cyclability. In fact, they behave like other NCIMs that we have recently investigated [9]. Indeed, by minimizing the size of the crystallites the formation of defect bonds is favoured, particularly at the crystallite surface, acting as reversible grafting sites for Li. Moreover, the cation-anion bonding would be weakened not

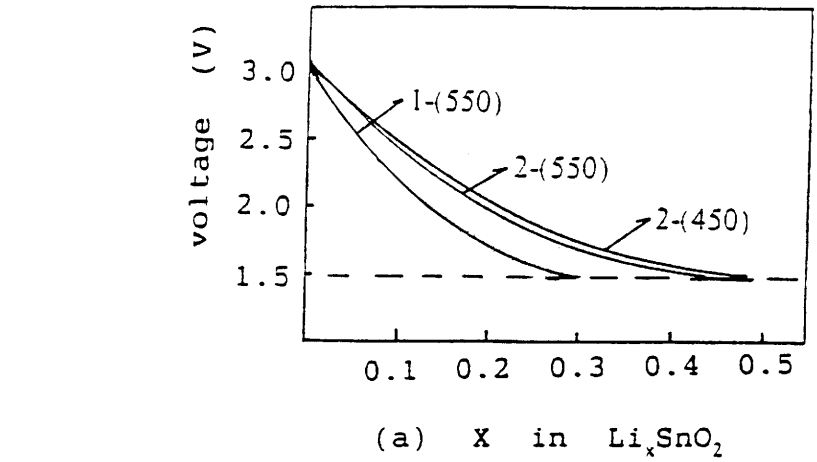

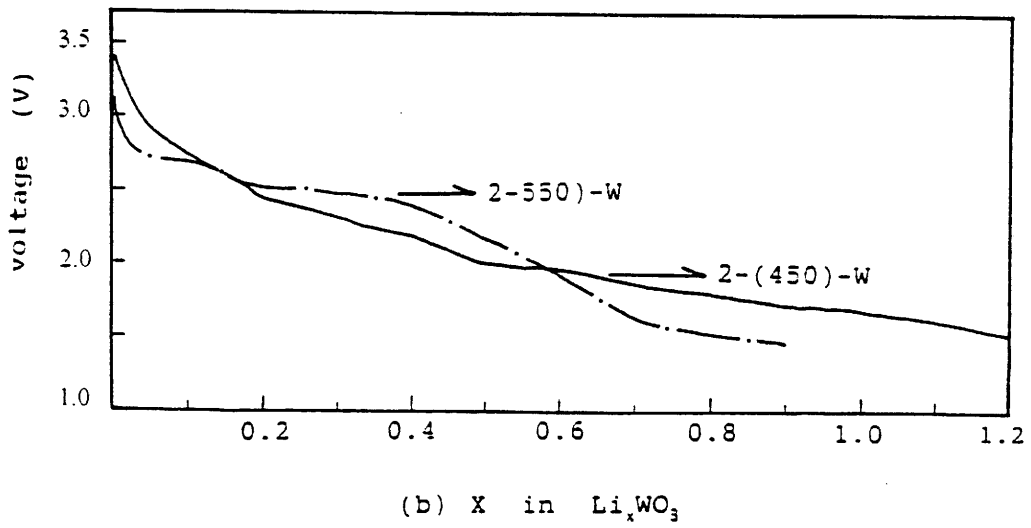

Fig. 7. Reversible 10th discharge curves of (a) $Li/Li^+/Li_xSnO_2$ and (b) $Li/Li^+/Li_xWO_3$ cells between voltage limits of 1.5 - 3.1V (a), and of 1.8 - 3.1V (b), vs Li. The current density was $50\mu A/cm^2$ for an electrode weight of 35mg.

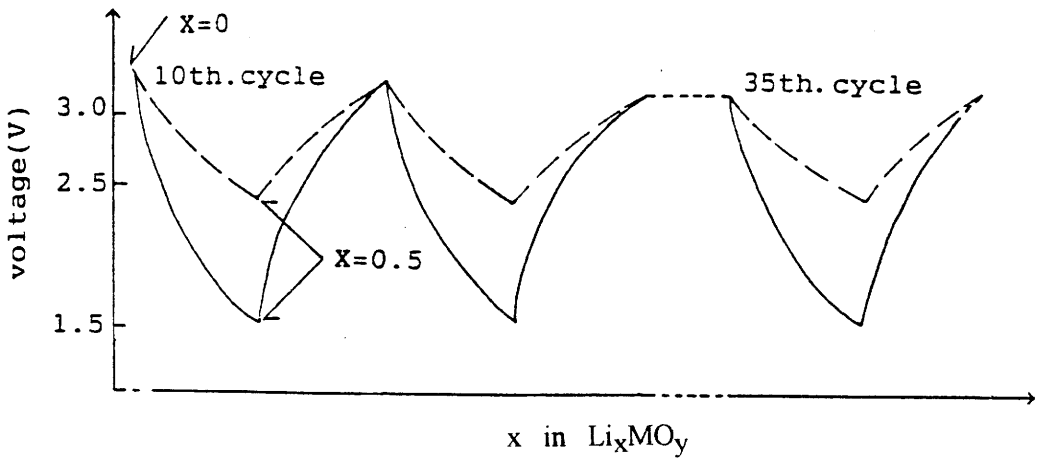

Fig. 8. Series of charge-discharge curves for $Li/Li^+/Li_xSnO_2$ (——) and $Li/Li^+/Li_xWO_3$ (-----) cells using 2-(450) and 2-(450)-W electrodes.

only in the grain boundary region, but also within a grain close to its surface; therefore, the electrochemical insertion of Li^+ would also occur through an easy bonding rearrangement. Let us point out that for WO_3 these "non-conventional" insertion mechanisms should occur in addition to the well known intercalation mechanisms of Li within the cristallites and allowed by their tunnel type structure. However, in order to check the validity of the discussions and conclusions made here, further investigations of *insitu* IR and Raman spectroscopy and of the evolution of electrode-equilibrium potentials as a function of the Li insertion rate are necessary; these measurements are in progress.

REFERENCES

1. E.E. Kohnke, J. Phys. Chem. Solids **23** (1962) 1557.
2. K.L. Chopra, S. Major, D.K. Pandya, Thin Solid Films, **102** (1983) 1.
3. C. Kemball, H.F. Leach, I.R. Shannon, J. Catalysis, **29** (1973) 99.
4. J.L. Aucouturier, P. Hagenmuller, J. Portier, J. Salardenne et al. Proc. 2nd Intl. Conf. on Chemical Sensors, Bordeaux, France (1986).
5. K.F. Poulter, J.A. Pryde, Brit. J. Appl. Phys. Ser. **1** (1968) 169.
6. P.V. Wright, Brit. Polymer J., 7 (1975) 319.
7. B. Morrel, Doctoral Thesis, University of Bordeaux, France, (1991).
8. S.D. Han, G. Campet, J. Portier, C. Delmas and J.C. Lassegues in Proc. of GFECI meeting in Clermont-Ferrand (1993) 15.
9. G. Campet, S.J. Wen, S.D. Han, M.C.R. Shastry, J. Portier, Mat. Sci. Eng. B **18** (1993) 201 and references therein.
10. J.A. Chapman and E. Lilly, J. Phys. C **934** (1973) 455.
11. G.N. Greaves, J. Non-Cryst. Solids **11** (1973) 472.
12. E.W. Thornton, P.G. Harrison, Trans. Faraday Soc. **171** (1975) 461.
13. Braune and Knoke, Z. Phisik Chem., **135** (1928) 49.
14. Landolt-Bronstain, Physikalisch-Chemche Tabellen, **2** Teil (1975).
15. W. Vedder, D.F. Hornig, J. Chem. Phys. **35** (1961) 1560.
16. W.A. England, M.G. Cross, A. Hamnett, P.J. Wiseman, J.B. Goodenough, Solid State Ionics, **1** (1980) 231.
17. S.D. Han, J.C. Lassegues and G. Campet (in preparation for Phys. Stat. Sol (a)).
18. J.F. Goodman and S.J. Gregg, J. Chem. Soc. (1960) 1162.
19. M.J. Fuller, M.E. Warwich, A. Walton, J. Appl. Chem. Biotecnol. 28 (1978) 369.
20. S. Kittika, K. Morishige, T. Fujimoto, J. Coll. Inter. Sci. **72** (1972) 191.

21. J. Portier, G. Campet, J. Etourneau, M.C.R. Shastry, B. Tanguy, J. Alloys and Compounds (communicated).

22. Q. Zhang, J.R. Dahn, K. Colbow, J. Electrochem. Soc., **139** (1992) 2046.

II. 3. INFLUENCE OF THE pH VALUES OF THE SOL-GEL STATE ON PROPERTIES OF SnO_2 POWDERS OBTAINED FROM A SOL - GEL ROUTE.

(publication)

Submitted to Active and Passive Electron Comp.

Influence of the pH values of the sol-gel state on the properties of SnO_2 powders obtained from a sol-gel route.

S.D. Han, G. Campet, J. Portier and M.A. Kennard
Laboratoire de Chimie du Solide du CNRS, Université Bordeaux I, 351 Cours de la Libération, 33405 Talence cedex, FRANCE.

J.C. Lassègues
Laboratoire de Spectroscopie Moléculaire et Cristalline, Université Bordeaux I, 351 Cours de la libération, 33405 Talence cedex, FRANCE.

Y.M. Son
Korea Institute of Energy Research, 71-1 Jang-dong, Yoosung-gu Taedok Science Town, Taejon 305-343. KOREA.

ABSTRACT

The evolution of the specific surface area and crystallite size of SnO_2 powders, prepared from a sol-gel process has been studied as a function of the calcination temperature of the stannic hydroxyde colloid, and for two different pH values (7.5 and 12.5) of the colloïdal state. The samples were characterized by TGA, IR spectroscopy, BET and XRD techniques. The crystallite size and specific surface area were strongly affected not only by the calcination temperature, and unexpectedly, by the initial pH value of the colloïdal state. A framework model, relating the pH dependence to the resulting properties is presented.

1. INTRODUCTION

Stannic oxide is an n-type semiconductor with a tetragonal rutile structure [1] and a large indirect band energy gap. It has attracted considerable attention due to the variety of applications related to its unique electrical, optical and catalytic properties. For example, stannic oxide is used in transparent heaters for windsheild defrosting, in anti-reflection coating for solar cells, as a transparent electrode for electrochromic devices, as a sensing material for combustible gas sensors, and as an electrocatalyst for organic oxidation reaction [2-4]. For the last two applications finely grained SnO_2 powders are used. These powders have generally been obtained through two different methods: one involves the oxidation of elemental tin with acids (HNO_3, H_2SO_4 etc.) and the other utilizes the well-known sol-gel route [3-4].

We have prepared fine particles of SnO_2 powder from this conventional sol-gel method. It involves the dispersion of stannic hydrate in aqueous ammonia to give a sol. The sol is later "solidified" through stages of stiffening and polymerization to give a gel (gelation). The gel so obtained is thoroughly washed with distilled water, filtered, dried and finally heated to high temperatures to obtain the required material. The evolution of the properties of SnO_2 powders, prepared with this technique, has been previously investigated, as a function of reaction temperature, time and ambiant calcination [5]. In this paper we report the correlation between the pH value of the stannic hydroxyde colloidal state and the physical properties of the resulting powders.

2. EXPERIMENTAL

2. 1. SnO_2 powder preparation

A stannic hydrate precipitate was obtained by dropwise addition of 28 % ammonium water to a solution of stannic chloride up to pH 12.5 . The temperature of the stannic chloride solution was maintained near 3°C with an ice-water bath. The excess of ammonium water and

ammonium chloride were removed by repeatedly washing with distilled water followed by filtering.

The pH of the stannic hydrate gel progressively decreased from an initial value of 12.5 after the first filtering to 7.5 after washing and filtering 9 times .

Two kind of SnO_2 powders will be investigated here as a function of the calcination temperature of the gel, one is obtained from a stannic hydroxide gel at pH = 12.5, the other from a gel at pH = 7.5.

The sample name, gel pH value and calcination temperature for each sample is listed in table 1.

Table 1 Sample identification

sample	sol-pH values	gel-calcination temperature (°C)
7-350	7.5	350
12-350	12.5	350
7-550	7.5	550
12-550	12.5	550

The rate of heating and cooling during calcination was 1°C/min and was controlled using an Eurotherm controller.

2. 2. Sample characterization

TGA analysis was carried out up to 600°C in dry air with a heating rate of 3.3°C/min, using a Setaram thermobalence. The infrared spectra of SnO_2 powders, preliminary dried at 200°C for 2hrs, were measured at room temperature using the KBr technique. The sample were manipulated in an argon filled dry box in order to prevent water absorbtion after drying. A

Perkin-Elmer infrared spectrometer (model PE 983) was used to obtain the absorbance of samples in the range of 200~4000cm^{-1}.

X-ray powder data were obtained with a Philips Spectrogoniometer (P.W 1050) using filtered Cu Kα radiation. The Scherrer [6] and Warren formula [7] were used to calculate the average crystallite size from the width of the main diffraction peak at half height (the factor β was corrected using the x-ray diffraction pattern of standard silicon powder).

The specific surface area of the samples was measured by BET using a Micromeritics system (Accusorb) and nitrogen as the adsorbate gas. All samples were out-gased at 150°C for 5hrs.

Electrical conductivity measurements have been carried out on samples that were isostatically pressed at 5 tons/cm^2 in a steel die of diameter 13mm. The two probe DC method was used and the experiments were performed under dynamic vaccum (10^{-3} Torr) between 223K and 375K. For the determination of conductivity, a bias voltage of 1.0 V was applied across the pelletized sample and the resulting current was measured using a pico-ammeter/vc 'tage source (Keithley 487). Silver paste was used for electrical contacts.

3. RESULTS AND DISCUSSION

TGA results of pH 7.5 and pH 12.5 stannic hydrate gels are shown in fig. 1. The weight loss (~16%) reported in fig.1 accounts for a smooth decomposition continued until the temperature reaches ~550°C. Our observations of weight loss are in agreement with the reports of other workers [8]. The two samples exhibited a difference in weight loss at 350°C and 550°C of 2.9 % and 1.4 % respectively. The decomposition takes place in two or three stages ((i), (ii), (iii)) depending on whether the pH of the gel is 7.5 or 12.5, as depicted in the figure. Stages (i) and (ii) corresponds to the removal of adsorbed water and hydroxyl groups respectively. A adsorbed molecular water is indeed entirely removed by drying at about 200°C [9]. On the other hand hyroxyl groups which are more strongly bound to the cations than adsorbed water are, therefore, removed at higher temperature. Residuals of ammonium salt (NH_4Cl) and ammonium hydroxide, remaining from the synthesis are likely

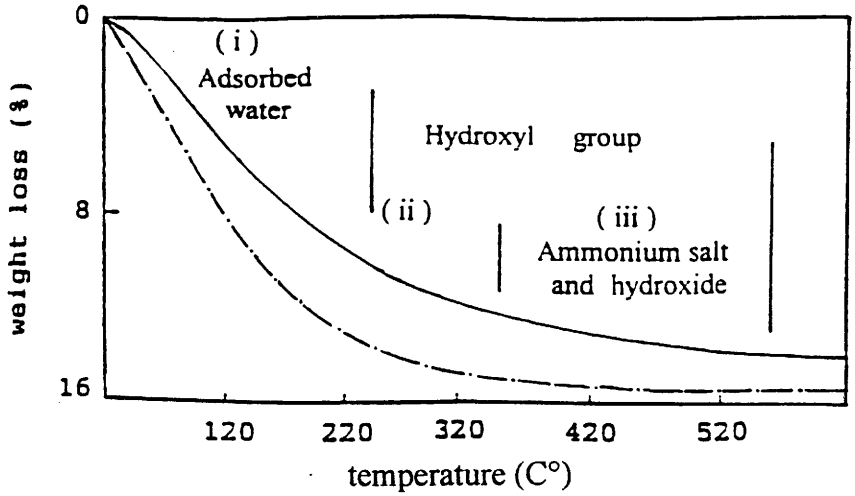

Fig. 1. TGA profiles of hydrated SnO_2 gels, recorded in dry air. (—pH = 7.5, --- pH = 12.5) Before measurements the samples were " pre-dried " in dry air at 60°C, for 2hrs.

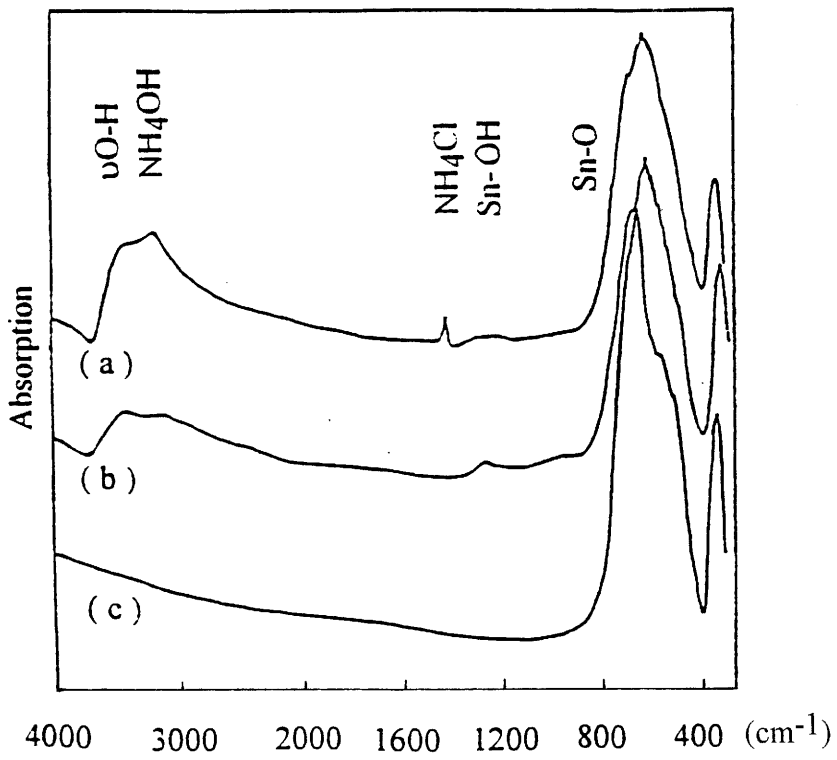

Fig. 2. Infrared absorption spectra; (a): sample 12-350, (b): sample 7-350, (c): samples 12-550, 7-550.

to occur for the gel being at pH12.5, and account for stage (iii). The IR spectrum of sample 12-350 reported on fig.2a reveals an absorption peak at 1400~1420cm^{-1} (ν_4 mode of NH_4^+ [10]). This indicates that unwashed, NH_4Cl, that is present in the stannic hydrate gel at pH12.5, remains up to a calcination temperature of 350°C (sample (12-350)). It is likely that NH_4Cl has little interaction with the SnO_2 framework.The ammonium chloride probably behaves as a coprecipite which has little or no interaction with the SnO_2 framework.

The broad features between 3040 and 3500cm^{-1} observed for samples 12-350 and 7-350 (IR spectra of fig.2a and b) have been assigned to hydroxyl groups associated with surface cations in the SnO_2 rutile structure [11, 12]. As expected no adsorbed water, characterized by its deformation mode δOH_2 at 1620cm^{-1}, was revealed in the IR spectra. On the other hand the traces of ammonium ions, which would occur for sample 12-350, also contribute to the 3040~3500cm^{-1} absorption band in fig.2a (ν_1 (3040cm^{-1}) and ν_3 (3145cm^{-1}) modes of NH_4^+ [13]).

It is of interest to examine whether the ammonium chloride, the hydroxyl and ammonium groups, present in the stannic hydrate gel at pH 12.5, influence the physical properties of the resulting SnO_2 powders. Fig.3 shows the x-ray diffractograms (XRD) for samples 7-550 and 12-550, from which the average crystallite sizes have been estimated. The XRD are characteristic of the SnO_2 rutile structure, as expected. However, and most interestingly, the crystallite size are significantly different: ~75Å for 7-550 and ~506Å for 12-550 although the calcination conditions are identical. On the other hand the powders obtained from the two stannic hydrated gels calcinated at lower temperature ($T < 350°C$) have similar crystallite sizes (fig.4).

The specific surface area of the powders varies inversely with the calcination temperature. When the calcination temperature is larger than 350°C (fig.5), it is larger or equal to 350°C (fig.5), i.e. it varies inversely with the size of the particles (the accepted definition being that many crystallites make a particle). For lower calcination temperatures ($T < 350°C$) the departure of adsorbed water and, probably, of weakly bound hydroxyl groups is responsible for the increase of the specific surface area. The specific surface area of sample 12-350 is larger than that of 7-350 (fig.5) even though the crystallite size appears to be nearly the same

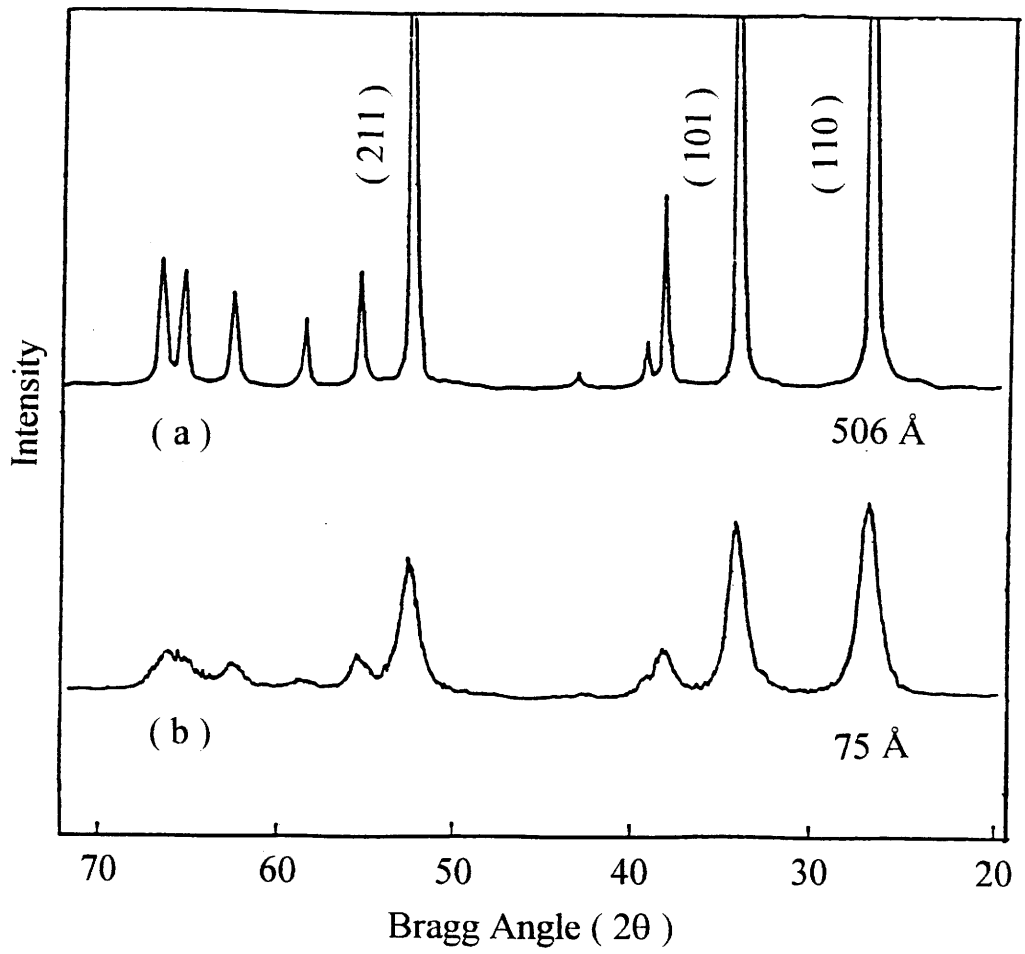

Fig. 3. X-ray diffractograms of, 12-550 (a), and 7-550 (b) samples (±6Å).

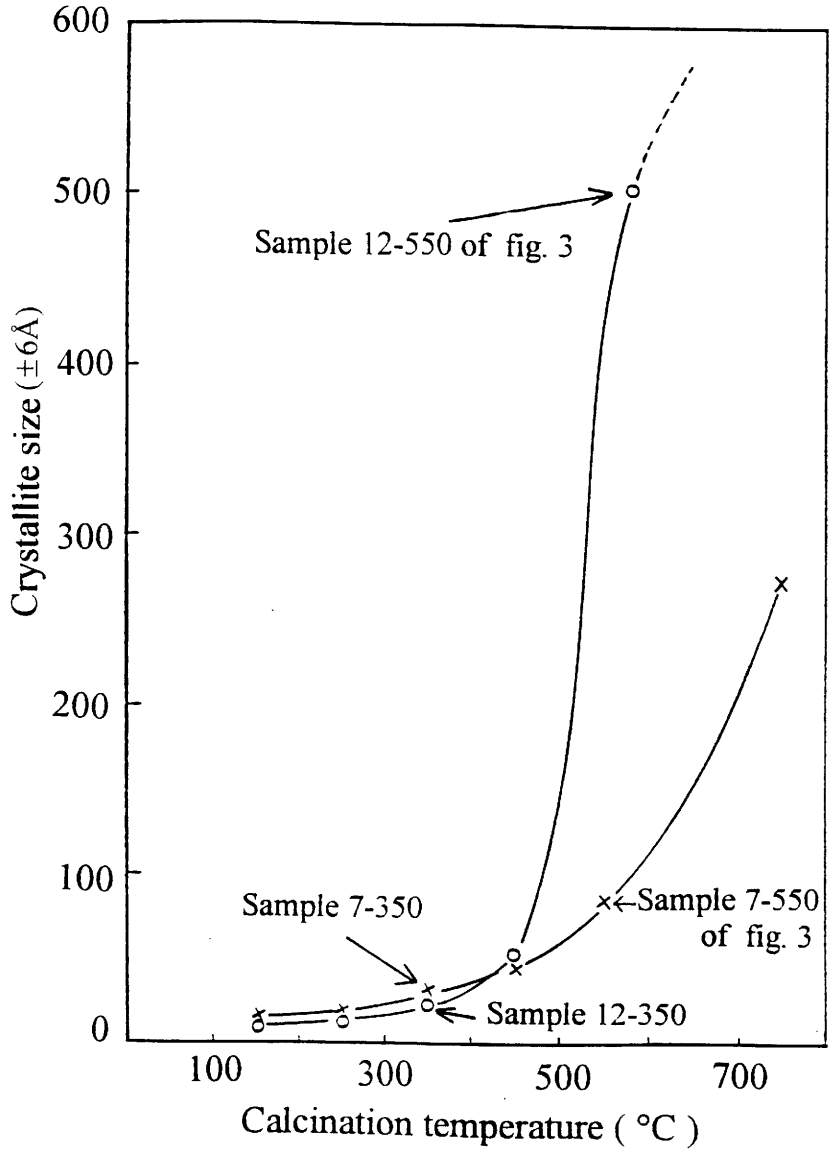

Fig. 4. Evolution of the crystallite size as a function of the calcination temperature of the two stannic hydrated gels (o: pH12.5, x: pH7.5)

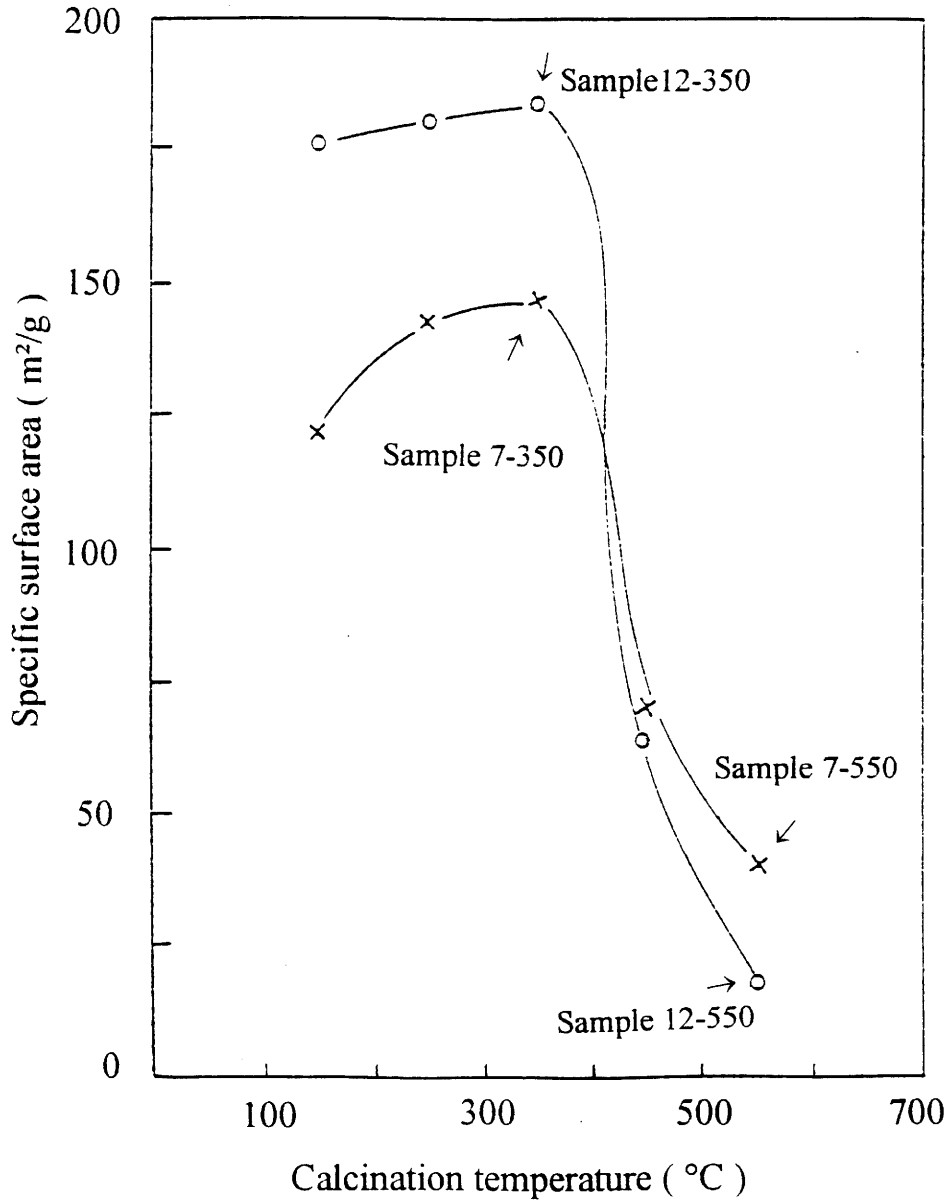

Fig. 5. Evolution of the specific surface area as a function of the calcination temperature of the hydrated SnO_2 gel, (o: pH 12.5, x: pH 7.5).

by x-ray diffraction. That can be explained as follows. We have shown that hydroxyl and ammonium groups and, also, ammonium chloride are present in higher proportions for sample 12-350. It is likely that these species are in the pores of the particle and could cause larger pore volume, as depicted in schematically fig.6. Consequently,this would result in larger specific surface area, as observed for sample 12-350 (fig.5). Thus the sharpest decrease of the specific surface area for T > 350°C, observed for the powders from the gel at pH12.5 (fig.5), is induced by the complete departure of the above mentioned species, leading to a closing of pore. The overall reaction accounting for the departure of the species might be expressed as follows,

$$SnO_{2-x-y}(OH)_x(OH)_y(NH_4)_y + z\,NH_4Cl \qquad (1)$$

$$\downarrow \sim 350°C \text{ (surf. cat.)}$$

$$SnO_{2-y}\square_y + (y+z)\,NH_3(\uparrow) + y\,H_2O(\uparrow) + z\,HCl(\uparrow) \qquad (2)$$

In fact the surface of the tin oxide, very likely might act as catalyser for the departure of the hydroxyl and ammonium species. Indeed ammonium chloride begins to be sublimated and decomposed above ~350°C [14]. According to (1) and (2), oxygen defficient tin oxide powders, $SnO_{2-y}\square_y$, arise from the calcination of the stannic hydrate gel at pH12.5. Moreover the hydrogen involved in (1) might enhance the reduction process and, therefore, enhances the oxygen-vacancy concentration. On the other hand it is well established that oxygen defficiency (as well as interstitial Sn) gives rise to n-type conductivity [15,16]. Under such a circumstance the conductivity of sample 12-550, for instance, should be significantly higher than that of sample 7-550, which should be more stoichiometric. The large difference in the conductivities between the two samples (fig.7) supports this hypothsis, It also explains the observed darker (greyish) coloration of sample 12-550 compared with 7-550. However, the higher rate of oxygen vacancies in the oxide 12-550 does

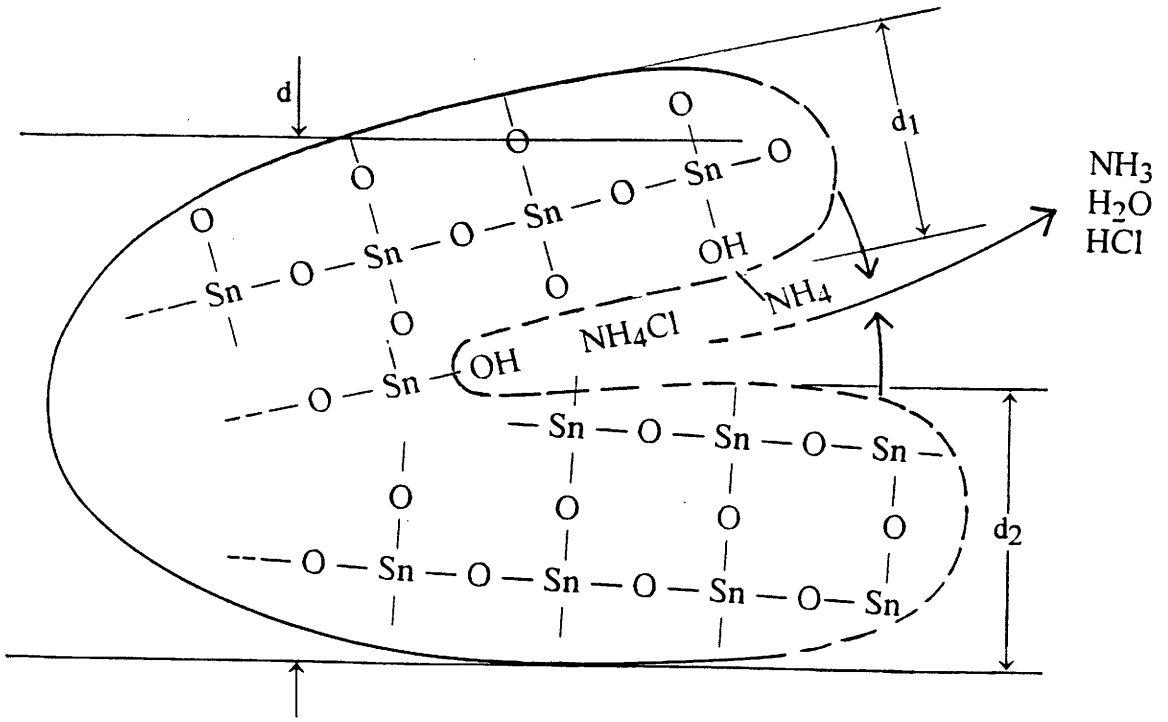

Fig. 6. Probable framework of SnO_2 powder issued from gel at pH12.5 and calcined at $T \leq 350°C$. The sublimation of NH_4Cl at $T \geq 350°C$ promotes the departure of the hydroxyl and ammonium groups leading to the closing of the pores. (The crystallite size, d is sharply increased by $d_1 + d_2$).

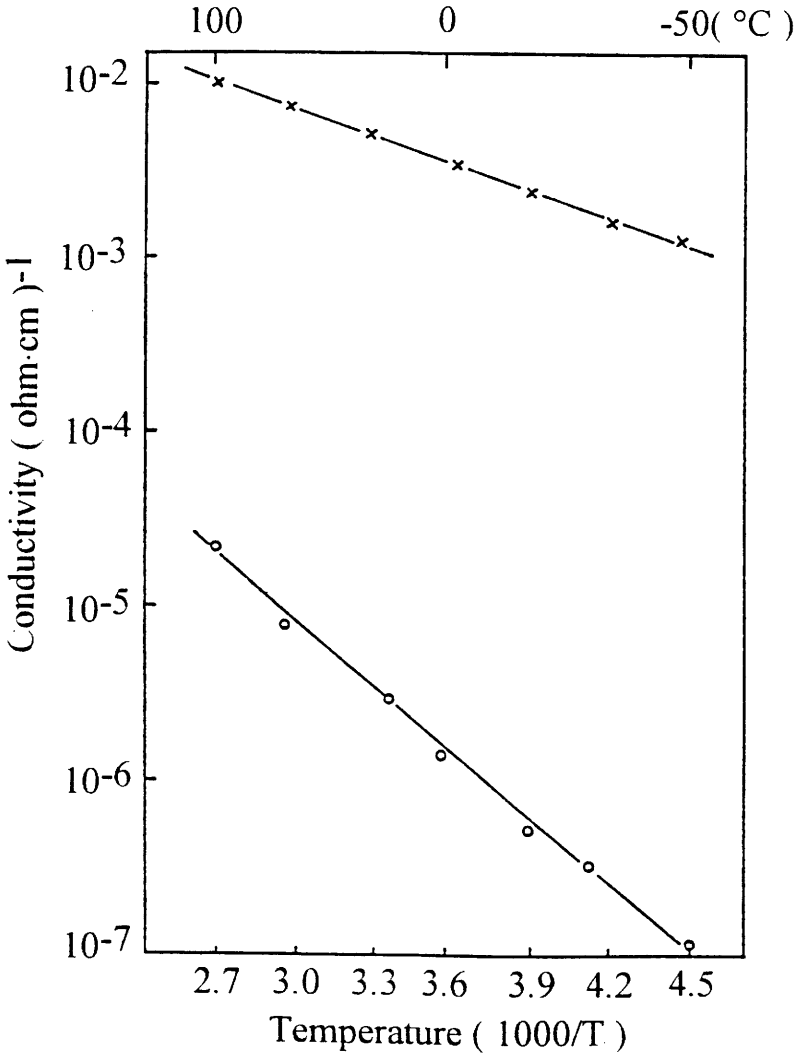

Fig. 7. Electrical conductivity as a function of temperature for 12-550 (x) and 7-550 (o) samples.

not account, in itself, for its much higher conductivity. Recall from fig. 3 that the oxide 12-550 produces larger crystallites than the oxide 7-550. Consquently the grain boundary effect, which inhibits the DC conduction, is minimized in sample 12-550, so that its conductivity is larger. It also sugests that the reaction (1) causes not only the closing of the pores but, in addition, promotes the crystal growth process. Indeed, the closing of the pores results in the " matching " of crystal site atoms(-- Sn - O - Sn --). It means that the crystallite size is sharply increased by ($d_1 + d_2$), as seem in fig. 4 and 6, in the 350 ~ 550 °C range. Let us finally recall that no significant difference between the size of the crystallites of the two oxides will be observed if the calcination temperature is lower than ~350°C (fig.4). Indeed at these calcination temperature ammonium chloride is not sublimated [14] and, consequently, reaction (1) cannot proceed.

4.CONCLUSION

The specific surface area and crystallite size of SnO_2 powders are affected not only by the calcination temperature, but also by the pH values of the colloidal state. Hydroxyl groups, ammonium hydroxide and ammonium chloride are present in the gels prepared at pH 12.5. They account for the larger pore volume, and as well as higher specific surface area observed for the SnO_2 powders calcined below 350°C. When the powders are heated above 350°C these species volatilize. This results in a sharp decrease of the specific surface area, and a large increase of the crystallite size.

REFERENCES:

1. E.E. Kohnke, J. Phys. Chem. Solids 23 (1962) 1557.
2. K.L. Chopra, S. Major, D.K. Pandya, Thim Solid Film, 102 (1983) 1.
3. C. Kemball, H.F. Leach, I.R. Shannon, J. Catalysis, 29 (1973) 99.
4. J.L. Aucouturier, P. Hagenmuller, J. Portier, J. Salardenne et al. Proc. 2nd Intl. Conf. on Chemical Sensors, Bordeaux, France (1986).
5. J.F. Goodman and S.J. Gregg, J. Chem. Soc., (1960) 1162.
6. P. Scherrer, Gottinger Nachrichter 2, (1918) 98.
7. A Guinier, Théorie et technique de la radiocristallographie, New York (1955).
8. M. J. Fuller, M. E. Warwick, J. of Catalysis. 29 (1973) 441.
9. E.W. Thonton, P.G. Harrisson, Trans. Faraday Soc., 171 (1975) 461.
10. W. Vedder, D.F. Horning, J. Chem. Phys.35 (1961) 1560.
11. R. S. Katiyar, P.Dawson, M.M. Hargreave, G.R. Wilkinson, J. Phys.C; Solid State Phys., 4 (1971) 2421.
12. W.A. England, M.G. Cross, A. Hammett, P.J.Wiseman, J.B. Goodenough, Solid State Ionics, 1 (1980) 231.
13. Ladolt-Bronstain, Physikalisch-Chemche Tabellen, 2 Teil (1975).
14. Braune and Knoke, Z.Phisik Chem., 135 (1928) 49.
15. H.J. Van Daal, Sold State Comm., 6 (1968) 5.
16. Z.M. Jarzebski, J.P. Marton. J. of Electrochemical Society., 123 (1976) 299.

II. 4. MECHANISMS OF THE REVERSIBLE ELECTROCHEMICAL INSERTION OF LITHIUM OCCURING WITH NCIMs (Nano-Crystallite-Insertion-Materials)

(publication)

To be published in J. of Active and Passive Electron Compon.

Mechanisms of the reversible electrochemical insertion of lithium occuring with NCIM$_S$ (Nano-Crystallite-Insertion-Materials)

S.D. Han, N. Treuil, G. Campet, J. Portier, C. Delmas*

Laboratoire de Chimie du Solide du CNRS
351 cours de la Libération - 33405 Talence - France

J.C. Lassègues

Laboratoire de Spectroscopie Moléculaire et Cristalline du CNRS
351 cours de la Libération - 33405 Talence - France

A. Pierre

Department of Mining - Metallurgical and Petroleum Engineering
University of Alberta - Edmonton - Alberta, T6G-2G6 - Canada

* *Author for correspondance*

Keywords : Nanocrystallite - dangling bond - lithium insertion

ABSTRACT

A new family of insertion-compound electrodes so called NCIM$_s$ (Nano-Crystallite-Insertion-Materials) has been proposed : the major requirement is that the electrode materials have to be polycristalline with a crystallite and particle size as small as possible (the accepted definition being that many crystallites make a particle). Indeed by minimizing the size of the crystallites the formation of defects is favoured, particularly at the crystallite surface, acting as reversible (de)grafting sites of Li^+. Also related to that the cation-anion bonding is weakened not only in the grain boundary region but also within the crystallite close to its surface : then the electrochemical insertion of Li^+ takes place through easy bonding rearrangements.

1. Introduction

In the last 20 years much attention has been focussed on A_xMO_2 - type intercalation compounds (A=Li, Na and M=Co, Ni, Mn...) which are used as positive electrodes in reversible alkali electrochemical cells (see for example refs. 1).
However, a very long-term cyclability (i.e. over 10^3 cycles) might be hardly achievable, particularly for corresponding electrodes having a large grain size, probably because the Li^+ (de)intercalation process slightly perturbs the host lattice.[1]

Some of us have patented, a few years ago, a new strategy and related experiments that have enabled us to put forward a rather new family of insertion-compound electrodes able to sustain long-term Li^+ electrochemical cyclability [2]. The major requirement is that the electrode materials are polycristalline with a crystallite and particule sizes as small as possible. Therefore we later called the polycristalline electrode materials $NCIM_s$ (for nano-crystallite-insertion material) [3, 4].
Table 1 gives important examples related to mixed-valency metal oxides [2, 5].
For clarity the examples listed in Table 1 have been divided into two classes, I and D, according to whether the resistivity tends to increase (class I) or to decrease (class D) upon the electrochemical Li^+ insertion process.

Table 1 - Some nanocrystallite insertion materials

Sample	Class	Average grain size (Å)	Insertion rate x (measured in $LiClO_4$ (p.c.), 1.5V<V(Li)<3.5V)
Li_xSrTiO_3	D	80	$0 \leqslant x \leqslant 0.3$
Li_xCrO_2	I	30	$0 \lesssim x \leqslant 1$
$Li_xMn_2O_3$	I	50	$0 \lesssim x \lesssim 2$
$Li_xFe_2O_3$	D	150	$0 \lesssim x \lesssim 0.5$
Li_xNiO_2	I	60	$1 \leqslant x \leqslant 2$
Li_xCuO_2	I	50	$1 \lesssim x \lesssim 2$
Li_xWO_3	D	40	$0 \leqslant x \lesssim 2$

Rather similar considerations were reported by Barloux et al. and concern the spinel $LiMn_2O_4$ [6]. Also apparently related to that, Kumagai et al. [7] have reported that the positive electrode $MnO_2.yV_2O_5$ was formed by incorporation of V_2O_5 into MnO_2 matrices and the crystallinity of the oxide decreased with increase in V_2O_5 content incorporated : they have shown that the amount of Li^+ ions which can be reversibly electrochemically (de)insered increased with increasing y value, i.e. with decrease in the crystallinity ; it reached about 1 Li^+ per mole of transition metal with y = 0.6 [7].

In this paper the framework of the model accounting for the reversible electrochemical Li^+ insertion occuring in the $NCIM_s$ is presented.
We also show, for the first time, that the model accounts for the evolution of the open circuit voltage or the electrodes, vs the fraction, x, of the alcali.

1. Voir la remarque p.20.

2. Mechanisms of the reversible electrochemical insertion of lithium occuring with $NCIM_s$

First of all, by minimizing the size of the crystallites we tend to :

(i) favour the formation of defect bonds, particularly at the crystallite surface (of its vicinity), such as anions adjacent to cation vacancies : ***these defects may act as reversible (de)grafting sites for Li^+.***

(ii) weaken the cation-anion bonding not only on the grain boundary region but also within the grain close to its surface : ***then the electrochemical insertion of Li^+ may be expected to occur through easier bonding rearrangements [3].***

That is depicted here-below for $SrTiO_3$-NCIM, ***taken as a non-limiting but illustrative example.***
First of all fig. 1 illustrates the electron conduction via $[Ti:3d]_{sub}$ or $[Ti:3d]_{bw}$ energy states :

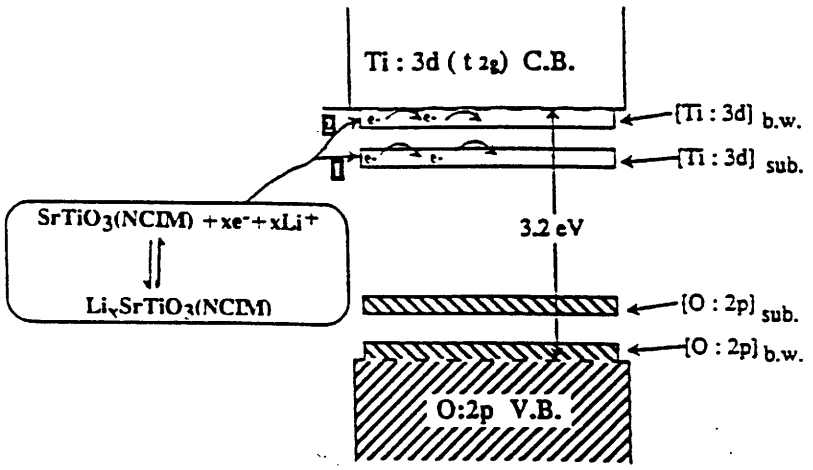

Fig.1 - Simplified band energy scheme of $SrTiO_3$-NCIM

- $[Ti : 3d]_{sub}$ represents deep subband-gap energy states arising from cation defects adjacent to an anion vacancy. They are lowered below the Π^*conduction band of $Ti^{4+} : 3d^0(t_{2g})$ parentage. Conversely anion defects adjacent to cation vacancies occur. They introduce acceptor states $[O : 2p]_{sub}$ arising from the $O^{2-} : 2p^6$ valence band. According to the model the latter defects act as reversible (de)grafting sites for Li^+, (see (i)).
- the $[Ti : 3d]_{bw}$ and $[O : 2p]_{bw}$ energy states originate from Ti-O bond weakening. This bond weakening induces Li^+ (de)insertion as mentioned above (see (ii)).

We will see, now, that the model accounts for the differences observed between the open-circuit voltage (OCV) vs x (the fraction of the alkali) curves related to polycrystalline electrodes having different sizes of crystallites. For sake of simplicity, such a behavior is illustrated only for two n-type electrodes Li_xSnO_2 and Li_xWO_3 (fig. 2a, b).

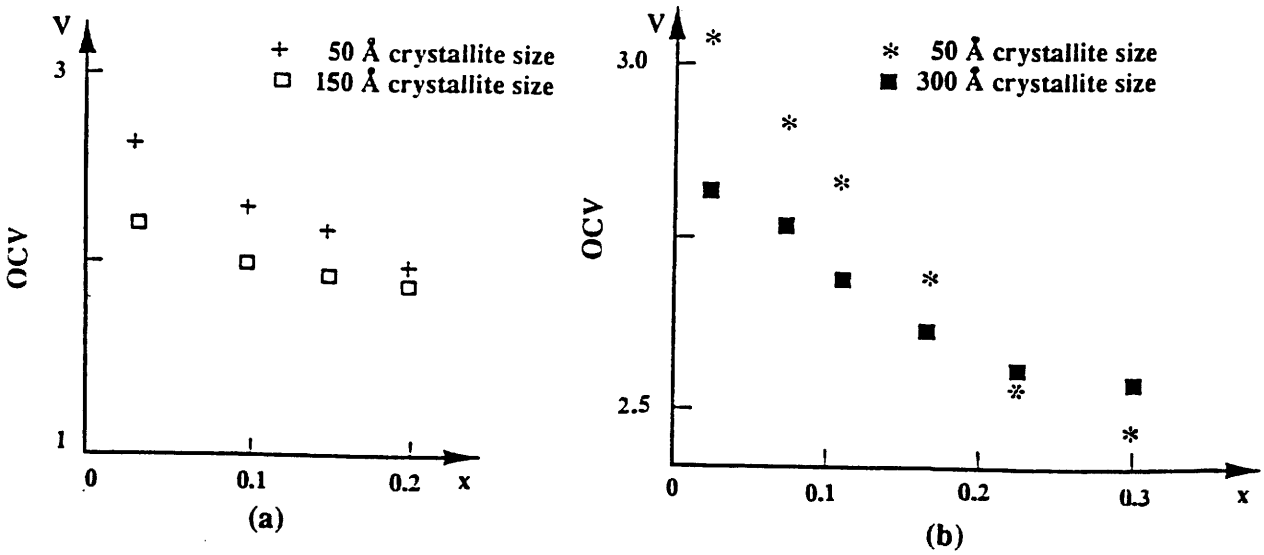

Fig.2 - Equilibrium OCVs vs x for some Li / $LiCF_3SO_3$ / NCIMs (a : Li_xSnO_2 ; b : Li_xWO_3) .

The concentration of the "sub" and b.w." states increases as the crystallite size is reduced. This obviously causes, ***only for the lower x values***, a pushing of the Fermi-energy (E_F) (i.e. higher electron affinity) and thereby of OCV towards cathodic values. Indeed, for the lower x values, the OCV are higher for the electrodes having the smallest crystallite size (fig. 2a and 2b for $x \lesssim 0.15$).

For higher x values ($x >> 0.15$) and when the inside-crystallite structure is well adapted for the reversible intercalation of lithium as occurs for Li_xWO_3, an inversion of the OCV is observed (fig. 2b) : indeed for $x >> 0.15$ all the subband gap energy states $[W^{6+} : 5d^0]_{sub}$ and $[W^{6+}\ 5d^0]_{bw}$ (the "twin states" of $[Ti^{4+} : 3d^0]_{sub}$ and b.w. reported in fig. 1) are filled with electrons : therefore the lithium intercalation within the nanocrystallites can now take place ; it is accompanied with a "delocalization" of the injected electrons in the conduction band. On the other hand it is well established that the band-energy width increases as the crystallite size decreases [8] ; therefore the WO_3 electrodes having the smallest crystallite size have their conduction-band edge shifted towards anodic values : this causes a decrease of E_F, and thereby of OCV, towards anodic values (as it is illustrated on fig. 2b for $x >> 0.15$).

References

1. J. Rouxel, in F. Levy (ed.), Physics and Chemistry of Layered Materials, vol. VI, Reidel, Dordrecht, 1979.
   K. Mizushima, P.C. Jones, P.J. Wiseman and J.B. Goodenough, Solid State Ion., 3-4 (1981) 171.
   C. Delmas, J. Braconnier, A. Maazaz and P. Hagenmuller, Rev. Chem. Miner., 19 (1982) 343.
   J. Molenda, Solid State Ion., 21 (1986) 263.
   S. Miyazaki, S. Kikkawa and M.Koizumi, Synth. Met., 6 (1983) 211.

2. J.P. Couput, G. Campet, J.M. Chabagno, M. Bourrel, D. Muller, R. Garrié, C. Delmas, B. Morel, J. Portier and J. Salardenne, Int. Appl. Publ. under PCT. Int. Pat. Class GO2F 1701, FO1 G9/00, C 23C 14/34, WO 91/01510, 1989.

3. N. Treuil, G. Campet, unpublished results : DEA report of N. Treuil. Bordeaux (1993).

4. G. Campet, S.D. Han, N. Treuil, MCR Shastry, J. Portier, C. Delmas, J.C. Lassègues, Mat. Sciences and Eng. B (submitted for publication).

5. B. Morel, Doctoral thesis, University of Bordeaux I (1991).

6. P. Barloux, J.M. Tarascon and F.K. Shokoohi, J. Solid State Chem. 94 (1991) 185.

7. N. Kumagai, S. Tanifuji, T. Fujiwara and K. Tanno, Electrochim. Acta, 37(6)(1992) 1039.

8. P.E. Lippens and M. Lanoo, Physical Review B, 39 (1989) 15.

II. 5. PHYSICAL AND (ELECTRO) CHEMICAL PROPERTIES OF THE INTER - CRYSTALLITE REGION IN METAL OXIDE POWDERS.

L'approche précédente (§II.4) donne une vision d'ensemble des mécanismes d'insertion electrochimique des ions Li^+ dans les NCIMs. Il convient maintenant d'approfondir le comportement électrochimique des NCIMs en précisant, notamment, l'influence non seulement de la taille des cristallites mais aussi de leur orientation. Cette étude (qui sera publiée ultérieurement) constitue l'objet du paragraphe suivant.

II.5.1. THE INTER-CRYSTALLITE (GRAIN BOUNDARY) REGION: AN ORIGINAL APPROACH.

II.5.1.1. General considerations.

Polycrystalline powders are formed with many crystallites, which grow rather independently from one another. Therefore their crystallographic axes have different orientations and account for a marked mismatching in the inter-crystallite (grain boundary) region.

Amorphous phases[1] may then occur in the inter-crystallite region which are in favor of efficient lithium (des) insertion (higher capacity and kinetic) [2-7].

On the other hand, the crystallites have different structural and physical properties. For example, fig.II.5.1 shows that (i) the spacing between the lattice planes, (ii) the surface packing density of the atoms in a lattice plane, (iii) the area per atom in a lattice plane, are different for the (001) and (110) lattice planes in the bcc and fcc structures [8]. Consequently nearly each crystallite has peculiar work function and Fermi energy (surface) which have an influence on its electrochemical behavior as shown below.

Let us first recall that the work function $e\Phi$ is fundamentally concerned with the crystal plane through the relation [9]:

$$e\Phi = (- e\varphi) - \mu \qquad (1)$$

where φ and μ are the electrostatic and chemical potentials respectively. Using polycrystalline tungsten as a non-limiting but illustrative example, we see that the work-function values related to different lattice planes, and reported in table II.5.1, are indeed significantly different. It is also established that $e\varphi$ depends upon variation of the Li doping concentration in the NiO material [11].

---

1. "Modèle nanocrystallin "de l'état amorphe de Chakraverty [1].

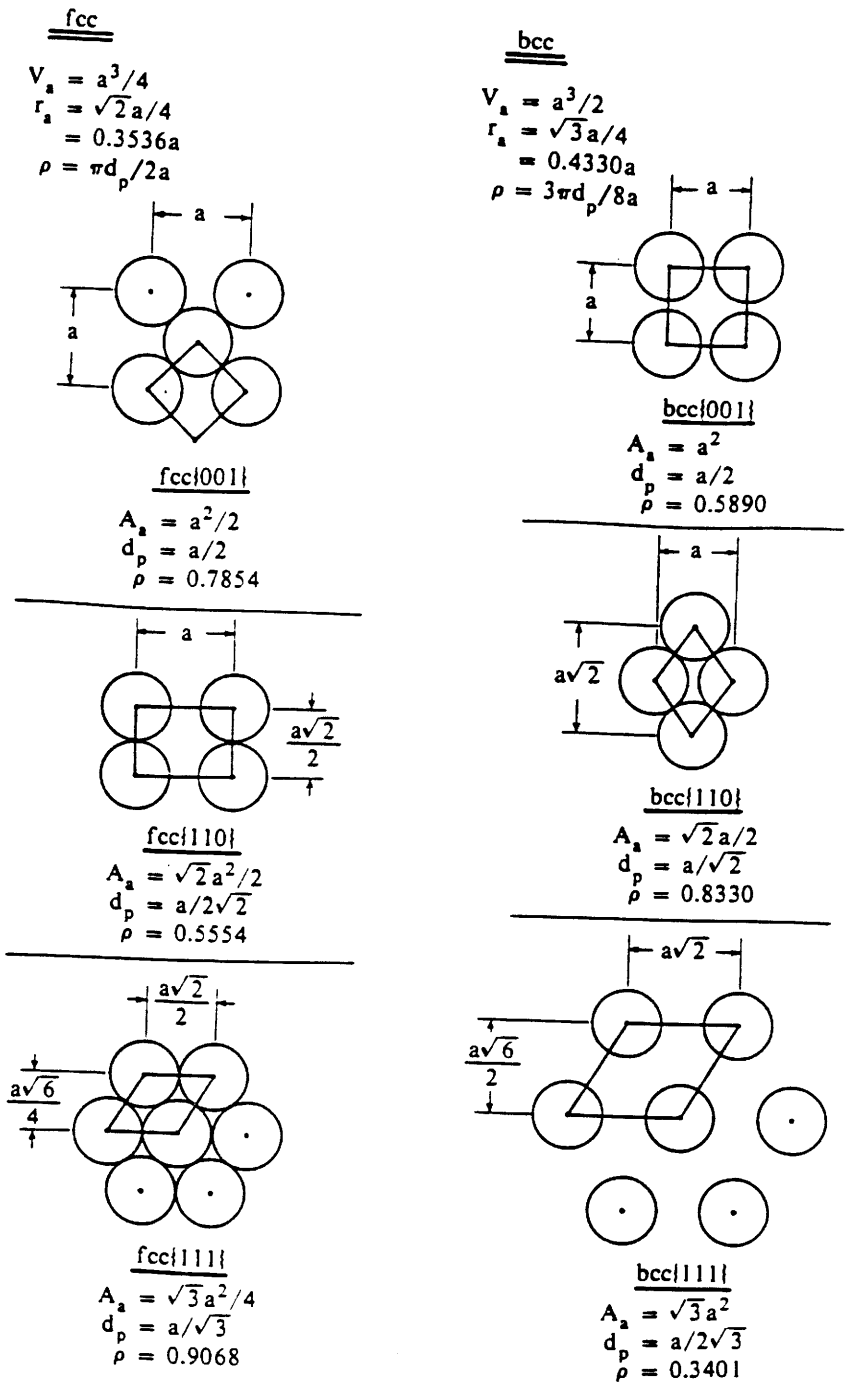

Fig. II. 5. 1 The geometry, to scale, of the common faces of the fcc and bcc structures. The maximum packing of hard spheres is assumed. a = the side of a cubic unit cell, r_a = the atomic radius, d_p = spacing between lattice planes, ρ = surface packing density of the atoms in a lattice plane, A_a = area per atom in a lattice plane[8].

Table II. 5. 1 The electron work function for each plane in the polycrystallite tungsten metal[10].

crystal planes	work function(eV)
(100)	4.63
(110)	4.25
(111)	4.47
(113)	4.18
(116)	4.30

II.5.1.2. The model accounting for lithium (des) insertion in the powdery electrodes.

The work function differences between the crystallites generate, in the inter-crystallite region, a potential barrier (V) and an accumulation layer (W). That is illustrated on the fig.II.5.2 showing the energy band diagram of the inter-crystallite region between two crystallites of tungsten metal having different lattice-plane orientations (110) and (100). The potential barrier depicted on the fig.II.5.2 can be expressed as:

$$\Delta V = e\,[\varphi(\,hkl\,) - \varphi(\,h'k'l'\,)]\,/\,2 \qquad (2)$$

Which is equal to 0.19 eV according to the values listed in table.II.5.1 [between (100) and (110) plane].

In fact the energy diagramm for oxide semiconductors represented in fig.II.5.2 can be described as follows: the crystallite face (hkl), which has the lowest work function will looses electrons in favor of the crystallite face (h'k'l') having the highest work function. This electron movement proceeds until the Fermi energies of the two inter-crystallite faces equalize. It results in a space charge region and an accumulation layer accounting, respectively, for an upward and downward shift of the energy levels near the interfaces (fig.II.5.2).

Consequently, even if no amorphous phase occurs in the inter-crystallite region (§II.5.1.1.), the interface region will have different physical properties than the bulk of the crystallites. In general, it would be also expected that ΔV (Δ eφ) is formed at their boundaries due to the difference of the impurity concentration , composition and phases (crystal, amorphous state)

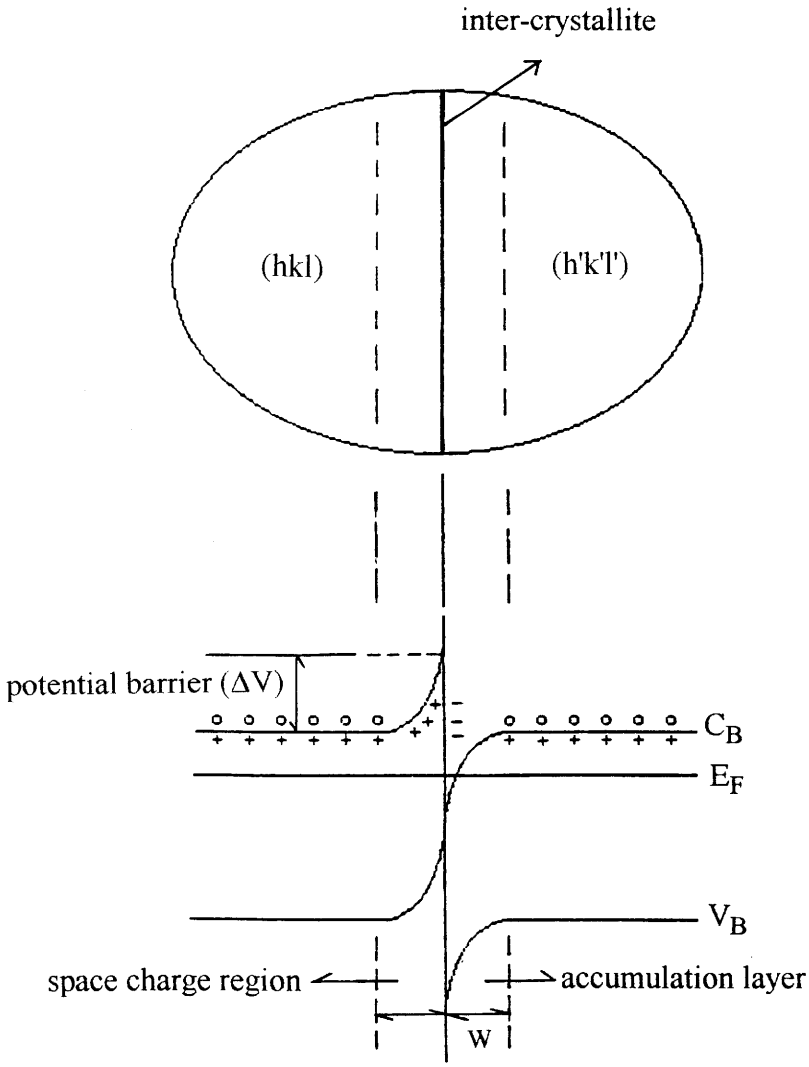

Fig. II. 5. 2. Energy band model of an interface (an intercrystallite) of a semiconductor particle.

in materials. In the accumulation region, the electron concentration is much higher than in the bulk. That should cause a lowering of the activation energy for carrier transport in the direction parallel ($\sigma_{//}$, $D_{//}$) to the inter-crystallite in favor of faster Li^+ electrochemical insertion (higher kinetic).

On the other hand when the carriers move in a perpendicular direction to the former one ($\sigma_{\perp}$, $D_{\perp}$), they have to overcome the potential barrier, V (fig.II.5.2). Nevertheless the height of the potential barrier can be modulated by the current applied during the Li^+ (des) insertion process.

We have, thus, shown that the inter-crystallite region should be more favourable for electrochemical (des) insertion of lithium ions than the bulk region due to:

(i) higher capacity (i.e. higher rate of lithium (des) inserted) as shown particularly in the § II. 2 and II. 4, and references therein.

(ii) faster (des) insertion process of lithium ions (i.e. higher kinetic), as shown here.

The amount, Q, of inserted Li^+ ions in the electrodes can be expressed, under certain conditions (see below), using the empiric formula

$$Q = A.W.N_d \qquad (3)$$

Where A.W. is the volume including, particularly, the accumulation layer (fig.II.5.2) or /and the above mentioned amorphous phase (§II.5.1.1) in the inter-crystallite region. N_d designates a carrier concentration close to that occuring in the accumulation region.

In fact, the reaction (3) would be:

(i) fully valid when the inside crystallite structure does not allow lithium intercalation.

(ii) partially valid when the inside crystallite structure is adapted for lithium intercalation; under such a circumstance reaction (3) applies for the lowest Q values (§II. 4).

Q is proportional to the parameter x which intervenes in the following expression.

$$xLi^+ + xe^- + MO_y \rightleftharpoons Li_xMO_y \qquad (4)$$

II.5. 2. CRYSTAL SIZE EFFECTS FOR LITHIUM INSERTION PROCESS IN THE Li_XSnO_2, Li_XWO_3 AND Li_XTiO_2 ELECTRODES.

II.5. 2. 1. Study of Li_XSnO_2 electrodes.

The fig.II.5.3. shows the lithium-insertion curves, V = f (x), for two powdery Li_XSnO_2 electrodes having different sizes of crystallites: 75Å (as it occurs for NCIM), and 506Å.

The higher insertion voltage observed for the NCIM electrode, i.e. having the smaller crystallites, can easily be justified based on the above reported argumentations (§II.2, §II.4 §II.5.1.2.). Moreover, for both samples the potential, V = f (x), smoothly decreases with x (fig.II.5.3); it illustrates regular Fermi-energy changes of the electrodes undergoing no significant structural changes. Indeed only a textural change, namely a reduction of the size of the crystallites is observed, accounting for a significant broadening of the x-ray diffraction peaks (fig.II.5.4). On the other hand, the d-spacing between the lattice planes tend to diminish as x increases (table II.5.2). It would imply that the crystallites undergo an uniform compressive stress which causes a contraction of the unit cell.

II.5.2.2. Study of Li_XWO_3 electrodes

The voltage curves reported in the fig.II.5.5 for Li_XWO_3 electrodes, having different crystallite-sizes, notably differ from those related to Li_XSnO_2 (fig.II.5.3).

However, as it occured for SnO_2, the highest voltages are observed for the NCIM (59Å crystal size). Moreover, for this sample uniquely, the potential monotonously diminishes with x (fig.II.5.5). The potential evolution, V(x), observed for the other electrodes account, in fact, for the successive phase transitions occuring during the electrochemical process, namely from monoclinic ($x \leq 0.02$) to tetragonal ($x \leq 0.15$), then finally cubic. Such results were previously reported by other authors [12,13]. The abrupt potential decease, as seen in fig. II 5.5, and the successive phase transitions are indicative of the variation of the Fermi energy in the crystallite.

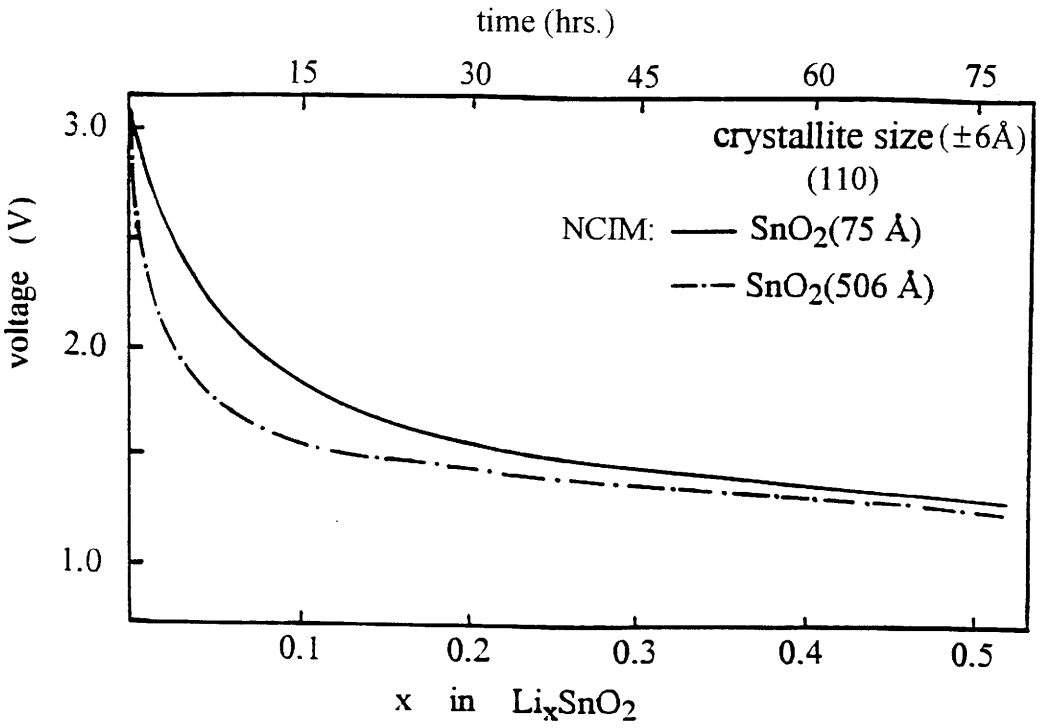

Fig. II. 5. 3 Discharge curves for Li / $LiCF_3SO_3$ / Li_xSnO_2 cells using SnO_2-NCIM (75Å) and SnO_2 electrode having larger crystallites (506Å).
I = 50μA/cm², weight of SnO_2 = 42mg and weight of carbon black = 8mg.

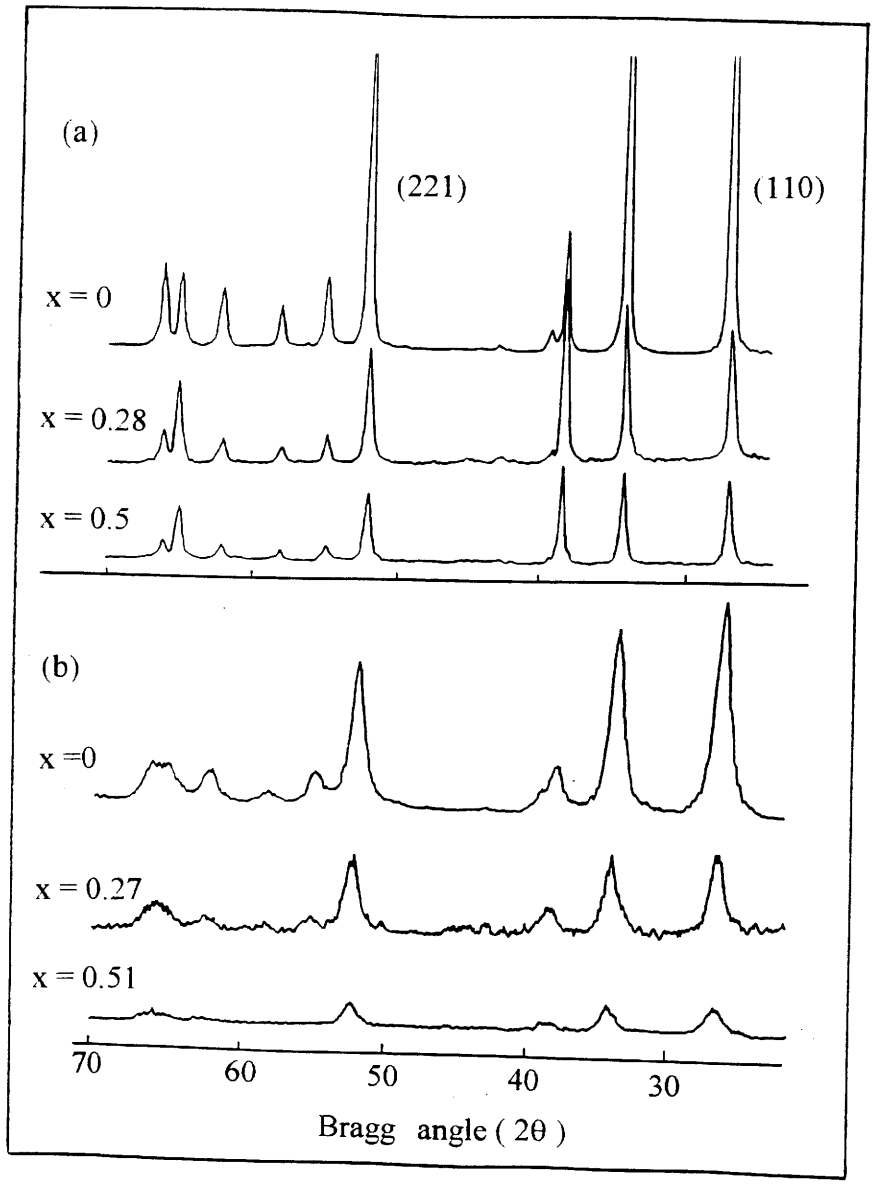

Fig. II. 5. 4 X-ray diffractograms of the Li_xSnO_2 powders. (a) : SnO_2 with larger crystal size [506Å for (110) plane]. (b) : SnO_2 with smaller crystal size [75Å for (110) plane].

Table II. 5. 2 The d-spacing decrease of the main crystalline peaks for Li_xSnO_2.

hkl	I/I_1	d(Å)				
		x=0	x=0.05	x=0.17	x=0.28	x=0.5
110	100	3.3453	3.3693	3.3650	3.3451	3.3329
101	80	2.6407	2.6559	2.6539	2.6412	2.6336
211	65	1.7641	1.7698	1.7693	1.7641	1.7624
220	18	1.6756	1.6810	1.6807	1.6758	1.6722
002	8	1.5930	1.5980	1.5960	1.5918	1.5912
310	14	1.4988	1.5025	1.5035	1.4990	1.4972
112	18	1.4387	1.4402	1.4382	1.4372	1.4363
301	16	1.4158	1.4184	1.4186	1.4162	1.4156

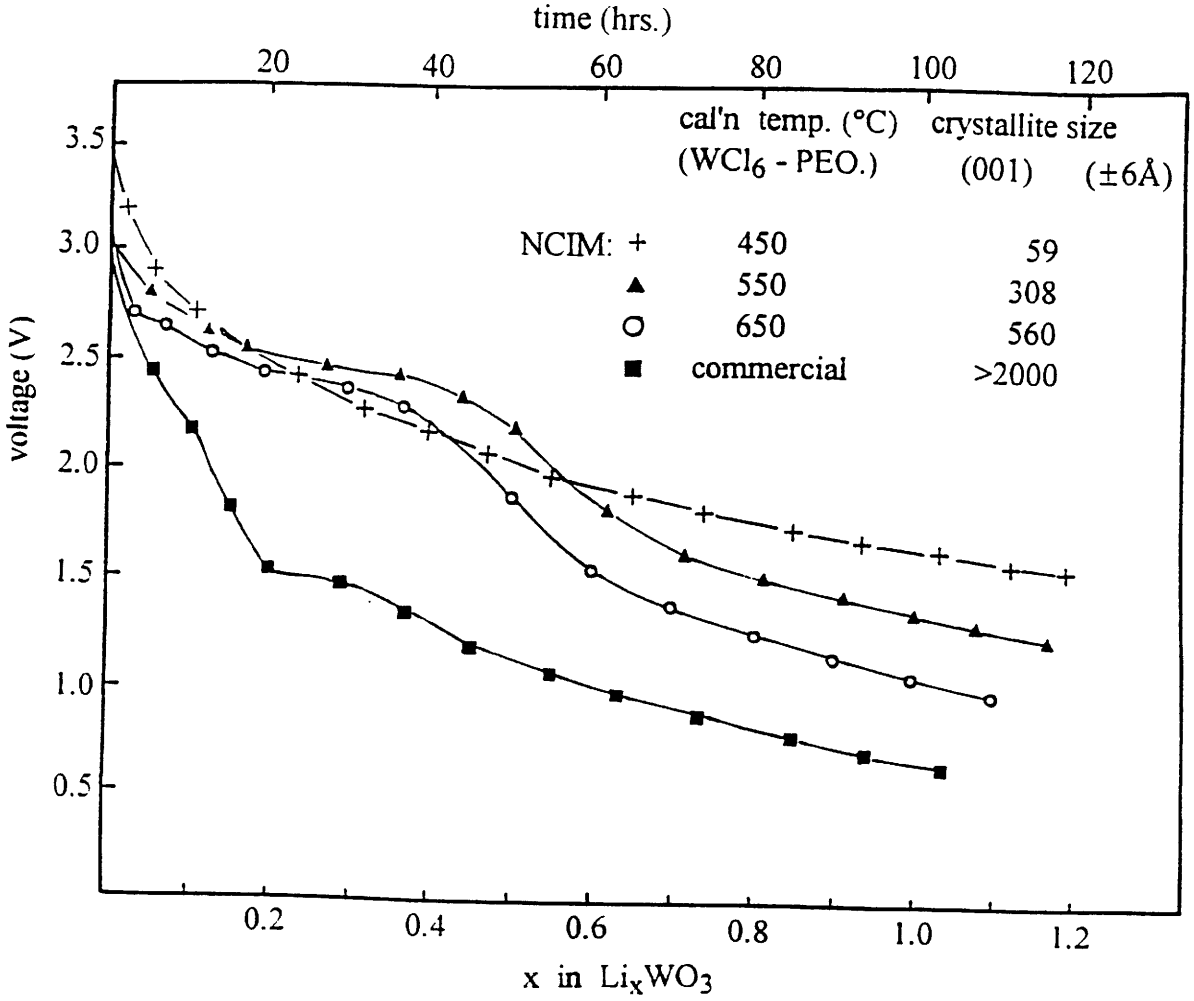

Fig. II. 5. 5 Discharge curves for Li / $LiCF_3SO_3$ / Li_xWO_3 cells using the various WO_3 powders having different crystallite size.

I = 50μA/cm², weight of WO_3 = 42mg and weight of carbon block = 8mg.

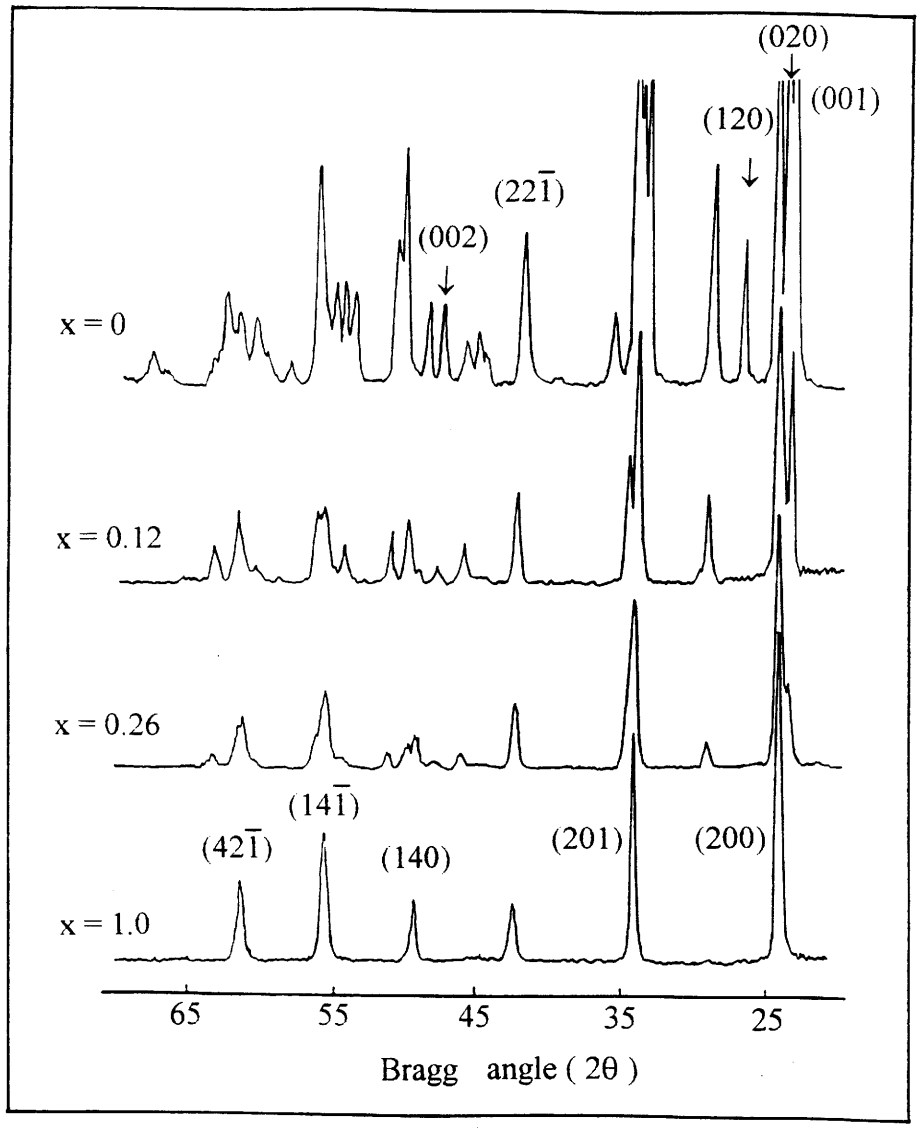

Fig. II. 5. 6 X-ray diffractogram of Li_XWO_3 electrodes prepared at 650°C [560Å crystal size for (001) plane].

The fig.II.5.6 shows the XRD of Li_XWO_3 electrodes, prepared at 650°C (560Å crystal size) , for different x values. Although some peak positions remain practically unchanged, other peaks are progressively shifted or disappear due to the above reported structural changes. It would imply that the crystallites undergo a non uniform compressive stress during the lithium insertion. Considering the tiny variation of the peak related to the (221) lattice plane, for instance, it can be reasonably assumed that Li^+ ions hardly diffuse into it. That is not the case for the peak related to the (020) lattice plane, into which the Li^+ ions should easily diffuse.

We will follow now our above reported considerations (§ II.5.1.1.) according to which the energy state and structure of each lattice plane deeply affect the electrochemical insertion process. We can, thereby, reasonally assert that: (i) the (221) lattice plane has a too low work function inhibiting efficient lithium insertion, (ii) the (200) one has a much larger work function in favour of lithium intercalation. To our knowledge these work functions are not known yet.

II. 5. 2. 3. Study of Li_XTiO_2 electrodes.

The lithium insertion curves [V = f(x)] are reported on figure II.5.7 for three powdery electrodes having the anatase structure. Here again the highest voltages occurs for the NCIMs due to their higher capacity for lithium insertion and the easier diffusion of lithium ions in the inter-crystallite region. The abrupt variation of the curves, within $0.3< x <0.6$ account for structural changes (fig. II.5.8) causing strong Fermi energy (and thereby potential) variation.

The XRD, shown in figure II.5.8, clearly show that the (103), (004) and (112) peaks planes are shifted and broadened upon Li-insertion, while the (101), (105), (211), (213) and (116) peak planes are split. The peak-splittings account for a change of the tetragonal (anatase) symmetry of TiO_2 to orthorhombic [14]. Consequently a shortening of Ti-Ti distances occurs, causing stronger Ti-Ti bond formation enhancing the electrical conductivity [15].

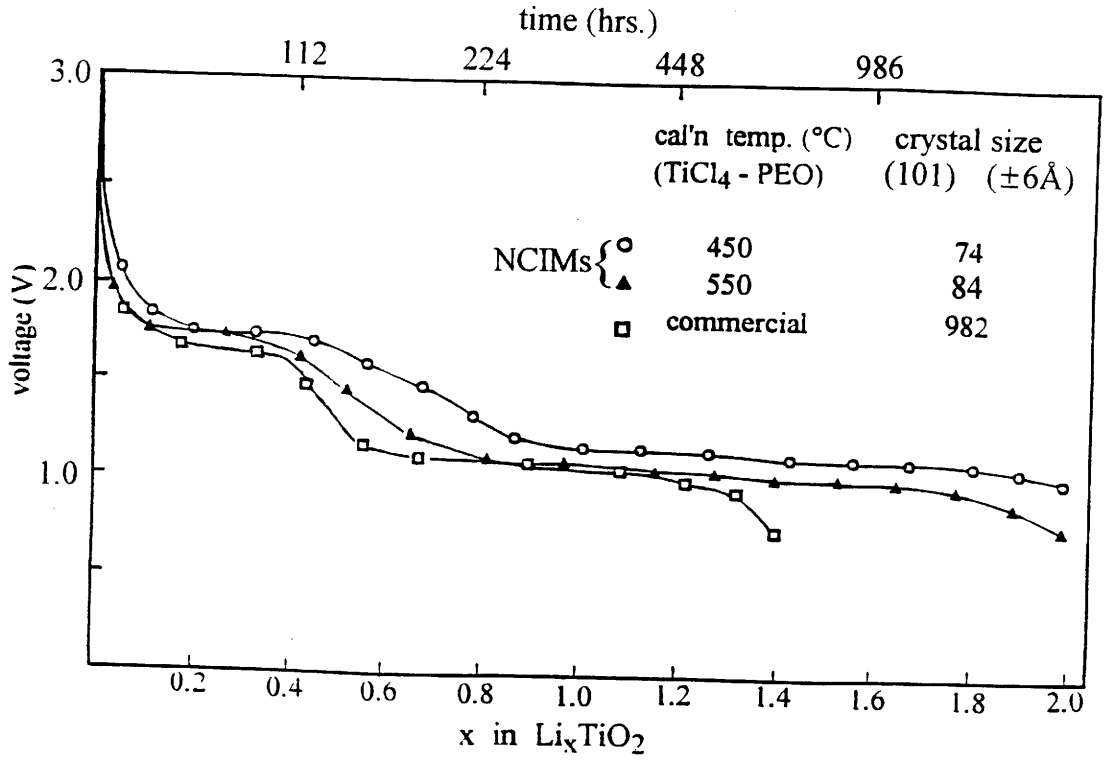

Fig. II. 5. 7 Discharge curves for Li / $LiCF_3SO_3$ / Li_xTiO_2 cells using TiO_2-NCIMs (74Å and 84Å crystal size) and commercial powder (982 Å). (The electrolyte may be decomposed from the near 1.2 V.)

Remarque: *Cette figure complète en fait la précédente (fig. II. 1.9, p24). Les échantillons de TiO_2 étudiés sont, ici, plus cristallisés (c' est à dire que la talle moyenne des cristallites est plus élevée). Corrélativement, le taux de lithium que l'on peut insérer réversiblement est plus faible que dans le cas précédent, ce qui est en accord avec le modèle poposé (p64 - 74).*

Alors que le taux de lithium inséré, réversiblement, pour l'échantillon le moins cristallisé (fig. II.1.9, p.24) correspondait à x = 0.95, il correspond ici à:

-x = 0.8 pour TiO_2-NCIMs (74 et 84Å)

-x = 0.6 pour TiO_2 commercial.

La valeur, x =0.6, trouvée pour TiO_2 commercial est en accord avec celle reportée dans la littérature [16].

Au delà de x ~ 0.6 (TiO_2 commercial) ou x = 0.8 (TiO_2-NCIM) on continuerait à insérer le lithium bien que l'on soit dans la zone "critique" de décomposition de l'électrolyte. En effet, une modification des diagrammes de diffraction X est observée (fig. II. 5.9, p87). Mais cette insertion est irréversible. Les résultats correspodants seront reportés dans la thése de D. Camino.

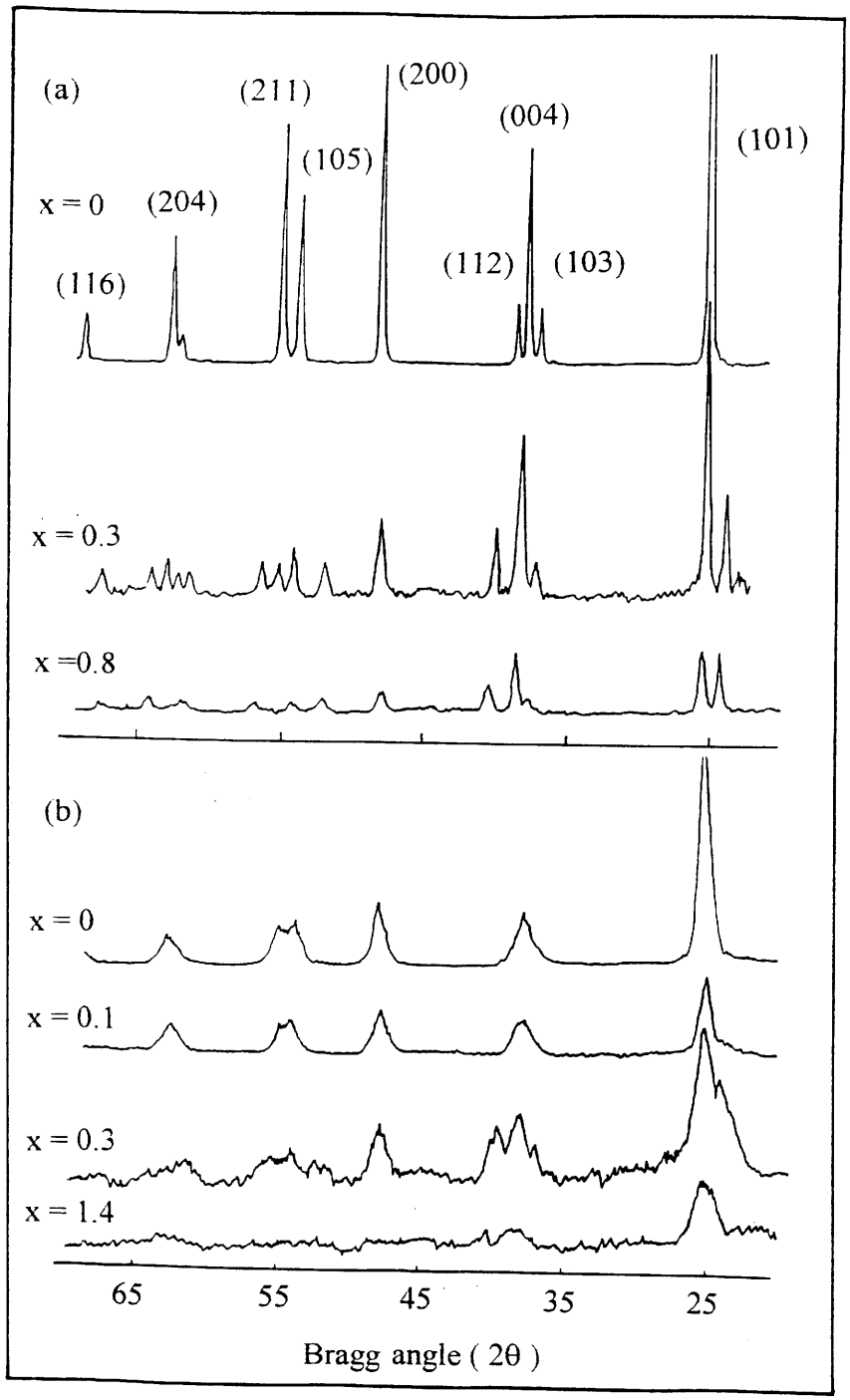

Fig. II. 5. 8 X-ray diffractograms of the Li_xTiO_2 powders. (a) : TiO_2 with larger crystal size [982Å for (101) plane]. (b) : TiO_2 with smaller crystal size [74Å for (101) plane].

II. 5. 3. CONCLUSIONS

An original approach has been proposed to describe the energy band state of the inter-crystallite region, together with a model accounting for the lithium insertion (desinsertion) in the powdery Li_XMO_y materials.

REFERENCES

1. B.K. Chakraverty, Congrès Interational sur les couches minces, Cannes suppl. de la revue le vide. 147 (1970) 427.
2. J -P. Couput, G. Campet, M. Chabagno, D. Bourrel. R. Muller, C. Garrié, C. Delmas, B. Morel, J. Portier and J. Salardenne, Int. Appl. Publ. under PCT. Int. Pat. Class, GO2F 1701, FO1 G9/00, C 23C 14/34, WO 91/0151, 1989.
3. G. Campet and J. Portier, S. J. Wen, J. of Active and Passive Electron Comp., 14 (4) (1992) 225.
4. G. Campet and J. Portier, ibid., 14 (4) (1992) 219.
5. G. Campet, B. Morel, M,Bourrel, J. M. Chabagno, D. Ferry, R. Gorié, C. Quet, C. Geoffroy, J. Videau, J. Portier, C. Delmas and J. Salardenne, Mater. Sci. Eng., B8 (1989) 303.
6. B. Morel, Doctoral Thesis, University of Bordeaux I, 1991.
7. Barloux, J. M. Tarascon and Shokoohi, J. Solid State Chem., 94 (1991)185.
8. G. Burn, Solid State Physics, Academic Press, (1985) 672.
9. C. Herring and M. Nichols, Revs. Modern Phys. 21 (1949) 185
10. CRC. Handbook of Chemistry and Physics (1988-1989)
11. J. Deren and Ziolkowski, Bull. Acad. Polon. Sci. Sér. Sci. Chim. 14 (1966) 443.
12. K. H. Cheng and M. S. Whittingham, Solid Sate Ionics, 1 (1980) 151.
13. Q. Zhong, J. R. Dahn and K. Colbow, J. Electrochem. Soc. 139 (1992) 2407
14. R. J. Cava, D. W. Maurphy, S. M. Zahurak, A. Santoro and R. S. Roth, J. Solid State Chem. 53 (1984)1176.
15. B. Z. Christiansen, k. West, T. Jacobsen and S. Atlung, Solid State Ionics, 28-30 (1988) 1167.
16. Tstomu, Ohzuku, et al., J of Power Source, 14 (1985) 1952.

Chapitre III

Etude des" électrodes nanocomposites" : $(POE)_8$ - SnO_2 (WO_3, TiO_2) - C

Nous désignons par le terme d' << électrode nanocomposite >>, telle que $(PEO)_8$ - SnO_2 - C ou ($PEO)_8$ - WO_3 - C ou finalement $(PEO)_8$ - TiO_2 - C, un mélange intéractif de trois phases. L' une d'entre-elles, telle que SnO_2 ou WO_3 ou TiO_2, est à base NCIM, c'est à dire est constituée de nanocristallites capables d'insérer réversiblement les ions Li^+ (c.f. chapitres I et II).

Il s'agissait d'étendre, ici, les concepts développés dans le chapitre précédent à des matériaux d'électrode hybrides, de caractère organique inorganique. Nous souhaitions en tout premier lieu que l'étude abordée dans ce chapitre permette ultérieurement l'essor d'une nouvelle classe de matériaux riches d'intérêt sur le plan fondamental. Notre objectif revêt également l'aspect appliqué de la recherche; il consiste en l'élaboration d'électrodes (cathodes et anodes) à armature polymère pour des générateurs électrochimiques <<souples>>, peu encombrants et non poluants, de type <<rocking-chair>> (c.f.chap.I).

L' étude décrite ici est destinée à être publiée ultérieurement. C'est dans cette optique qu'elle est, d'ores et déjà, présentée en anglais.

III.1 ELECTROCHEMICAL PROPERTIES OF ORGANO-METAL (OXIDE) COMPOSITE MATERIALS.

III.1.1 Introduction.

There are various classes of organo-mineral materials.

One class refers as solid-polymer electrolytes; they are ionically conducting phases formed by dissolving salts in polar polymers and might advantageously take the place of some conventional liquid electrolytes commonly used in batteries, for example [1]. Electrochemical cells based on liquid electrolytes are indeed likely to present practical problems associated with the escape of corrosive, flammable or toxic liquids. Furthermore, it is not generally possible to miniaturise such cells nor to produce special configurations such as thin film structures.

Another class of such materials, symbolized as <<organo-mineral composites>>, involves an interacting mixture of an organic compound with (i) metal-oxide powders, or/and (ii) metal-powders. They can be used as active electrodes intended for soft and no lumbering solid-state devices such as film-based supercapacitors, rechargeable batteries...[2, 3].

In fact the two classes of materials, above mentioned, have to fulfil critical conditions:

(i) adequate ionic conductivity associated with negligeable (or high) electronic conductivity as far as electrolytes (or electrodes) are concerned.

(ii) ability to form good interfacial contacts with the adjacent phases.

(iii) good mechanical properties (such as not being brittle as it occurs for certain ceramics, but being able to <<elastically relax>> when they are submitted to the stress arising from the volume change in the adjacent phase for example).

(iv) ease of processing and manufacturing as it occurs for some large-scale manufactured polymers using continuous production .

Up to now, by far the biggest efforts have focussed into the development of H^+ or Li^+ conducting polymer electrolytes for supercapacitor or battery applications, respectively. Due to the negligible electronic conductivity and ease of manufacturing of some of these

materials, such as Li^+ conducting PEO (polyethylene oxide), the cell design can involve thin electrolyte film of large surface area [4]. The solid-state lithium batteries, which are close to commercialisation and are manufactured with such a polymer, use a lithium anode[1] (negative electrode) and an << organo-mineral composite >> cathode. The later involves an interacting mixture of a lithium-conducting polymer electrolyte (such as lithium conducting PEO) with carbon-black and an intercalation compound such as V_6O_{13} [4, 5].

We will focuss here on such type of << organo-mineral composite >> electrodes. However the later will use, apparently for the first time, the NCIMs: SnO_2 or WO_3 , as insertion compounds[2] , instead of the intercalation compounds V_6O_{13} or TiS_2. The advantages of these materials, being then in nano-crystallite form, have been quoted in chapters I and II.

III. 1. 2. EXPERIMENTAL.

III. 1. 2. 1. Sample manufacturing.

The NCIMs (SnO_2 , WO_3 , TiO_2), prepared as indicated in chapter II, were intimately mixed with carbon black and PEO (molecular weight : 5 x 10^6, Aldrich), in the proportions[3] (wt. %) : MO_y (39%) + PEO (37%) + C (8%) corresponding to the standard ratio O/M = 8.

---

1. Voir les remarques formuleés au chapitre I (§I - 1).

2. Les électrodes hybrides à base de TiO_2- NCIM sont actuellement étudieés par N. Treuil et D. Camino. Les résultats correspondants, qui s'apparentent à ceux observés avec les autres NCIMs, SnO_2 et WO_3, seront reportés dans leur thèse.

3. PEO. is << permeable >> to the electrolyte (lithium conducting-propylene carbonate) choosen here for electrochemical experiments . Therefore there is no need of adding lithium salts as a fourth component . In fact POE acts as a mechanical support.

The resulting powder was added to acetonitrile (CH_3CN being a solvent for PEO). The solution was energetically stirred until an homogeneous gel was formed. The gel state sample was cast on carbon textile[4](16 wt. %) and allowed to dry at room temperature in order to get a flexible film (0.1 ~ 0.5 mm thick and 13 mm diameter). The films were further heated in dry air at about 60°C for 24 hrs, in order to remove the last traces of solvent and finally stored in the inert argon atmosphere of a glove box.

III. 1. 2. 2. Electrochemistry.

Electrochemical (des)insertion of lithium were realized in bottle type cells having two electrodes. The composite films was used as cathode, and the lithium metal was used as both reference and anode. The electrolyte was a 1M. Li CF_3SO_3 - propylene carbonate (PC, which was previously dried by fractional distillation under vacuum using molecular sieves) solution coated onto glass filter papers. Electrochemical experiments have been carried out in glove box. The XRD pattern were obtained with a Phillips PW 1050 spectrometer using CuKα radiation.

III. 1. 3. ELECTROCHEMICAL PROPERTIES OF THE COMPOSITE ELECTRODES.

The framework of the flexible electrodes is depicted in fig. III. 1. The carbon textile contributes as the main conduction path for electrons in the insulated PEO[5], and carbon black[5] serves as electronic connection between the carbon textile and the metal-oxide particles.

---

4. *KYNOL ^{TM} activated carbon fibres, thickness 0.5mm, specific surface area 2000m^2/g.*

5. *The pure POE sample exhibits a room-temperature (ionic) conductivity of about 5 x 10^{-8} Ω^{-1} cm^{-1} and undergoes a glass transition at Tg = - 65°C [6, 7].*

6. *Carbon black possesses: (i) a surface area (measured using the BET technique) of 1250 m^2/g, (ii) a resistivity of 10^{-3} Ω^{-1} cm^{-1}, (iii) an average grain size of 300Å [8].*

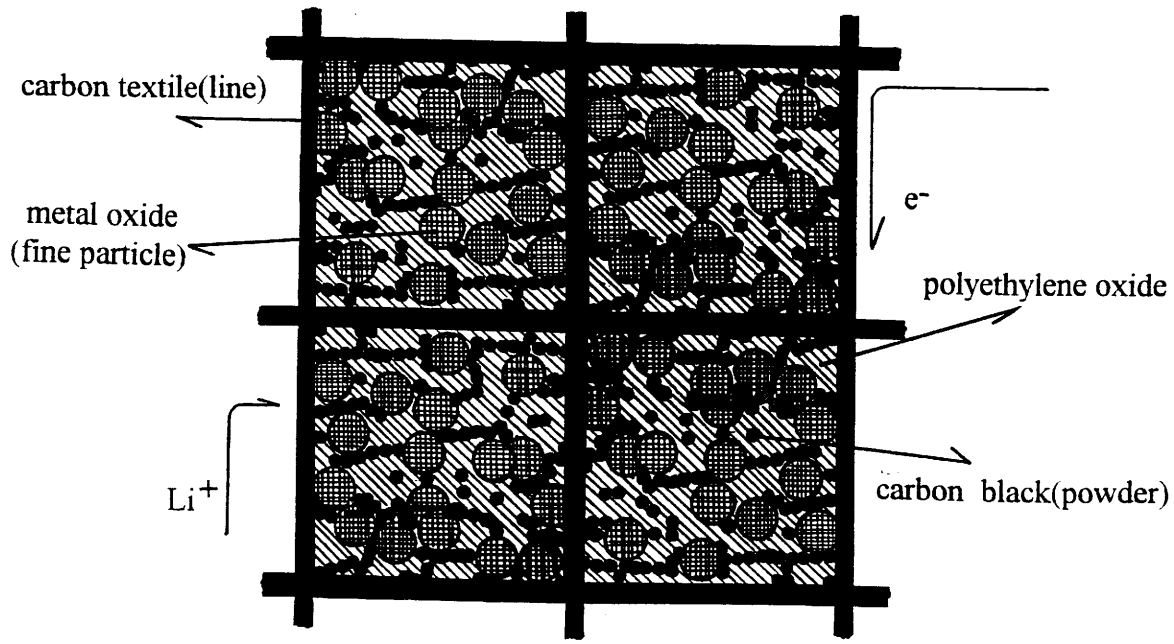

Fig. III.1 Structure of metal oxide - polymer (PEO) - carbon conductor (textile + powder) composite electrode.

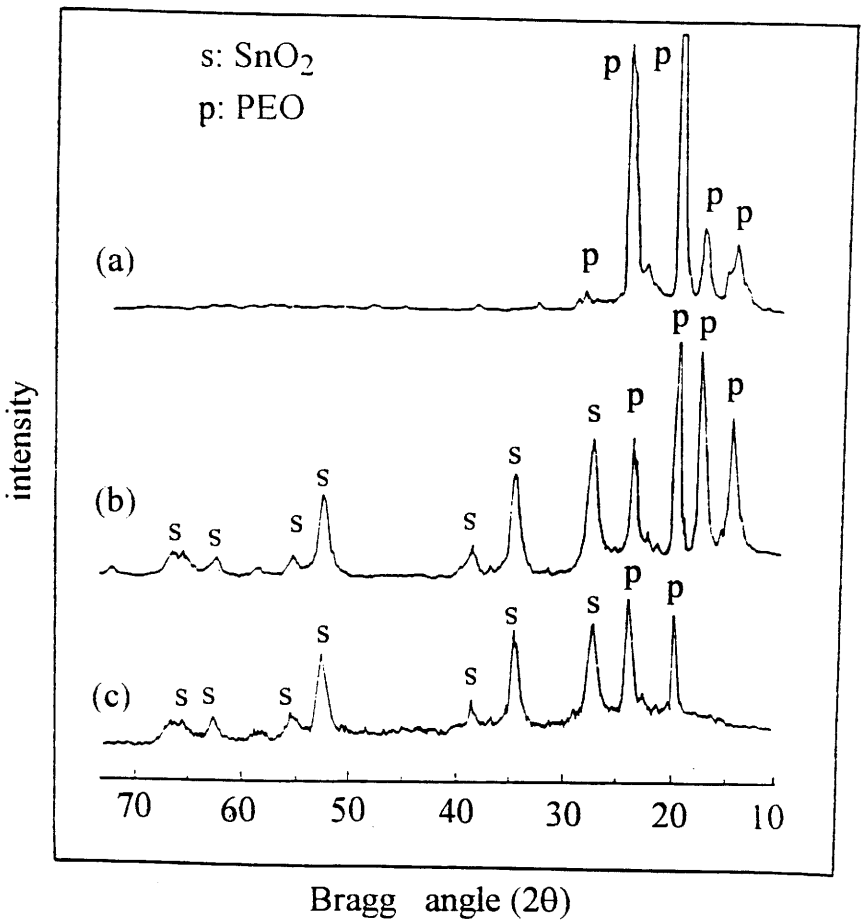

Fig. III. 2 XRD pattern of composite electrodes:

(a) : PEO heated in dry air at 60°C for 4 hrs.

(b) :composite electrode (PEO+SnO_2+C) after treatment in dry air 60°C for 4hrs.

(c) : same composite electrode as in (b), but after lithium insertion ($Li_{0.4}$ PEO+ SnO_2 + C).

The crystallinity of POE sharply diminishes (i.e. the helix-reapeat distance is reduced) when the composite electrode, which is permeable to the contacting electrolyte, has undergone lithium insertion (fig.III.2. a, b, c). This change in crystallinity, together with the electrolyte impregnation, causes a high Li^+ conductivity of the electrode; moreover the size of the metal oxide particles should also be lowered due to the manufacturing process used for the composite electrode. Consequently efficient lithium (des)insertion must occur for such an electrode (§II.2). This favourable situation is depicted in fig.III.3 and III.4 showing the third desinsertion-insertion curves for:

PEO + C, PEO + SnO_2-NCIM + C, SnO_2-NCIM + C electrodes

and for

PEO + WO_3-NCIM + C, WO_3-NCIM + C electrodes.

The higher rate of lithium, which is reversibly inserted, indeed occurs for the PEO-metal oxide electrodes: PEO + SnO_2-NCIM + C or PEO + WO_3-NCIM + C .

Let us quote that the two first cycles, which are not reported here for sake of simplicity, are not reversible and the charge exchanged is lower than that measured during the reproducible following cycles. The lack of reversibility observed during the two first cycles is the consequence of the volume change of the electrodes as they are progressively impregnated with the electrolyte.

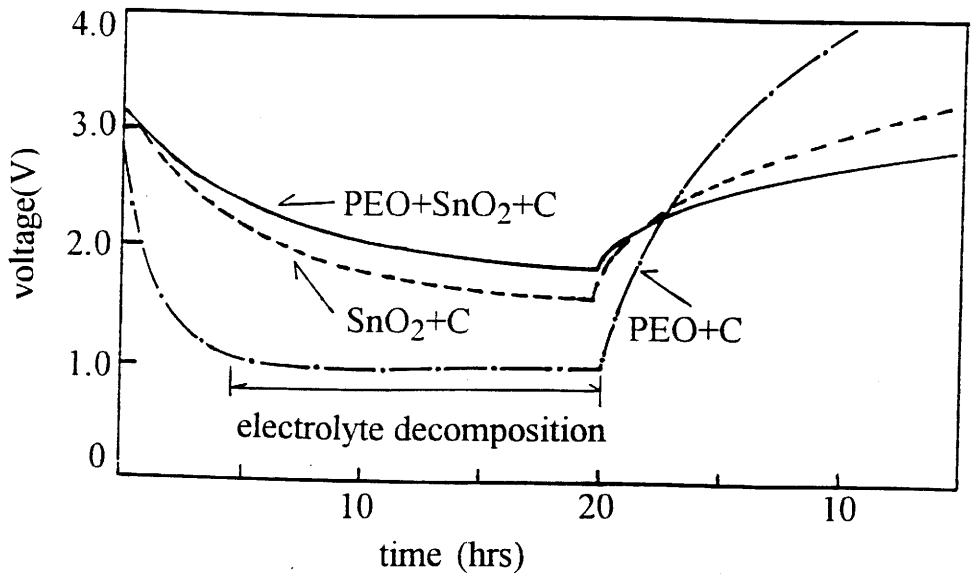

Fig. III. 3 Third Li - insertion and desinsertion curves for composite electrodes using SnO_2-NCIM (~50Å), as shown in curves - - - - and ——. For comparison the curve related to the composite electrode having no SnO_2 (curve — · —) is also reported. The sample was individually mixed as the amount of 39mg (PEO), 37mg (SnO_2) and (or) 24mg (C). I = 50μA/cm².

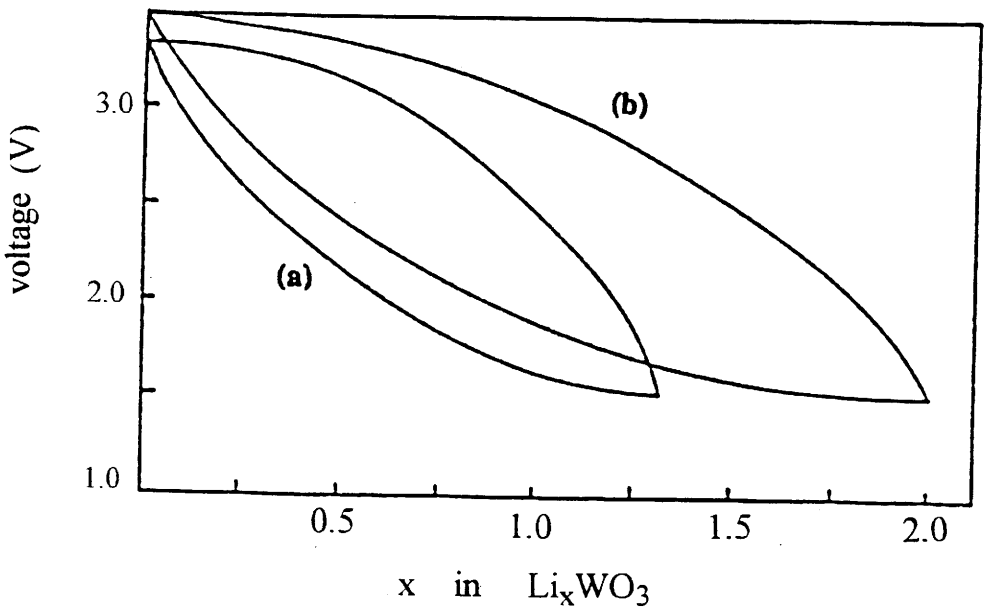

Fig. III.4 Third discharge - charge curves for ; (a) : Li / CF_3SO_3-PC / WO_3 (59Å) + C cell, (b) : Li / $LiCF_3SO_3$ - PC / PEO + WO_3 (59Å) + C cell . The sample was individually mixed as amount of 36mg (PEO), 35mg (WO_3) and 21mg (C). I = 50μA/cm².

REFERENCES

1. C. A. Vincent, Chemistry and Industry, 17 August (1992) 602.
2. M. A. Ratner and D. F. Shriver, MRS. Bulletin, Sept. (1989) 39.
3. T. Kanbara, M. Inami and T. Yamamoto, J. of Power Sources, 36 (1991) 87.
4. F. Capuano, F. Croce and Scrosati, ibid, 37 (1992) 369.
5. D. F. Shriver and G. F. Farrington, Chem. and Eng. News, 6 (1985) 42.
6. R. G. Linford (Editor), "Electrchem. Sci. and Tech. of Polymers", Elsevier Co., NY, 1987.
7. F. L. Tanzella, W. Bailey, D. Frydrych, G. C. Farrington and H. S. Story, Solid State Ionics, 5 (1981) 681.
8. F. Carmona, Ann. Chim. Fr. 13 (1988) 395.

III. 2. TiO_2 - POLYMER NANO-COMPOSITES BY SOL-GEL.

(publication)

REMARQUE:

Les propriétés électrochimiques des électrodes composites ont été présentées en premier lieu dans le paragraphe précédent, par souci de clarté. Toutefois cette étude a été menée en parallèle avec une investigation plus complète des matériaux, et toujours poursuivie à l'heure actuelle. La publication, présentée dans le paragraphe suivant illustre notre démarche générale en prenant TiO_2 comme exemple.

TiO_2-POLYMER NANO-COMPOSITES BY SOL-GEL

A. C. Pierre[1], G. Campet[2], S.D. Han[2], E. Duguet [2] and J. Portier[2]

(1) Department of Mining, Metallurgical and Petroleum Engineering, The University of Alberta Edmonton, Alberta, T6G-2G6, Canada.

(2) Laboratoire de Chimie du Solide, Université de Bordeaux I, 351 cours de la libération, 33405, Talence, France.

ABSTRACT

Sol-gel processes make it possible to develop new hybrid electrolyte materials of the type ceramic-polymer, known as Nano-Crystallite-Insertion-Material (NCIM). They can be used in reversible alkali electrochemical cells after insertion with cations such as Li^+. In the present study, TiO_2 - polyethylene oxide hybrid materials were synthesized, from $TiCl_4$ and from Ti ethoxide. Their structure is analyzed in relation with the processing parameters. A primary evaluation of the nanoscale composite materials for reversible Li insertion was done.

1. Introduction

Recently, the investigation of new organic-mineral hybrid copolymers was undertaken for possible applications as batteries electrodes and electrochrome devices. For instance complexes such as $(PEO)_8SnCl_4$ or $(PEO)_8SnCl_4,4H_2O$, where (PEO) stands for polyethylene oxide, were prepared [1]. Other hybrid materials made from the same chemical components include nanocomposites comprised of fine SnO_2 grains made by sol-gel, embedded in a PEO matrix [2]. More recently the development of TiO_2 nanoscale insertion composites materials were proposed[3]. These nanoscale grains provide many broken bonds in surface where reversible alkali adsorption could be achieved.

In the present study, we focused on the fabrication of such hybrid materials with TiO_2 nanoscale

phase, by controlled hydrolysis of mixed solutions of metal and polymer precursors. The polymer chemical precursor was PEO, while 2 ceramic precursors were investigated: $TiCl_4$ and the ethoxide $Ti(OC_2H_5)_4$. The fabrication and structure of these materials is presented.

2. Experimental

The chemical products used in this investigation were from Aldrich. The PEO, in which EO stands for $-CH_2CH_2O-$ and P for "poly", had an average molar mass of 100,000. The $Ti(OC_2H_5)_4$ was a 20% solution of technical grade ethoxide in ethanol. The $TiCl_4$ was 99.9% pure. It was a liquid with the aspect of water kept under nitrogen in a sure-seal bottle. This product reacts very violently with any trace of water and produces a HCl gas. It was always transferred under nitrogen with needles, in the present study.

Some polymer reference samples were only made by hydrolysis of PEO without any TiO_2. Similarly, some TiO_2 reference samples were only made by hydrolysis of each Ti precursor. Then, a range of $(PEO)_nTiO_2$ hybrid materials with n = 4 to 16 were synthesized with each Ti precursor. Two different dry solvents were used: acetonitrile and pentanol. The effects of slow hydrolysis by air humidity and fast hydrolysis in excess water were compared. The structure of synthesized hybrids were analyzed up to 600°C by powder X-ray diffraction, and scanning electron microscopy (SEM). Preliminary Li insertion was carried out on one material.

3. Results

The reference TiO_2 samples made at 20°C from $TiCl_4$ or from $Ti(OC_2H_5)_4$ by hydrolysis with an excess of water or by the air humidity were all amorphous (Fig.1a). They crystallized to anatase form at 180°C (Fig. 2d). As for PEO, it showed the crystalline X-ray diffraction data in Fig.1e, both for the initial powder or when drying to a strong polymer film. The hybrid $(PEO)_nTiCl_4$ materials made were the same in dry pentanol or in dry acetonitrile, for a given set of precursor

content and hydrolysis conditions. When hydrolyzed by air humidity, they were X-ray amorphous for n = 4 (Fig.1b). For n = 8, the X-ray structure was a mixture of amorphous TiO_2 and crystalline PEO (Fig.1c). For n = 16, the amorphous spectrum of TiO_2 was no longer observed (Fig.1d). However, while the hydrolysis of mixed $(PEO)_8TiCl_4$ solutions by air humidity led to a crystalline PEO phase (Fig.1c and Fig.2a), hydrolysis of the same solutions by excess water led to completely X-ray amorphous hybrid materials (Fig.2b).

SEM observations of all samples hydrolyzed by air humidity actually showed the presence of 2 phases, even in the X-ray amorphous $(PEO)_4TiCl_4$ material. Each phase was separated in macroscopic domains several 100 μm in extent. One phase had the aspect of PEO while the second phase was a very viscous brown gel which did not dry at 20°C. The viscous gel could be dried with difficulty under vacuum at 65°C and it gave gel fibers with a high TiO_2 content and some residual chlorine, according to qualitative EDX analysis. For n = 4, both phases were rather featureless, while for n = 16 the extensive planar agglomeration of PEO crystallites formed during drying could be observed. The aspects of both phases for n =8 can be seen in Fig.3a.

The only homogeneous samples according to SEM observations (Fig.3b) and with an amorphous X-ray diagram (Fig.2b), were made by hydrolysis in excess water of mixed $(PEO)_8TiCl_4$ solutions.

By comparison with $TiCl_4$, all $(PEO)_nTi$ materials made from mixed PEO and $Ti(OC_2H_5)_4$ solutions, and hydrolyzed by air humidity or by excess water, showed the X-ray pattern of crystalline PEO as in Fig.1c or Fig.1d. In all samples hydrolyzed by air humidity, the 2 phases were easily distinguished under the SEM. A thin layer of TiO_2 gel segregated and formed on top of the PEO (Fig. 3c). In Fig.3c, the PEO appears to be above because the dried samples was observed from below. An EDX analysis confirmed the fibers mostly consisted of a TiO_2 gel, while the particles linked by the gel were mostly PEO. On the contrary, in the $(PEO)_8Ti$ sample hydrolyzed by excess water, phase separation occurred on a uniform nanoscale, to make a uniform composite throughout the sample (Fig.3d). The TiO_2 phase consisted of sub micron fibers (Fig.4) linking an open packing with uniform porosity of PEO flakes .

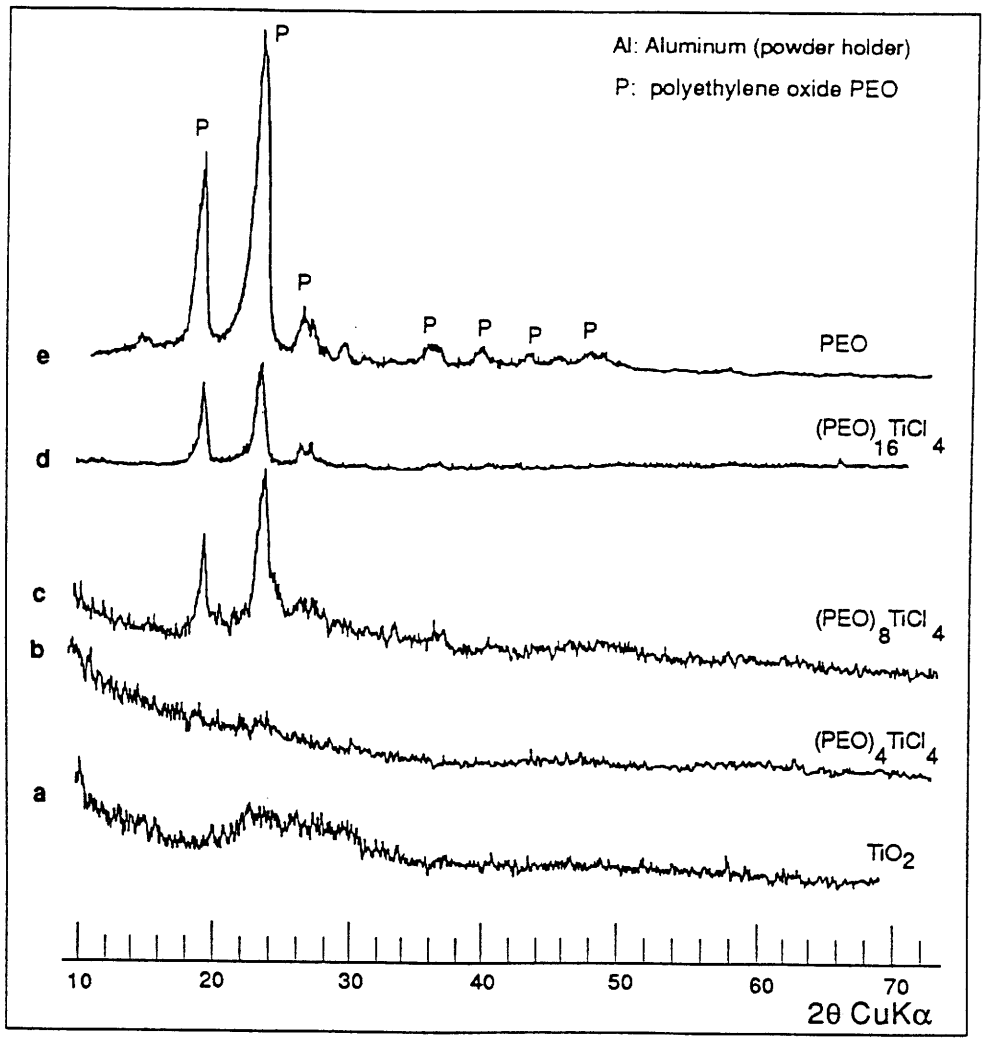

Figure 1 - X-Ray diffraction spectra of hybrid $(PEO)_nTiCl_4$ materials made by hydrolysis by air humidity in dry pentanol. The Spectra of PEO and of TiO_2 from $TiCl_4$ obtained in the same conditions are also reported.

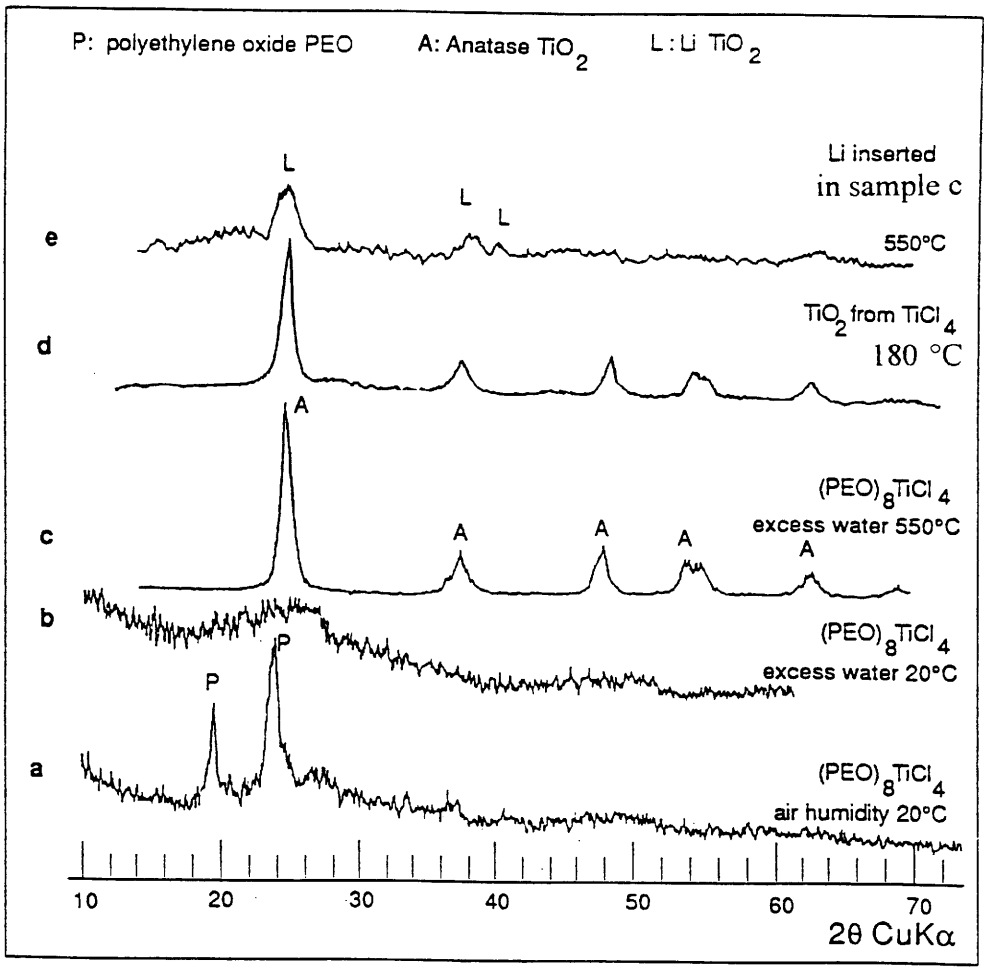

Figure 2. X-ray diffraction spectra of $(PEO)_8TiCl_4$ hybrids made by hydrids of mixed pentanol solution: (a) by air humidity at 20°C; (b) by excess water at 20°C; (c) by excess water, after heat treatment at 550°C; In (d) TiO_2 made in excess water at 20°C from $TiCl_4$, then crystallized at 180°C. (e) by excess water after insertion of Li and heat treatment at 550°C.

TGA analysis showed that the polymer phase in all hybrid materials was progressively destroyed from 200 to 350°C. Then the TiO_2 crystallized in the anatase form as shown in fig. 2c for amorphous $(PEO)_8TiCl_4$ sample hydrolyzed in excess water the pyrolised at 550°C (Fig.2c) . Li insertion is now being studied in this last sample, and preliminary results showed that such an insertion is reversible. The Li insertion composite gives a $Li_{2.0}TiO_2$ compound by heat treatment at 550°C (Fig. 2e).

4. Discussion

PEO is known to be an excellent host material for a number of salts and a detailed review of their structures and properties was provided by Ratner and Shriver [4] . These materials are good ionic conductors above their glass transition T_g, due to a molten micro-environment where the ions can move by a local liquid-like process. They can be mostly made with monovalent cations such as Na^+, Li^+,K^+ and Ag^+. The backbone oxygen of EO act as Lewis-base sites to complex the alkali. The cations are strongly solvated by these oxygen. These materials also show complex phase diagrams [5]. At high temperature, a single elastomeric liquid or amorphous phase with high conductivity is present. At lower temperatures, 2 phases are usually present, which can be a liquid and a polymer. Obviously, all of our $(PEO)_nTiCl_4$ with $n \geq 8$ showed this mixture liquid + PEO-like structure. The liquid led to a TiO_2 gel type phase.

The hybrid materials synthesized in this study can be divided in 3 categories. A first category with homogeneous SEM and X-ray aspects only comprised the $(PEO)_8TiCl_4$ material made by simultaneous hydrolysis of PEO and $TiCl_4$ in excess water. This is consistent with the fact that all the precursors in this study undertake fast hydrolysis, and that hydrolysis occurred in many nucleation centers in excess water. Hence, this materials was either homogeneous on an atomic scale, or heterogeneous on a scale well below the μm. Actually, the formation of anatase in all samples near 400°C, including this sample, indicates that we always had 2 phases. In the $(PEO)_8TiCl_4$ sample hydrolyzed in excess water, these heterogeneity were too fine to be

observed under the SEM.

This view is comforted by the structure of samples made from Ti-ethoxide hydrolyzed in excess water, by comparison with the same samples hydrolyzed by air humidity. Both samples belong to a same second category of materials showing a PEO-like X-ray diffraction and a SEM heterogeneous aspect. However, when hydrolyzed by air humidity, macroscopic phase separation occurred as in samples from $TiCl_4$. With $Ti(OC_2H_5)_4$, the phase separation was even more extensive than with $TiCl_4$ since a TiO_2 gel layer formed on top of the polymer (Fig.3c). In excess water samples, it was replaced by a fine sub micron size dispersion of amorphous TiO_2 gel fibers linking planar PEO crystallite aggregates uniformly throughout the sample (Fig.3d).

Overall, in all materials hydrolyzed by slow diffusion of water, hydrolysis occurred on a smaller number of nucleation centers. Hence, phase separation occurred on a macroscopic scale. Differences between the color of the TiO_2 gel phases, in samples made from $TiCl_4$ versus $Ti(OC_2H_5)_4$, is certainly due to the presence of Cl^- anions with the first precursor.

Even the $(PEO)_4TiCl_4$ sample hydrolyzed by air humidity, which belonged to a third category with an X-ray amorphous pattern, was macroscopically phase separated. The amorphous X-ray appearance of both phases is due to the high $TiCl_4$ proportion leading to abundant HCl formation during hydrolysis. Crystalline PEO polymer is known to have a comb structure [6], where the comb-like teeth consist of short chains oligoethers which contain the Lewis-base [7]. If the teeth are too long, the materials looks like crystalline PEO, which occurred in our case for $n \geq 8$. If the teeth are too short, an amorphous structure forms, which obviously occurred with the highest $TiCl_4$ proportion.

In all cases, the feasibility of nanoscale hybrid composites is consistent with the fast nucleation of TiO_2 particles which remain separated from each other by the simultaneous formation of polymer aggregates, in fast hydrolysis conditions. The fact that the TiO_2 nanoscale phase transformed to anatase instead of rutile during heat treatment, cannot be attributed to the Cl^- anions, since these anions lead to rutile in the reference TiO_2 samples and they were not present when using the ethoxide. Rather, this is consistent with the action of backbone oxygen in the PEO network on the

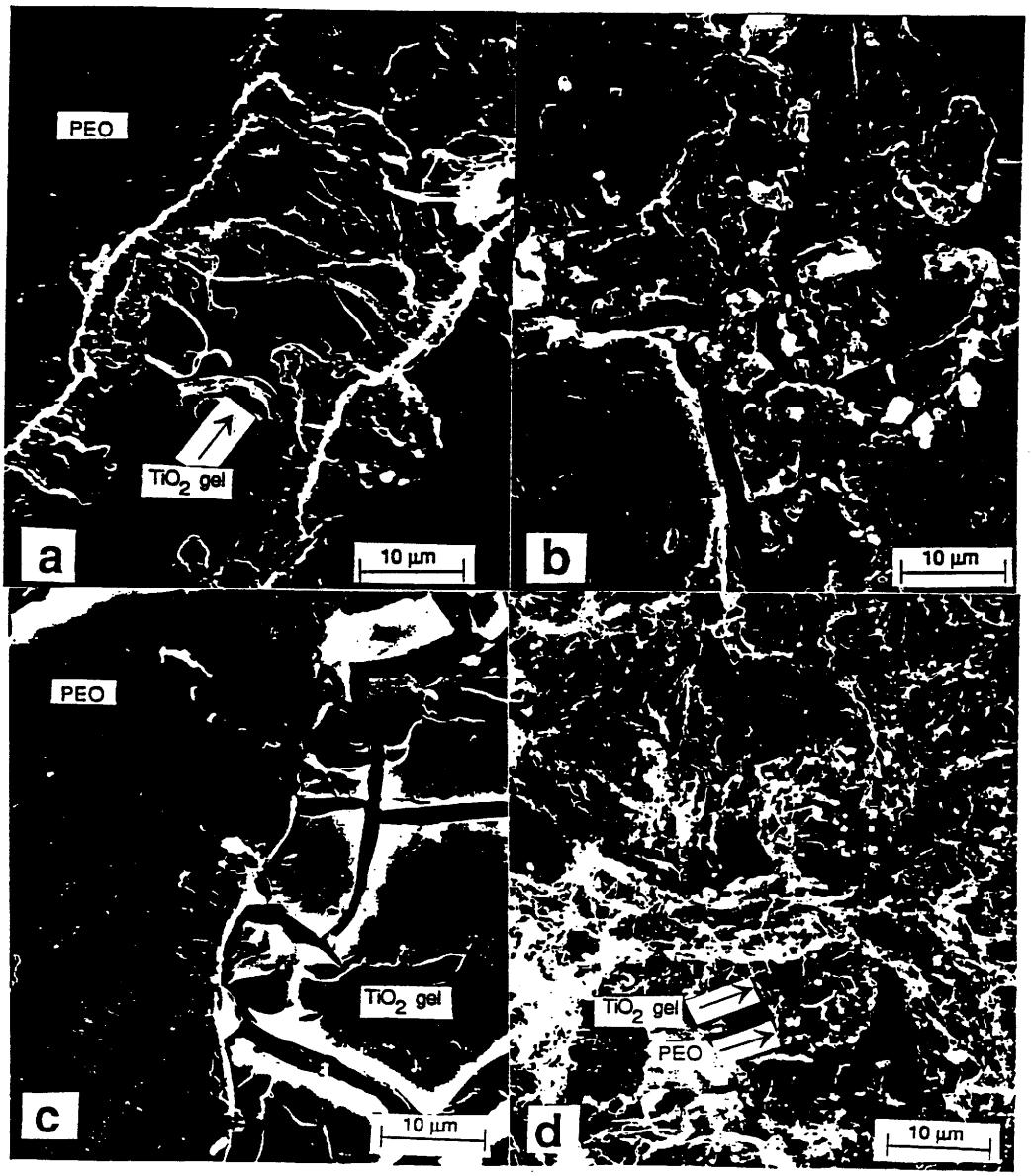

Figure 3. SEM micrographs of $(PEO)_8TiCl_4$ samples in dry pentanol by hydrolysis at 20°C: (a) by air humidity; (b) by exces water. $(PEO)_8Ti$ samples made from $TI(OC_2H_4)_4$ at 20°C in dry pentanol, hydrolyzed: (c) by air humidity; (d) by excess water.

Figure 4 - SEM micrographs of the $(PEO)_8Ti$ samples in Fig.3d, made from $Ti(OC_2H_5)_4$ at 20°C in dry pentanol, hydrolyzed by excess water.

Ti cations. The nanosacle structure of the $(PEO)_8TiCl_4$ sample hydrolyzed in excess water is also consistent with the easy and reversible insertion of Li, as indicated in preliminary results. Further investigations are now underway to characterize and understand better the Li insertion process in these materials.

5. Conclusions

Hybrid PEO-TiO_2 materials with a range of structures from completely X-ray amorphous and SEM homogeneous to completely phase separated, were synthesized. This could be achieved by controlling the hydrolysis process and the nature of the precursor. Nanoscale TiO_2 gel-PEO composites were obtained by hydrolysis with excess water. Slow hydrolysis by air humidity always produces macroscopic heterogeneity.

REFERENCES

1 - P.V. Wright, Brit. Polymer J., 7, 319 (1975).

2 - D.E. Fenton, J.M. Parker, P.V. Wright, Polymer, **14**, 589 (1973).

3 - G. Campet, S.J. Wen, S.D. Han, M.C.R. Shastry, J. Portier, C. Guizard, L. Cot, Y. Xu, J. Salardenne, J. of Mat. Sci. and Eng. B, under publication, (1993)

4 - M.A. Ratner, D.F. Shriver, MRS Bulletin, **September** , 39 (1989).

5 - M. Minier, C. Berthier, W. Gorecki, J. Physique, **45**, 789 (1984).

6 - Y. Chatani, S. Okamura anf Y. Fuji, ACS Div. Poly. Chem. Poly. Preprints, **30**, 404 (1989).

7 - P.M. Blonsky, D.F. Shriver, P. Austin, H.R. Allcock, Solid State Ionics, **18/19**, 258 (1986).

Chapitre IV

MATERIAUX D'ELECTRODE POUR DISPOSITIFS ELECTROCHROMES

La première partie de ce chapitre (§IV. 1) est consacrée à l'étude des propriétés électrochimichromiques de NCIMs déposés en couches minces. Rappelons qu'il s'agissait ici de compléter les études antérieures sur les matériaux électrochromes, - effectuées conjointement par le LCS, LEMME, GRL -, et évoquées plus haut (chap. I et références correspondantes).

Les matériaux considérés jusqu'ici étaient déposés en couches minces par pulvérisation cathodique. Nous avons, ici également, utilisé la voie sol-gel plus facile à mettre en oeuvre que la pulvérisation cathodique.

C'est ainsi que nous avons élaboré par spin coating des contre-électrodes à base de Fe_2O_3-NCIM qui demeurent transparentes dans les états inséré et désinséré.

La deuxième partie de ce chapitre (§IV. 2) se démarque de notre stratégie principale. En effet nous avons, ici, complété les recherches initialement entreprises au LCS sur les électrodes transparentes; elles répondaient à un enjeu important du moment: il s'agissait d'améliorer les propriétes électroniques des électrodes ITO. En effet leur conductivité est encore prohibitive: trop faible, elle nuit à l'uniformité des processus de (dé)coloration des vitrages électrochromes, notamment ceux de grande surface. Pouvait-on alors améliorer la conductivité des ITO existants d'un facteur 2 environ, sans altérer leur transparence? Les résultats que nous avons obtenus en relation avec Y. Xu et le professeur Jean Salardenne, du LEMME, montrent qu' une solution avantageuse a été apportée.

IV.1. REVERSIBLE ELECTROCHEMICAL INSERTION OF LITHIUM IN FINE GRAINED POLYCRYSTALLINE THIN FILMS OF MIXED VALENCY-METAL OXIDES: application to $Li_xFe_2O_3$ thin film-electrodes prepared by the sol-gel process.

(publication)

Materials Science and Engineering, B18 (1993) 201 - 208

REVERSIBLE ELECTROCHEMICAL INSERTION OF LITHIUM IN FINE GRAINED POLYCRYSTALLINE THIN FILMS OF MIXED VALENCY-METAL OXIDES. APPLICATION TO $Li_xFe_2O_3$ THIN FILM-ELECTRODES PREPARED BY THE SOL-GEL PROCESS

G. Campet, S.J. Wen, S.D. Han, M.C.R. Shastry, J. Portier
Laboratoire de Chimie du Solide du CNRS, University of Bordeaux I, 351 Cours de la Libération, 33405 Talence, FRANCE.

C. Guizard, L. Cot
Ecole Nationale Superieure De Chimie, University of Montpellier, 8 Rue de L'Ecole Normale, 34053 Montpellier, FRANCE.

Y. Xu, J. Salardenne
Laboratoire d'Etudes des Matériaux pour la Microélectronique, University of Bordeaux I, 351 Cours de la Libération, 33405 Talence, FRANCE.

ABSTRACT

A new family of insertion-compound electrodes able to sustain long term Li^+ electrochemical cyclability in fine-grained polycrystalline-film form is presented. The major requirement is that the electrode materials have to be amorphous or polycrystalline with grain size as low as possible. Indeed, by minimizing the size of the crystallites the formation of defect-bonds is favoured, particularly at the crystallite surface, acting as reversible (de)grafting sites of Li^+. Related to that the cation-anion bonding is weakened not only in the grain boundary region but also within the grain close to its surface; therefore the electrochemical insertion of Li^+ can also occur through easy bonding rearrangement. These concepts are used to describe the electrochemical Li^+ (de)insertion of $Li_xFe_2O_3$ thin-film electrodes prepared by the sol-gel process.

1. INTRODUCTION

Over the last 15 years, much attention has been focussed on A_xMX_2 type intercalation compounds (A and M designating respectively alkali and transition metal elements: A = Li, Na,

and M = Co, Ni, Mn...; X = O, S, Se,...) which are used as positive electrodes in reversible-alkali electrochemical cells [1]. These compounds have a layered structure, which can often be described as an ordered rock-salt structure. The alkali ions can easily move from one to another octahedral environment between the $(MX_2)_n$ layers due to the rather weak Van der Waals type interaction between the layers. Among these materials the oxides Li_xMO_2 (M = Co or (and) Ni...), which can reversibly intercalate over 0.5 Li^+ per mole, have recently received a great interest [2,3]. However a very long term cyclability (i.e. over 10^3-10^4 cycles) might be hardly achievable, particularly for corresponding electrodes having large grain size, probably because the Li^+ (de)intercalation process slightly perturbs the host lattice.

On the other hand, concerning grain size we have shown in recent electrochemical studies of cells using Li_xCrO_2 or Li_xNiO_2 as the positive electrode in thin film form, that not only the cell reversibility but also the cell capacity were greatly enhanced when very fine crystallites were used [4-8]. Rather similar considerations concerning the spinel $LiMn_2O_4$ were reported by P.Barboux et al. [9]. Also apparently related to that N.Kumagai et al. have reported that the positive electrode $MnO_2.xV_2O_5$ was formed by incorporation of V_2O_5 into MnO_2 matrices and the crystallinity of the oxide decreased with the increase of V_2O_5 content incorporated : they have shown that the amount of Li^+ ions which can be reversibly electrochemically (de)inserted increased with increasing x value, i. e. with the decrease of crystallinity; it reached c.a. 1 Li / mole of the oxide with x = 0.6 [10].

2. A convenient approach to obtain thin film electrodes able to sustain long term Li^+ electrochemical cyclability

Some of us have patented, a few years ago, a new strategy and related experiments that have enabled us to put forward a rather new family of insertion-compound electrodes able to sustain, in thin film form, long term Li^+ electrochemical cyclability [4]. The major requirement being that the electrode materials are amorphous or polycrystalline with grain size as small as possible. Besides, as far as thin-film electrodes are concerned the electrode materials must obviously tightly adhere to the substrates [4]. Therefore we have later symbolized the polycrystalline electrode materials as MCIM (for "Micro-Crystallite-Insertion-Material") [11,12]. Table I gives significant examples related to mixed valency metal oxides [4,11,12].

For the sake of clarity the examples listed in table I have been divided into two classes, A and C according to whether the resistivity tends to increase (class A) or to decrease (class C) upon the electrochemical Li^+ insertion process. In fact this classification arises from the "rocking-chair" concept which has been used to manufacture electrochromic systems, based on

such class A electrodes (which generally change from transparent-to-coloured state upon Li^+ anodic desinsertion) and class C electrodes (which generally change from transparent-to-coloured state upon Li^+ cathodic insertion) [4]. For similar x values (table I) class A electrodes generally have deeper Fermi level than class C electrodes (thereby having higher Fermi level).

Let us quote that the reversible electrochemical (de)insertion of lithium was previously demonstrated, by numerous authors, for some of thin film electrodes of composition reported in table I, such as Li_xIrO_2 [13,14] and more particularly Li_xWO_3 electrodes [15]. However, to our knowledge, except for WO_3 [15] the literature data was inadequate for describing and understanding the long term cyclability rate sustained by the other MCIM reported in table I. In order to remedy this situation, at least partially, we have set up a tentative model accounting for the reversible electrochemical insertion mechanisms [4,8,16]. The framework of this model will be outlined again here. First of all let us quote that by minimizing the size of the crystallites we tend to: (i) weaken the cation-anion bonding, not only in the grain boundary region, but also within the grain close to its surface; the electrochemical insertion of Li^+ would then occur through easy bonding-rearrangements [8]; (ii) favor the formation of defect-bonds, particularly at the crystallite surface, such as anion adjacent to cation vacancies and, conjunctively cation adjacent to anion vacancies; the former defects would act as reversible (de)grafting sites of Li^+ [4,8,16].

In support of these views we were able to show that several aspects of the transport data can, in some cases, be consistently explained using the equations of the transport coefficients developed by Mott [17] (for conduction occurring in band tail below the conduction band mobility edge as it occurs in event (i)) or by Davis-Mott [18] (for conduction taking place in deep subband-gap localized states at the Fermi-energy as it occurs in event (ii)). In event (ii) the $T^{-1/4}$ dependence of $L n\sigma$ can be observed; for example fig.1 illustrates this situation for Li_xNiO_2 electrodes for which the average crystallite size we could deduce by TEM was about 60 Å (table I) [8]. Other conduction mechanisms, under investigation at the present time, can occur such as carrier delocalization above the mobility edge for some class C electrodes and for high x value . Let us also quote that some particular cases, not reported in table I for the sake of clarity and for which small polarons would dominate the conduction process, are worth noticing. These events, presently under investigation, deal with composite electrodes based on micro-crystallites (< 30 A size) of mixed-valency metal oxides dispersed in conductive polymers [19]. All other concepts mentioned above can be visualized using a schematic band-diagram. Fig. 2 shows that of $SrTiO_3$ based MCIM (table I) whose physical properties have been detailed elsewhere [20-23]. Rather similar simplified band-energy scheme would normally apply for other MCIM also. Fig.2 illustrates the electron conduction occurring, in the grain-boundary region including the vicinity of the grain-surface (within the grain), via $[Ti : 3d]_{sub}$ or $[Ti :3d]_{b.w.}$energy states. The $[Ti:3d]_{sub}$ symbolizes deep subband gap energy states arising from cation-adjacent to anion-vacancy defects and lowered about 0.6 eV below the Π^* conduction band of $Ti^{4+}:3d^0$ (t_{2g}) parentage [23]. Let us point out that efficient reversible Li^+ (de)insertion, accounting for the electrochromic properties, is essentially observed in stoichiometric $SrTiO_3$ based MCIM and not in strongly oxygen deficient crystallized electrodes

[4,23]. Consequently the $[Ti:3d]_{sub}$ occurring in the $SrTiO_3$ based MCIM would mainly arise from broken titanium bonds in such a way that rather similar concentration of broken oxygen bonds occurs at cation vacancies. The latter defects introduce acceptor states, $[O:2p]_{sub}$, lifted out the $O^{2-}:2p^6$ valence band (fig. 2); the related cation vacancies act as reversible grafting sites for Li^+.

The $[Ti:3d]_{b.w.}$ and $[O:2p]_{b.w.}$ energy states, which are close to the conduction and valence band edges respectively (fig. 2), originate from Ti-O bond weakening. Indeed a reduced symmetry mainly introduces band tailing [23]. As mentioned above the Ti-O bond weakening takes place not only in the grain boundary region but also within the grain close to its surface. From the foregoing discussion it follows that:

(i) when negative and positive bias are applied to the MCIM based $SrTiO_3$/ITO coated glass electrode (with ITO symbolizing the well known transparent and conductive indium-tin-oxide film used here to get electrical contact) the coloration and bleaching phenomena are alternatively observed:

$$\underset{\text{(no color)}}{SrTiO_3} + xLi^+ + xe^- \text{<------>} \underset{\text{("green blue")}}{Li_xSrTiO_3} \quad (0 < x < 0.3) \qquad (1)$$

(ii) for rather low x values ($x < 0.1$) the Fermi-energy lies in the band of the $[Ti:3d]_{sub}$ localized states (fig. 2); the electrons injected in the electrode according to equation (1) move between the states via a phonon assisted tunneling process (the conduction mechanism is rather similar to that suggested for Li_xNiO_2) [23,24]. Consequently nearly no optical reflectivity is measured in the IR region; on the other hand optical absorption related to the filling of the $[Ti^{4+}:3d^0]_{sub}$ is observed:

$$[Ti^{4+}:3d^0]_{sub} + e^- \text{<-------->} [Ti^{3+}:3d^1]_{sub} \qquad (2)$$

The Li^+ ions which are electrochemically (de)inserted according to equation (1), move via a hopping process between the above mentioned O- defects (fig. 2).

(iii) when all $[Ti:3d]_{sub}$ energy states (fig. 2) are filled up with electrons, and thereby the O- defects are grafted with Li^+, the $[Ti^{4+}:3d^0]_{b.w.}$ energy states are progressively filled with electrons as x increases (beyond about 0.1); the electrochemical insertion of Li^+ simultaneously takes place through easy bonding rearrangement:

$$[Ti^{4+}\text{-}O^{2-}]_{b.w.} + e^- + Li^+ \text{<------>} [Ti^{3+}:3d^1]_{b.w.} + O^{2-}\text{-}Li^+ \qquad (3)$$

More extended state conduction which would have induced some IR reflectivity and which could have been related to efficient Li^+ intercalation within the micro-crystallites, was not achievable for the Li_xSrTiO_3 electrodes [4].

On the other hand the "more conventional intercalation compound " Li_xWO_3 can sustain efficient Li^+ intercalation within the micro-crystallites, but once the subband-gap energy states $[W^{6+}:5d^0]_{sub}$ and $[W^{6+}:5d^0]_{b.w.}$ (the "twin states" of $[Ti^{4+}:3d^0]_{sub}$ and b.w. reported in fig.2) are filled with electrons. That is observed for x>0.3 for the WO_3-based MCIM reported in table I [4] .

Using precisely WO_3 as a third non-limiting but illustrative example it can be shown that the corresponding simplified band-energy diagram (not reported here as it is rather similar to that of fig. 2) also accounts for the different shapes of the open circuit voltage (OCV) versus x curves related to Li_xWO_3 electrodes deposited at different substrate temperatures (fig. 3): the concentration of the $[W^{6+}:5d^0]_{sub}$ subband-gap energy states is obviously as the more large as the crystallite size is reduced; consequently for $x << 0.3$ and for films deposited at low substrate temperature (thereby having small grain size) a pinning of the Fermi energy within the $[W^{6+}:5d^0]_{sub}$ states will occur and be responsible for the high OCV observed (fig.3). Rather similar occurence can be observed for other class-C electrodes. Conversely, for class-A electrodes (table I) and for high x values, the subband - gap energy states related to the fine grained texture will generally cause a pinning of E_F above the valence band edge [8]. Fig.4 illustrates the later situation for Li_xCrO_2-based MCIM electrode (table I) whose behaviour is compared to that of well crystallized $LiCrO_2$ electrode [25]: indeed, a difference in the OCV of about 1 volt is observed between the two types of electrodes when they are in their quasi-reduced state (i.e. [Cr4+] << [Cr3+]).

3. Application to fine-grained $Li_xFe_2O_3$ thin film electrodes obtained by the sol-gel process

As mentioned above the capacity of polycrystalline thin-film electrodes, whose inside-grain structure does not allow efficient Li^+ (de)insertion, can be greatly improved if fine-grained electrodes are used.

Solution technique is one of the judicious ways to easily obtain films with small grain size [25]. Therefore we report herein the preparation of Fe_2O_3 thin film electrodes prepared by means of the sol-gel process [25]. This well known process consists of the condensation of metal oxide networks from solution precursors.

TABLE 1. Some microcrystallite insertion materials

Sample	Class	Average grain size (Å)	Insertion rate x (measured in $LiClO_4$ (polycrystalline), $1.5\ V \leqslant V(Li) \leqslant 3.5\ V$)
Li_xSrTiO_3	C	80	$0 < x < 0.3$
Li_xCrO_2	A	30	$0 < x \leqslant 1$
$Li_xMn_2O_3$	A	50	$0 < x < 2$
$Li_xFe_2O_3$	C	This study	
Li_xNiO_2	A	60	$0 < x < 2$
Li_xCuO_2	A	50	$1 < x < 2$
Li_xWO_3	C	70	$0 < x < 0.6$
Li_xIrO_2	A	60	$0 < x < 1$

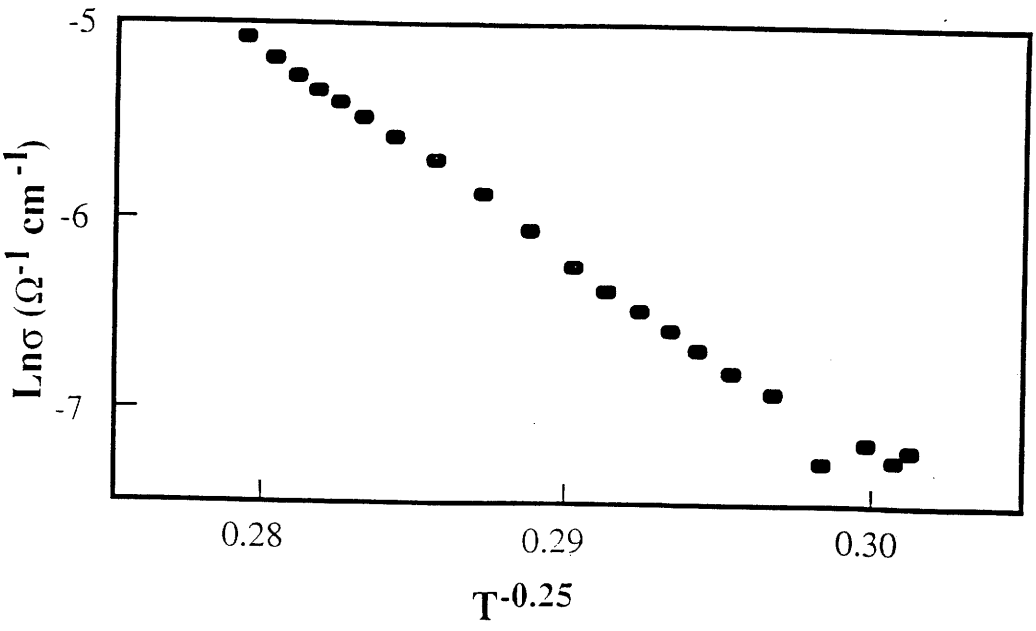

Fig. 1. $T^{-1/4}$ dependance of ln σ for Li_xNiO_2 (x=1) electrodes (Table 1) [8].

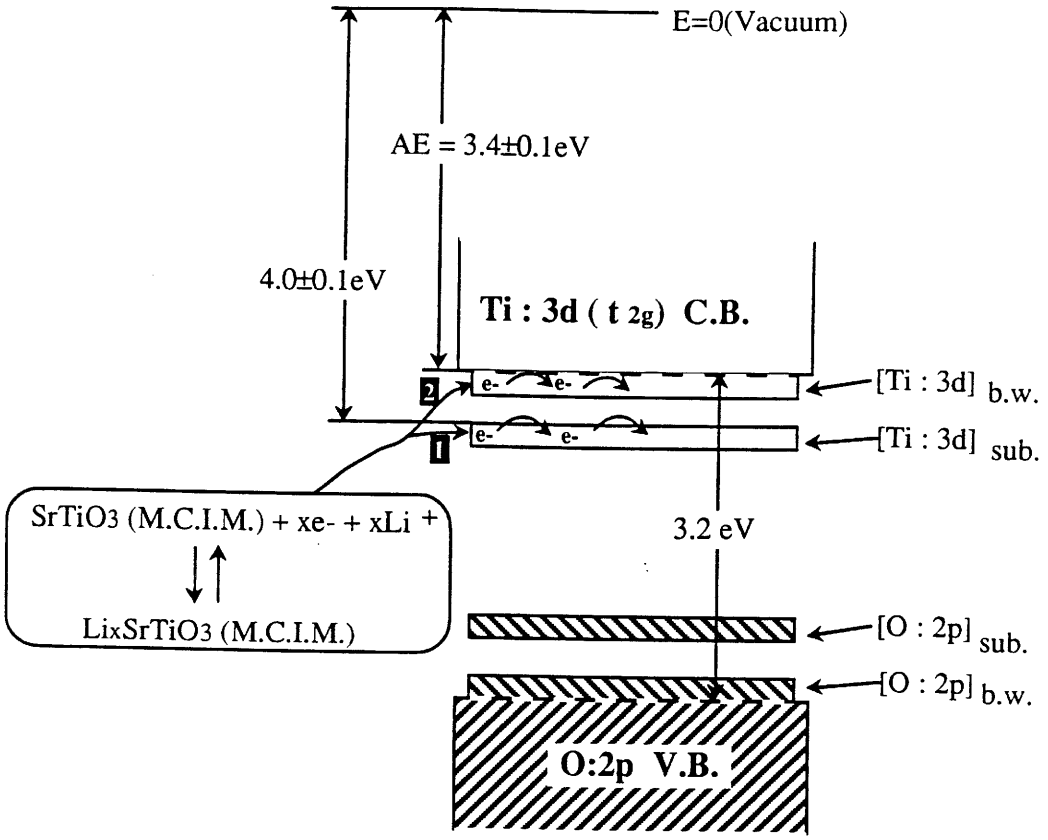

Fig. 2. Simplified energy scheme of the grain boudary within which electron and lithium conduction occur through the medium of respectively $[Ti:3d]_{sub.}$ (or $[Ti : 3d]_{bw}$) state and $[O: 2p]_{sub.}$ (or $[O:2p]_{bw.}$) related O- defects. CB, conduction band; VB, valence band.

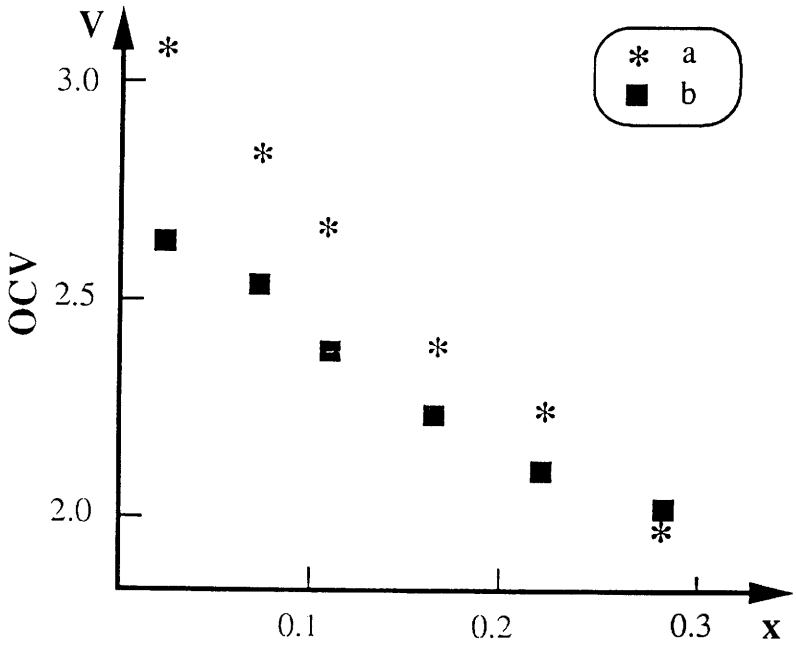

Fig. 3. Equilibrium open circuit voltages (OCV) for Li/ $LiClO_4$, PC./ $LiWO_3$ cells versus x (reversibly exchanged) [8,11].
a): RF. sputtered WO_3 (T_{substr} =70°C): average grain size of 70Å (as given in table1)
b): RF. sputtered WO_3 on hot substrate ($T_{substr.}$= 350°C): average grain size of 300Å.

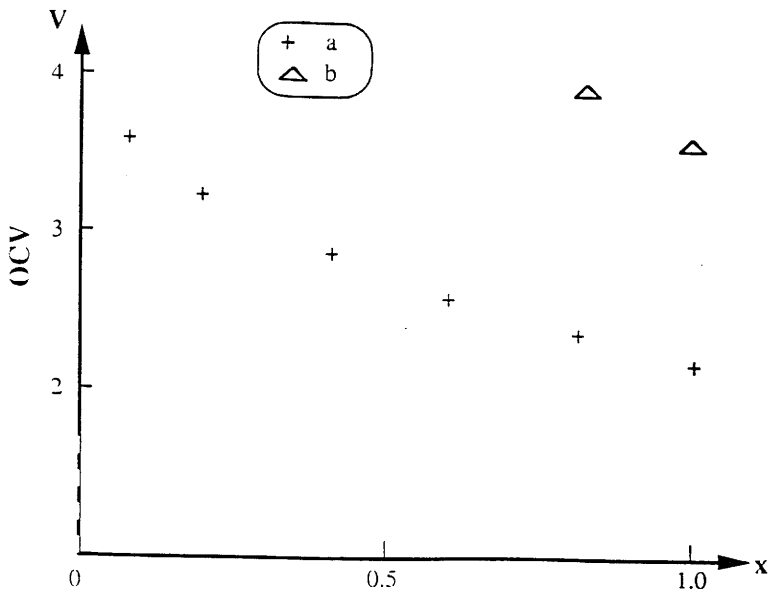

Fig.4. Equilibrium open circuit (OCV) versus x for Li/ $LIVIO_4$, PC./LI_xCrO_2 cells using:
a): fine-grained (80Å size as given in table 1) electrodes.
b): "more conventional" intercalation electrodes (from ref. [25]).

3. 1. Experimental

The films have been deposited at room temperature from the solution [1] to which was added 1 g of polyvinybutyral to get appropriate viscosity and adherence on the substrate. The spin-coating technique (acceleration speed: 40 rad.s^{-2}; rotating speed and time: 120 rad.s^{-1}, 30s) was used. ITGO [2] coated glass substrates (R = 10 Ω) were used for electrochemical and optical analysis.

Differential thermal analysis (DTA) and thermogravimetric analysis (TGA) were performed, as described in ref. [8], from 90°C to 800°C. In this prospect either films deposited on gold-leaf substrates (which provide samples easily weighed) or powdered samples, prepared by heating the solution [1] at 90°C (i.e. above the boiling point of pentanol) were used. X-ray diffractometry was carried out for both the films and powders. Optical absorption measurements were recorded using a Cary 17 ratio-recording spectrophotometer.

The electrochemical procedure makes use of a two electrode cell configuration, namely the iron-based film and a lithium electrode; both electrodes are immersed in a dehydrated $LiCF_3SO_3$ (1M) propylene carbonate electrolyte.

3 -2 Results and discussion

a) *TGA, DTA and X-ray analysis*

From the TGA, DTA and X-ray analysis shown in fig.5-7 we can draw the following conclusions. First of all the total weight loss observed was approximately 40% (fig.5). This took place in two main stages. The loss of polyviny butyral over by ~330°C (figs. 5 and 6) accounts for the first step. (fig. 7). This organic compound has high hydroxyl content; therefore, and according to IR spectroscopy [28], the samples treated at ~330°C are left with OH groups tightly bound to the crystallite surfaces. Under these circumstances the second endothermic process, occurring between ~330°C and 460°C (fig.5), illustrates a dehydratation process. However, all hydroxyl groups were eliminated (still according to IR spectroscopy [28]) once the powdered samples or the films have been heated in air at T>350°C for t>2hrs. As shown in fig.7.a the films treated at 350°C essentially develop the Maghemite (γ -Fe_2O_3) X-ray spectrum (the presence of Fe^{2+}, that would have accounted for the existence of unnegligeable traces of

[1] 4 g of iron (III) 2-4 pentanedionate are dispersed in 25 ml of pentanol. The solution is then intimately stirred up for 2 hours at 60 °C. 0.4 ml of H_2O are finally added to achieve the condensation of iron alcoxyde according to:

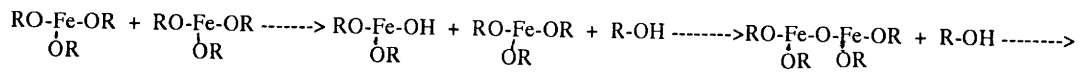

[2] ITGO symbolizes Ge-doped indium oxide films we have recently studied [26,27]; owing to their high carrier-mobility their conductivity and transparency in the visible can be higher than that of well known ITO (Sn-doped indium oxide).

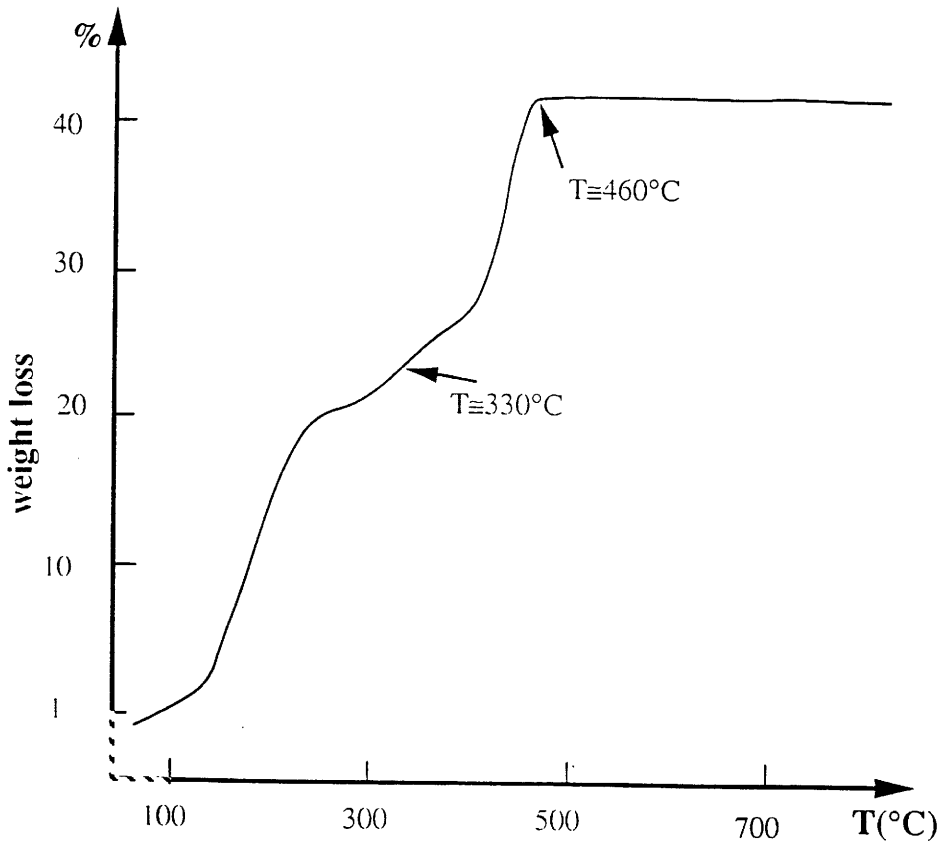

Fig. 5. Thermogravimetric analysis (TGA) performed, at a heating rate of 5°C / min. from 90°C to 800°C. Either films deposited on gold leaf substrates (which provide samples easily weighed) or powdered samples were used.

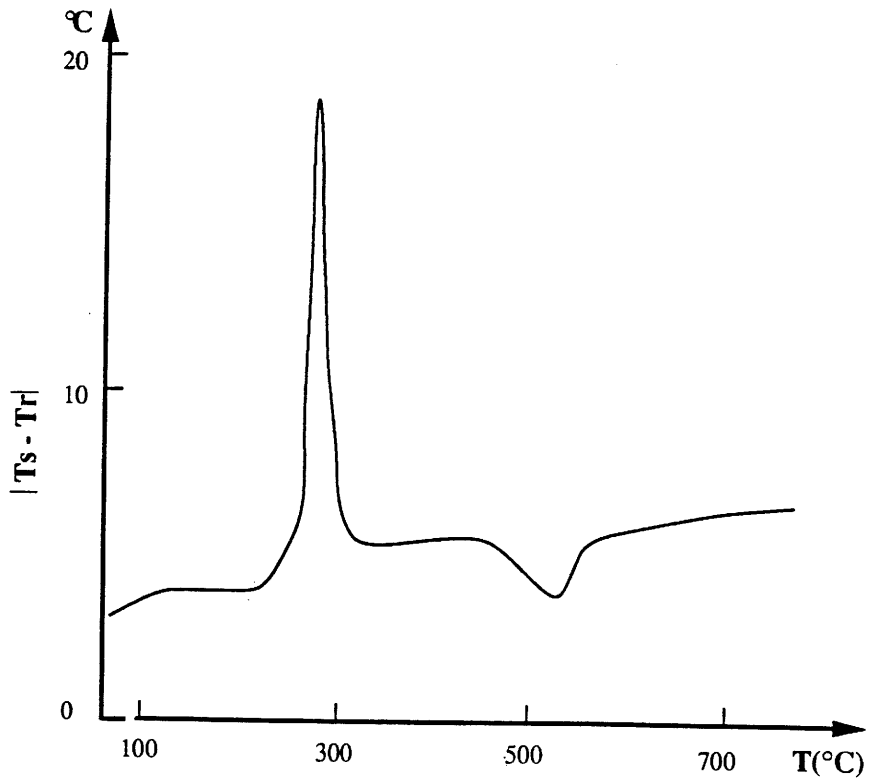

Fig. 6. Differential thermal analysis (DTA) performed in a similar way as TGA (fig. 5). Ts and Tr refer to sample and reference temperature respectively.

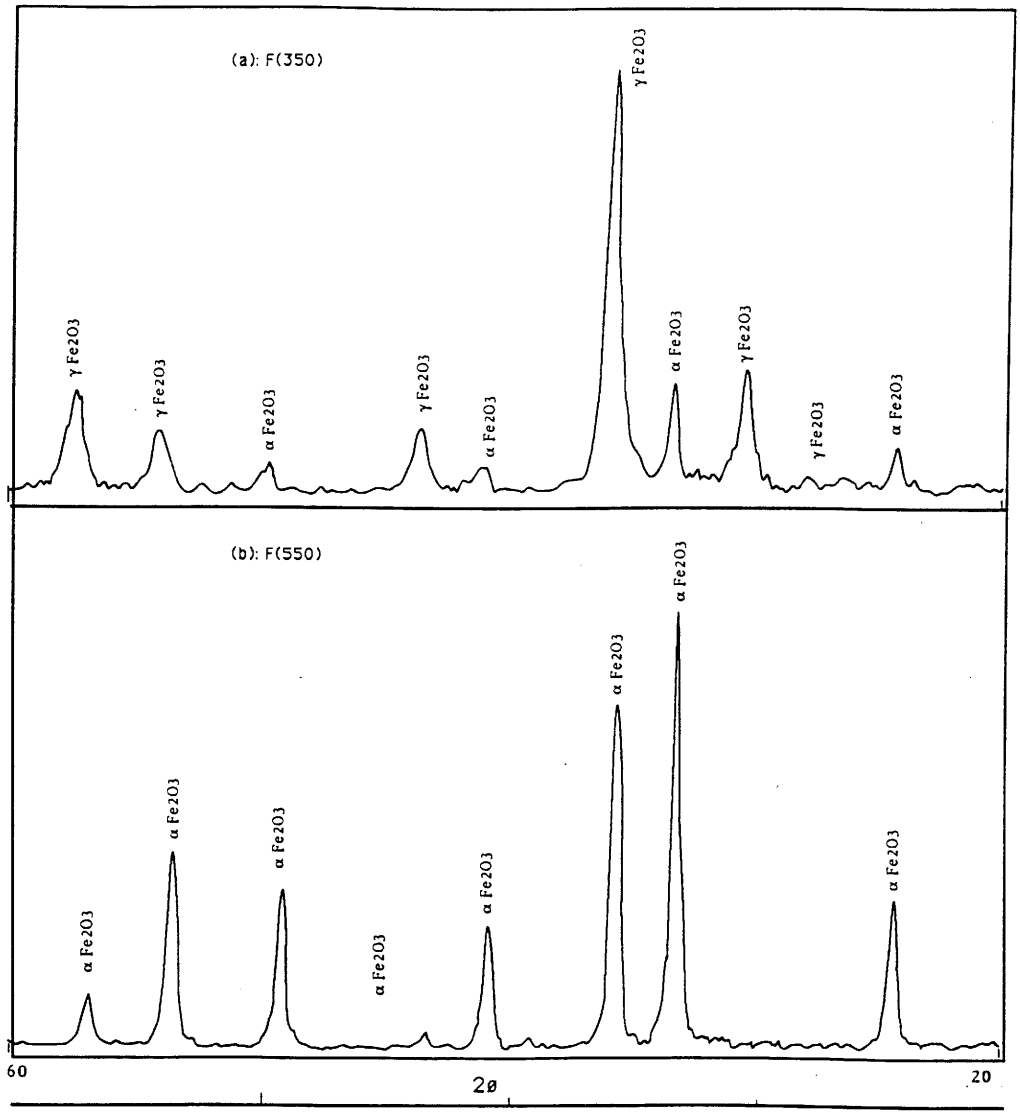

Fig. 7. X-ray diffractogrms for the Fe_2O_3 film heated at two different substrate temperatures: 350°C (fig.7a) and 550°C (fig.7b). The corresponding films are denoted as F(350) and F(550) respectively.

Fe_3O_4 was not revealed by Mossbauer spectroscopy). The X-ray spectrum allows an estimation of the mean-grain size, D≅150Å (deduced from the classical Scheerer's formula or from TEM measurements). When the samples are further progressively heated from 350°C to 800°C a broad exothermic peak is observed between 480-550°C (fig.6). It does not account for a significant change in stoichiometry because TGA shows no visible gas evolution (fig.5). The exothermic peak should in fact be associated with two events: (i) the increase of the grain size on the one hand, (ii) the structural change Maghemite -> hematite (α-Fe_2O_3) on the other hand. All that is indeed revealed by the X-ray pattern of samples treated at 550°C (fig.7.b), according to which the average grain size is D≅300Å.

Therefore in the following we have chosen to investigate the electrochemical lithium insertion /extraction in two types of Fe_2O_3 films, namely treated at 350°C on the one hand and at 550°C on the other hand. According to our assumptions remarkable difference would be observed in lithium reactivity between the two series of films symbolized hereafter respectively as F(350) and F(550) .

b) *Electrochemistry*

The electrochemical testing are processed within the following appropriate voltage range: 1.5V-3.5V so as to avoid electrolyte oxidation and ITO reduction [5].

As illustrated in fig.8, showing the cyclic voltammograms recorded between 1.5 V and 3.5 V at the sweep rate of 100 $s.V^{-1}$, the charge exchanged in cycling F(550) is about half that measured in cycling F(350). The voltammograms show complete reversibility. On the other hand the charges exchanged correspond to that measured when the potential is abruptly stepped between 1.5 V and 3.5 V; that illustrates a fast and reversible Li^+ (de)insertion at these potentials.

The knowledge of the range of film specific weight of 3-4 g/cm^3 gives the following average modulation of the lithium contents:

(i) for F (350)

$$Fe_2O_3 + 0.5\ Li^+ + 0.5\ e^- \text{<----------> } Li_{0.5}Fe_2O_3$$

(ii) for F (550)

$$Fe_2O_3 + 0.25\ Li^+ + 0.25\ e^- \text{<----------> } Li_{0.25}Fe_2O_3$$

Therefore the number of accessible sites for lithium in F (550) is approximately twice lower than that occurring for F (350) in good agreement with expectation (fig. 9). Let us, however, point out that we could have expected a more extended modulation of the lithium content for F (350) . Indeed it is well known that lithium can be electrochemically intercalated into the spinel

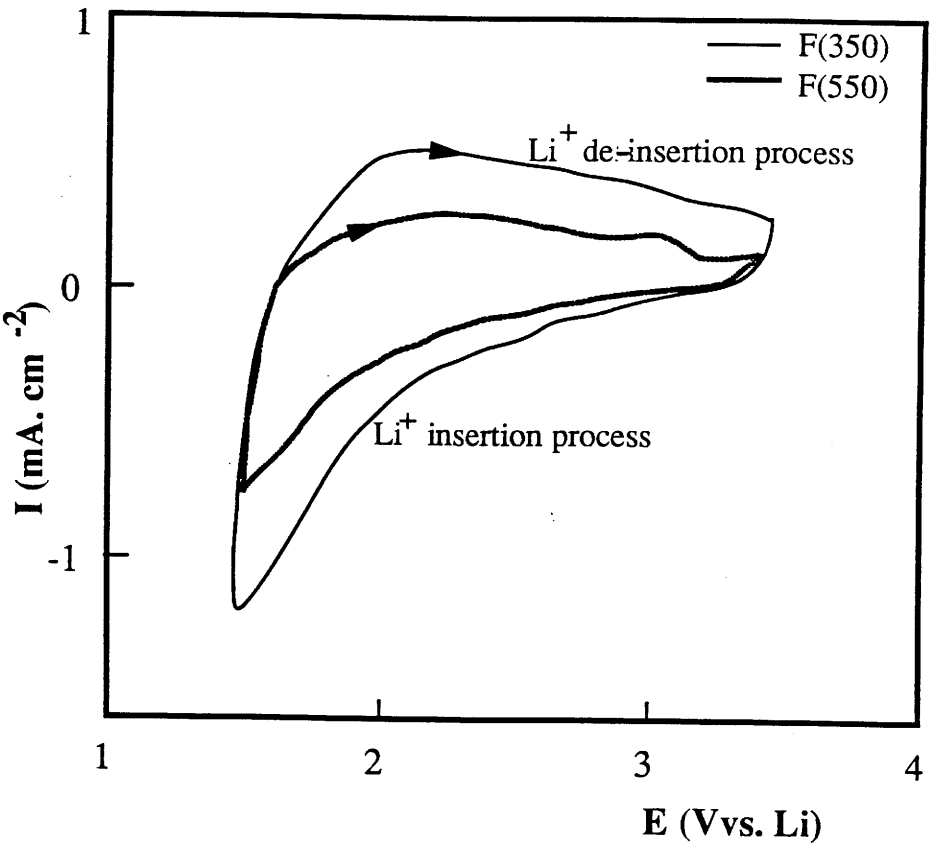

Fig. 8. Cyclic volammograms (50^{th}) of F(350) and F(550), scanning rate 100s/V.

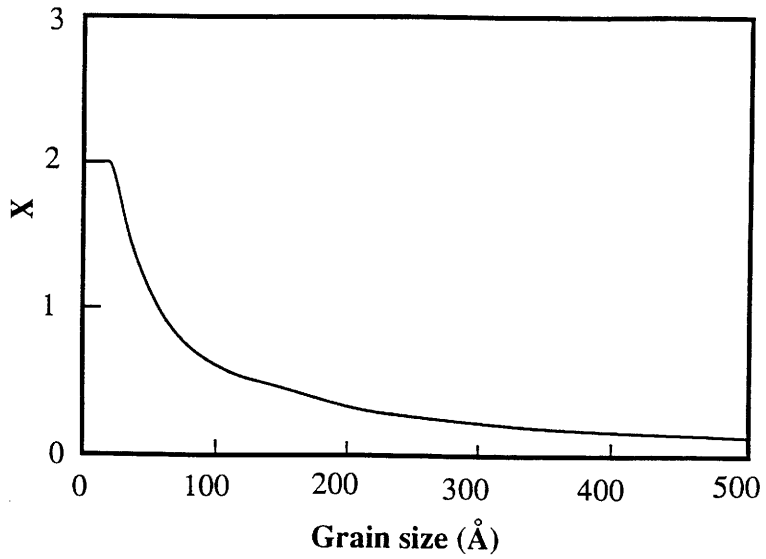

Fig. 9. Theoretical estimation of the rate x of $Li^{+}Fe_2O_3$, roughly assuming that x corresponds to the number of oxygen present at the spherical shaped grain surface.

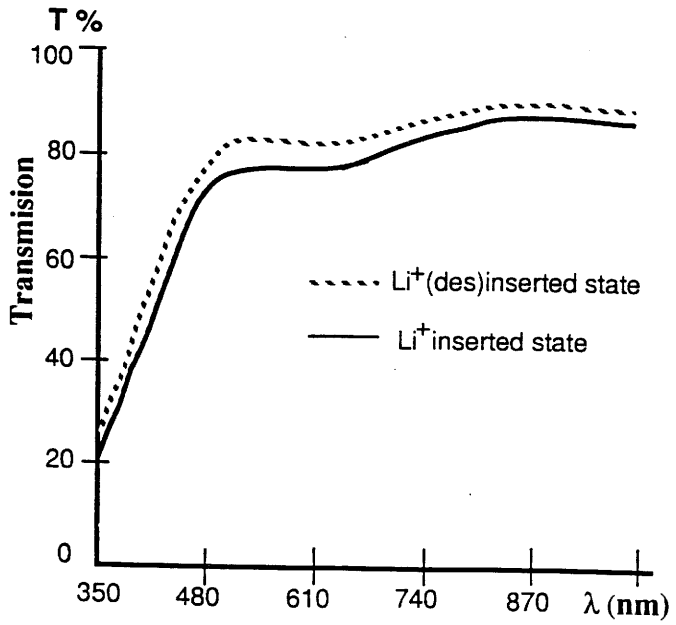

Fig. 10. Optical transmission spectra for Li^{+} inserted and desinserted F(350); rather similar spectra have been observed for F(550).

$Li_xFe_3O_4$ over a wide compositional range, $O \leq x \leq 2$ [29] ; unfortunately such an occurrence has not been observed for F (350) electrodes having similar structure.

The electrodes remain rather transparent in both inserted and desinserted state (fig. 10). Therefore they could be used as counter electrodes, similar to Li_xCrO_2 [8], in nearly-no-absorbing but reflective electrochemical windows using well crystallized WO_3 films as the "active" electrochromic electrode [15]. However, the as-deposited films do not adhere tightly enough to the substrates, contrarily to what occurred for the above mentioned Li_xCrO_2 electrodes deposited by sputtering and able to sustain 10^5 electrochemical cycles without significant degradation [8]. Indeed, here, the charge exchanged after 10^3 electrochemical cycles is half that measured during the first ones. On the other hand the material in itself is highly stable electrochemically because no apparent degradation occurs for Fe_2O_3-based "soft" composite electrodes, we have recently manufactured, and able to reversibly exchange about 1 Li^+ per Fe; these composite electrodes consist of very low grain size (about 30 Å) Fe_2O_3 powders prepared via the sol-gel route, finely dispersed in conductive polymer acting as a host matrix [30].

Finally fig. 11 shows the open-circuit voltage (OCV) values of $Li/LiClO_4$ p.c. $/Li_xFe_2O_3$ cells and for low x values. Higher OCV values occur for F (350) electrodes; they must be correlated to the higher density of subband-gap energy states fixing downwards the Fermi-energy as stated above for other class C electrodes..

4. CONCLUSIONS

The simple model we proposed for thin film electrodes listed in table I rather adequately fit most of experimental observations including Fe_2O_3-based MCIM electrodes . It is also conceivable that not only oxides but also other materials such as metal halides exhibit efficient Li^+ electrochemical (de)insertion in very fine-grained polycrystalline film form (or when the microcrystallites are finely dispersed in conductive polymers). The corresponding samples are then likely to have a large density of vacant sites at the crystallite-surface and its immediate vicinity, these sites being available for efficient electrochemical (de)insertion.

Concerning the Fe_2O_3 electrodes investigated here further study aiming at optimizing the electrochemical response by reducing the crystallite size to about 30 Å (fig. 8) is in progress. Such electrodes, deposited by sputtering or manufactured using the microcrystallites finely dispersed in conductive polymers, are under investigation.[3]

---

[3] Acknoledgments: The authors wish to thank Pr. J. B. Goodenough for very helpful discussions and the Groupement de Recherches de Lacq (ELF-AQUITAINE) for technical and financial support.

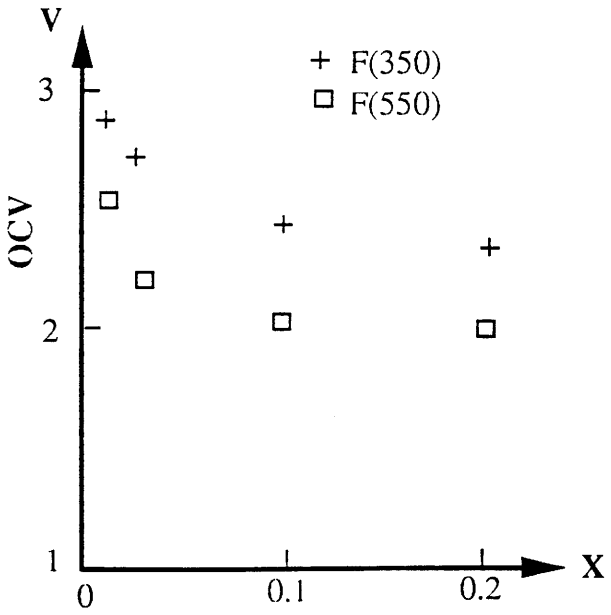

Fig. 11. Equilibrium open circuit voltage (OCV) versus x for $Li/LiClO_4$,PC./$Li_xFe_2O_3$ cells using F(350) and F(550) electrodes.

REFERENCES

(1) See for instance:

-J. Rouxel, in Physics and Chemistry of Layered Materials, F. Levy (ed), vol VI, Reidel (1979).
-K. Mizushima, P. C. Jones, P. J. Wiseman and J. B. Goodeuough, Solid State Ionics **3/4** (1981) 171.
-C. Delmas, J. J. Braconnier, A. Maazaz and P. Hagenmuller, Rev. Chem. Min. 19 (1982) 343.
-J. Molenda, Solid State Ionics, 21 (1986) 263.
-S. Miyazaki, S. Kikkawa and M. Koizumi. Synthetic Metals, 6 (1983) 211.

(2) C. Delmas and I. Saadoune, Solid State Ionics (in press).

(3) C. Delmas, I. Saadoune, A. Rongier, J. Power Sources (Submitted).

(4) J. P. Couput, G. Campet, J. M. Chabagno, M. Bourrel, D. Muller, R. Garrié, C. Delmas, B. Morel, J. Portier, J. Salardenne, Int. Appl. Publ. under PCT. Int. Patent. Class: GO2F 1701, FO1 G9/00, C 23C 14/34. WO 91/01510 (1989).

(5) G. Campet, J. Portier and S. J. Wen, J. of Active and Passive Electr. Comp. (in press).

(6) G. Campet and J. Portier, J. of Act. and Pass. Electron. Comp. (in press).

(7) G. Campet, B. Morel, M. Bourrel, J. M. Chabagno, D. Ferry, R. Gorie, C. Quet, C. Geoffroy, J. . Videau, J. Portier, C. Delmas and J. Salardenne, Mat. Sc. and Eng. B8 (1991) 303.

(8) B. Morel, Doc. Thesis (University of Bordeaux I, France, 1991).

(9) P. Barloux, J. M. Tarascon and F. K. Shokoohi, J. Solid State Chem. 94 (1991) 185.

(10) N. Kumagai, S. Tanifuji, T. Fujiwara and K. Tanno, Electrochem. Acta. 37, 6 (1992) 1039.

(11) G. Campet, unpublished result.

(12) S. J. Wen, J. C. Lassègues, G. Campet and S. D. Han, J. Act. and Pass. Electron. Comp. (submitted).

(13) S. Hackwood, A. H. Dayem and G. Beni, Phys. Rev. B, 26 (1982) 471.

(14) P.G.Pichup and V. I. Birss, J. Electrochem. Soc. 135 (1988) 41.

(15) See for instance:

-B. W. Fanghnan, R. S. Crandall and P. M. Heyman, RCA Rev. 36 (1975) 177.
-B. W. Fanghnan, R. S. Crandall and M. A. Lampert. Appl. Phys. Lett. 27 (1975) 275.
-P. Gerard, A. Deneuville, G. Hollinger and T. M. Duc, J. Appl. Phys. 48 (1977) 4252.
-O. F. Schirmer, V. Wittver, G. Baw and G. Brandt, J. Electrochem Soc. 124 (1977) 749.
-K. S. Kang, PhD. Thesis, London University (1979).
-H. M. Gupta and G. F. Leal ferreira, J. Appl. Phys. 50 (1979) 5036.
-P. Gerard, A. Deneuville and R. Courths, Thin Solid Films 71 (1980) 221.
-W. C. Dautremont-Smith, Displays 4 (1982) 3.
-R. R. Goldner, D. H. Mendelsohn, J. Alexander, W.R. Henderson, D. Fitzpatrick, R. D. Rouh, M. A. Parker and T. L. Rose, Appl. Phys. Lett. 43 (1983) 1093.
-D. H. Mendelsohn and R. B. Goldner, J. Electrochem. Soc. 131 (1984) 857.
-C. M. Lampert, Sol. En. Mat. 11 (1984) 1.
-M. Pham Thi and G.Velasco, Rev. Chem. Miner. 22 (1985) 195.
-J. S. E. M. Svenlon and C. G. Granqvist, Thin Solid Films, 126 (1985) 31.
-M. Green and A. Tavlos, Philos. Mag. B 51 (1985) 501.
-F.Bonino, L.Peraldo Bicelli, B.Rivolta, M.Lazari and F.Festorazzi Solid State Ionics 17 (1985) 21.
-H. Kaneko, F. Nagav and K. Miyake, J. Appl. Phys. 63 (1988) 510.
-O. Bohnke, Cl. Bohnke, A. Donnadieu and D. Davazoylen, J. Appl. Electrochem. 18 (1988) 447.
-R. B. Goldner, T. E. Haas, G. Seward, K. K. Wong, P. Norton, G. Foley, G. Berera, G. Wei, S. Schulz and R. Chapman, Solid State Ionics, 28 (1988) 1715.
-M. F. Daniel, B. Desbat, J. C. Lassègues and R. Carie, J. of Solid State Chem. 77 (1988) 127.
-M. Green and Z. Hussain, J. Appl. Phys. 69 (1991) 7788.

(16) C. Geoffroy, Doc. Thesis (University of Bordeaux I, France 1990).

(17) N. F. Mott, Philos. Mag. B 22 (1970) 7.

(18) E. A. Davis, N. F. Mott, Philos. Mag. B 22 (1970) 903.

(19) S. D. Han, G. Campet, S. J. Wen, J. C. Lassègues, J. Portier, In preparation for Mat. Sci. and Eng. B.

(20) G. Campet, Z. W. Sun, C. Puprichitkun, J. P. Manaud and J. Claverie, Phys. Stat. Sol. (a) 103 (1987) 175.

(21) Z. W. Sun and G. Campet, Mat. Sci. and Eng., B5 (1990) 455.

(22) Z. W. Sun and G. Campet, J. Act. Pass. Electron. Comp. 14 (1990) 47.

(23) G.Campet, C.Geoffroy, J.P.Manaud, J.Portier, Z.W.Sun, J.Salardenne and P.Keou Mat. Science and Eng.B8 (1991) 45 .

(24) P.Keou, Doc. Thesis (University of Bordeaux I, France 1990).

(25) S. Miyazaki, S. Kikkawa and M. Koizumi, Synthetic metals. 6 (1983) 211.

(26) S.J.Wen, G.Campet, J.Portier, G.Couturier, J.B.Goodenough, Mat. Science and Eng.B14 (1992) 92.

(27) S.J. Wen, Doc. Thesis (University of Bordeaux I, France 1992).

(28) S.D. Han, Doc. Thesis (University of Bordeaux I, France 1994).

(29) M.M. Thackeray, W.I.F.David, P.G. Bruce and J.B. Goodenough, Mater. Res. Bull. 18 (1983) 461.

(30) S.D. Han, G. Campet, S.J. Wen, J.C. Lassègues, J. Portier, In preparation for Solid State Ionics.

ANNEXE :

IV.2. LES ELECTRODES TRANSPARENTES: étude des propriétés électroniques (électriques et optiques) de semiconducteurs à base de In_2O_3

IV.2.1. Introduction; travaux antérieurs.

1. Du problème pratique vers l'approche fondamentale.

Certains oxydes (In_2O_3, SnO_2, ZnO, ...) possèdent la propriété remarquable qui est d'allier, sous certaines conditions de "dégénérescence", une conductivité de type métallique à une excellente transparence au rayonnement visible. La conductivité et la transparence les plus élevées ($\sigma_{25°C} \cong 8 \times 10^3 (\ \Omega\text{-cm}\ )^{-1}$ avec $T_{VIS} \geq 80\ \%$) avaient été obtenues par Granqvist et al. pour des films d'ITO[1].

Toutefois, les applications modernes, telles que les vitrages électrochromes pour bâtiments, exigeaient des valeurs de conductivité deux fois plus élevées, au moins, sans altération de la transparence.

La résolution de ce problème, d'ordre pratique, imposait un accroissement de la mobilité des porteurs sans abaissement de leur densité.

Une étude antérieure effectuée au LCS a ainsi porté sur l'étude systématique des facteurs limitant la mobilité électronique dans ITO (cf. 2, a, b et c). C'est ainsi que de nouvelles électrodes ayant les propriétés requises ont été proposées.

2. Une approche "chimique" des mécanismes de diffusion des porteurs pour l'amélioration des propriétés optiques et électroniques.

a. Etude de la diffusion des porteurs (électrons) par les impuretés neutres: propriétés électriques et structurales de monocristaux et de céramiques d'ITO.

Une étude comparative des propriétés optiques, électriques et structurales entre monocristaux et céramiques de mêmes compositions, effectuée antérieurement au LCS avait permis d'établir, pour la première fois, sensiblement la même limite, $x_{max.} \cong 0{,}02$, de solubilité de l'étain dans $In_{2-x}Sn_xO_3$ [2].

Au-delà de cette limite la phase $SnO_{2-\varepsilon}$ apparaissait et provoquait une chute de mobilité électronique (diffusion des porteurs par l'impureté neutre $SnO_{2-\varepsilon}$) (fig.IV. 1). Toutefois, lorsque $x \leq 0.02$, la mobilité croissait lorsque x augmentait.

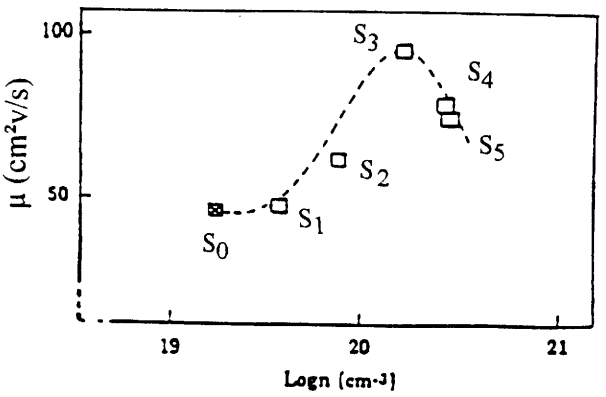

Fig. IV. 1 **Evolution de la mobilité en fonction de la densité électronique.**
■ monocristal de In_2O_3 (IO)
□ monocristaux de $In_{2-x}Sn_xO_3$ (ITO) avec
$x = 0{,}005$ (S_1) ; 0,01 (S_2) ; 0.02 (S_3) ; 0,04 (S_4) ; 0,08 (S_5).
Lorsque $0 \leq x \leq 0{,}02$, la conductivité augmentait avec x par suite d'un accroissement simultané de μ et n.

Une telle "heureuse" évolution avait pu être attribuée à une diminution de la masse effective des porteurs, liée à une modification du bord de bande.

b. Etude de la diffusion des porteurs par les joints de grains: propriétés de transport des céramiques à base de IO et d'ITO non dopées et dopées (Cu, F...).

Cette étude avait été consacrée à des céramiques et des films minces (remarquons que ces derniers pouvaient être considérés comme des céramiques de faible épaisseur). Une élévation de la mobilité électrique avait été observée pour des céramiques dopées par le fluor ou le cuivre. Cette élévation de la mobilité résultait d'un accroissement de la compacité [3].

c. Etude de la diffusion des porteurs par les impuretés ionisées: sur une nouvelle famille d'éléments dopants dans IO ou ITO, induisant une amélioration simultanée de la conductivité et de la transparence.

Les études précédentes avaient permis de se placer dans la situation idéale où la mobilité était limitée principalement par la diffusion des porteurs par les impuretés ionisées. Il était alors possible d'examiner l'influence directe de divers dopants sur les propriétés électroniques elles-mêmes, en particulier sur la mobilité. Deux règles simples permettaient de choisir le cation

idéal qui en se substituant à l'indium (ou à l'étain) dans IO (ou ITO) induisait un accoissement de la mobilité électronique.

Régle 1:

Il est souhaitable, mais pas indispensable, que le cation du dopant existe sous deux degrés d'oxydation.

La création des porteurs peut alors être illustrée par l'un des deux mécanismes:

In^{3+} est remplacé par $M^{(m-n)+} \rightarrow M^{m+} + ne^-$ dans la bande de conduction

In^{3+} est remplacé par $M^{m+} + (m-3)e^-$ dans la bande de conduction

Régle 2:

Le cation M^{m+}, associé au niveau donneur ionisé doit avoir:

* un fort pouvoir polarisant pour attirer fortement vers lui les anions (oxygène) afin de mieux écranter sa charge vis-à-vis des électrons de conduction,
* une électronégativité qui soit la plus faible possible afin d'affaiblir le pouvoir attractif du cation vis-à-vis des électrons de conduction (sans tenir compte de l'effet d'écrantage précité) [4,5].

Dans ces conditions, le dopage de In_2O_3 (IO) ou de ITO par Zr^{4+} et notamment par Ti^{4+} et Ge^{4+} s'est révélé être particulièrement prometteur (c.f. §IV. 2. 2. et IV. 2. 3.).

REFERENCES

1. Granqvist et al., J. Appl. Phys., 64 (1988) 5117.
2. S. J. Wen, G. Couturier, J. P. Chaminade, J. Solid State Chem. 101 (1992) 203.
3. S. J. Wen, G. Couturier, G. Campet, J. Portier, J. Claverie, Phys. stat. sol. (a) 130 (1992)407.
4. S. J. Wen, G. Campet, G. Couturier, J. Portier, J. B. Goodennough, Mat. Science and Engineering -B-8, 303 (1991).
5. J. Portier, G. Campet, B. Tanguy, J. Etourneau, Ecl. Quim. 17 (1992) 63.

IV. 2. 2 THE ELECTRONIC EFFECT OF Ti^{4+}, Zn^{4+} AND Ge^{4+} DOPING UPON THE PHYSICAL PROPERTIES OF In_2O_3 AND Sn-DOPED In_2O_3 CERAMICS:

application to the realization of new highly-transparent conductive electrode.

(publication)

Materials Science and Engineering, B19 (1993)285-289

The electronic effect of Ti^{4+}, Zr^{4+} and Ge^{4+} dopings upon the physical properties of In_2O_3 and Sn-doped In_2O_3 ceramics. Application to the realization of new highly-transparent conductive electrodes.

G. Campet*, S.D. Han, S.J. Wen and J. Portier
Laboratoire de Chimie du Solide du CNRS, Université de Bordeaux I, 351 Cours de la Libération, 33405 Talence, France.

Y. Xu, J. Salardenne
Laboratoire d'Etude des materiaux pour la Microelectronique,
Université de Bordeaux I, 351 Cours de la Libération, 33405 Talence, France.

Abstract

The electronic properties of In_2O_3 (IO) and Sn-doped In_2O_3 (ITO) ceramics doped with Ti^{4+}, Zr^{4+} or Ge^{4+} are investigated. The choice of the doping elements arises from their high value of the "Lewis acid strength". Related to that, it has been shown that the doping of IO or ITO ceramics with Zr^{4+} and most interestingly with Ti^{4+} or Ge^{4+}, increases both the carrier concentration and the mobility. This approach has been successfully applied to thin films, and new highly-transparent conductive electrodes have been realized.

---

* author to whom correspondence should be adressed.

1. Introduction

Transparent electronic conductors have beeen widely investigated during the last half century [1-5]. Some "exotic oxides" can be used as electrodes in optoelectronic devices in which it is necessary to collect electrons (or to apply an electrical voltage) and to transmit an optical beam through the electrodes simultaneously. (Remark: For these applications, metal and alloy based films cannot be used as electrodes because they reflect visible light. Most of the heavily doped n-type or p-type semiconducting films based on transitional metal compounds (for example, n^+-TiO_2, n^+-$SrTiO_3$, p^+-NiO,...) which possess the proper sheet resistance needed for electrode materials strongly absorb visible light. Thus the conditions to be met in such electrodes appear to be the following [6].

(1) The stoichiometric, or undoped, host compound should be an insulator with a conduction band edge (E_c) lying at at least 2.5 eV above the top of the valence band and at least 2.5 eV below the next higher conduction band. This condition is fulfilled in oxides where the conduction band is mainly the metal- 5s (4s) band such as In and Sn (and Zn) oxides; the next higher band is the metal-5p (4p) band, and the valence band is mainly the oxygen $2p^6$ band.

(2) The host compound should be doped so that it becomes an n-type semiconductor Moreover the doping must result in a degenerate conduction band with a low enough carrier concentration so that (i) the plasma frequency, ω_p, associated with the free carriers remains below the range and (ii) almost no electrons are trapped in localised states below the conduction band edge. It is the latter part of the second condition that appears to be difficult to fulfil in transition metal compounds (see the remark above).

In the case of indium oxide films, doping the parent compound has been accomplished by introducing oxygen vacancies, In_2O_{3-y} (IO), and also by substituting quadrivalent Sn^{4+} for In^{3+} ions, $In_{2-x}Sn_xO_{3-y}$ (ITO) [1-3]. In ITO films the oxygen vacancy concentration is generally much lower than that in Sn conenturation so that $y<<x$; besides segregation of $SnO_{2-\varepsilon}$ as a second phase limits the concentration "n" of mobile charge carriers [7]. $y<<x$ makes the electrical conductivity of ITO films primarily mobility limited

by scattering from the donor dopant ions. In the case of ITO films Hamberg and Granqvist obtained a transparency higher than 80% in the whole visible region, a resistivity as low as $1.9x10^{-4}$ S/cm, associated with a carrier mobility and a carrier concentration as high as 43 $cm^2/V.s$ and 8 x 10^{20} cm^{-3} respectively (based on Hall effect measurements). However, in spite of such high performances there is still a need for enhancing the conductivity and the transparency in the whole of the visible region due to the increasing sophistication of active and passive devices based on ITO thin films.

Therefore one important question arises; "Can the conductivity and the transparency of ITO be improved by doping with appropriate elements?" Given an upper limit on the charge carrier desity "n", which appears to be imposed by an intrinsic reduction limit of the In-O array [7], the search for a higher $\sigma = ne\mu$, should turn to search for a higher electronic mobility μ. Moreover, an enhanced carrier mobility may result in an enhanced transparency of the films [1]

$$\mu \propto \lambda / m^* A_{\text{free carriers}} \qquad (1)$$

Where, $A_{\text{free carriers}}$ symbolizes the photon loss due to free carrier absorption; λ and m^* designate, respectively, the photon wavelength and the carrier effective mass. It implies that in ITO based films an enhancement of the carrier mobility has to be carried out. That has to occur through the use of more appropriate dopants than Sn, whose scattering effect with regard to conduction band electrons is reduced. In fact we have recently shown [6], that the ideal dopant cation should have low electronegativity (χ) and ionic radius (r) associated with higher effective nuclear charge (Z^*). Indeed, such a cation, having high value of Z^*/r^2 will polarize the electron cloud of oxygen $2p^6$ valence band more strongly thereby screening its charge so as to weaken it as a scattering center [6]. Moreover a low electronegativity for the dopant cation would account for a weak interaction between the conduction band electrons and the dopant -cation. The empirical relation established by Zhang [8] is

$$L = Z^*/r^2 - 7.7 + 8.0 \qquad (2)$$

Where, L symbolizing, in Zhang's notation, the "Lewis acid strength" of the element, accounts for this approach [6]. Consequently high mobilities, and thereby high conductivities are likey to occur for ITO (IO) samples heavily doped with cations having high L values.

Following this guide-line, it appears that the use of Ge^{4+} or Ti^{4+} and to a lesser extent of Zr^{4+} as a doping element in ITO (partially or totally substituted to Sn^{4+}) would be judicious. Indeed, one has [8]

$$L(Ge^{4+}) \cong L(Ti^{4+}) = 3.06 >> L(Sn^{4+}) = 1.62 \qquad (3)$$

However

$$L(Zr^{4+}) = 2.03 > L(Sn^{4+}) \qquad (4)$$

Consequently, IO or ITO doped with Zr^{4+} or more particularly with Ti^{4+} or Ge^{4+} should have a higher conductivity, associated with a higher carrier mobility than a bare IO or ITO.

In order to investigate thoroughly the effect of doping of IO or ITO films on their electronic properties, it is worthwhile to study ceramics first. Indeed, the concentration of the doping element can be more easily modulated in ceramics than in thin films and hence its influence on the electronic properties can be more accurately investigated in ceramics (Remark: We have previously reported that Ge^{4+} doping of IO and ITO ceramics induces a significant enhancement in the carrier mobility [6]. Indeed, we will investigate here Ti^{4+} and Zr^{4+} doped IO and ITO ceramics and compare the results with Ge^{4+} doped IO and ITO ceramics.) Such a methodical approach, therefore, consisting of first studying ceramics and then thin films, will be followed here. We note at the outset that films have the same "disadvantages" as the ceramics, such as the relative small size of the grain, which can cause a drop in the carrier mobility: such a grain boundary effect has been studied elsewhere [9].

2. Experimental details

a. Sample preparation

All the samples were prepared under similar conditions. Powders obtained by intimately mixing 0.3g of the starting oxides (see Table 1) were cold-pressed in steel die and then isostatically pressed at 5 tons/cm^2. The pressed pellets were heated up to 1300°C at a rate of 100°C/h and then sintered at that temperature for 24 hours. They were subsequently cooled at a rate of 100°C/h.

The structure and texture of the sintered samples were examined using X-ray powder diffraction and by electron microscopy. For all the ceramics, the grain sizes (average ca 1μm) and densities (about 0.72, theoretical) were all comparable.There was no evidence of second phase formation at the grain boundaries for doping concentrations of 1at. % (i.e. corresponding to 100x = 2, as shown in the Table 1).

b. Thin film preparation

For the sake of clarity we will report here on two types of films: (1) "conventional" ITO films and (2) Ge^{4+}-doped ITO, symbolized as ITGO. Results on Ge^{4+}- doped IO and Ti^{4+} and Zi^{4+} doped IO and ITO films will be given elsewhere [10]; let us simply mention that they are consistent with our above mentioned approach.

The ITO and ITGO films were deposited on glass substrates using an RF magnetron cathodic polarisation technique with home made targets. The study has been systematically carried out using various targets of different compositions and various deposition conditions [11]. However, for simplicity we will present here only the ITO and ITGO films which have the highest electronic performances, within the frame of our experimental procedure reported in Table 2.

c. Electrical and optical measurements

Accurate values of conductivity, σ, (using A.C. Van der Pauw four probe technique), the carrier concentration "n" (from the Hall effect measurements in a magnetic field of 2.5T) and the Hall mobility μ (calculated using the expression $\mu = \sigma / n e$) have been carried out. In-Ga eutectic or silver paste ensured electrical contacts. Spectral transmission in the range 300-900nm were recorded on samples using a Cary 17 ratio-recording spectrometer.

3. Results and discussion

a. Ceramics: Ti, Zr and Ge doped IO and ITO systems

For an accurate comparitive study, we have chosen for all samples the same doping concentration equal to 1(atomic) %, i.e. corresponding to x = 0.02 (Table 1). A slight decrease in lattice parameters, consistent with the smaller size of the dopant (Ti^{4+}, Zr^{4+} and Ge^{4+}) relative to In^{3+} and Sn^{4+} is observed. Figure 1 shows the evolution of the room temperature Hall carrier mobility and carrier concentration as a function of doping element for undoped and Zr^{4+}-, Ge^{4+}- or Sn^{4+}-doped IO samples. Of particular note is the enhanced Hall mobilty in Ti^{4+}-, Zr^{4+}- and Ge^{4+}-doped IO samples compared with that of IO and ITO. We know that in heavily doped n-type semiconductors, as occurring here, the mobility is primarily limited by the scattering of electrons from ionized donor centers. Such scattering effect is reduced for Zr, Ti and Ge doped samples because the "Lewis acid strength" of the donor element is high (as we have shown above) and thereby accounts for the evolution of the electronic properties illustrated in Fig. 1. Finally Fig. 2 shows the increase in carrier mobility when the ITO (Sn/(In+Sn) = 0.01) is doped with Zr or more particularly by Ti or Ge. This significant result is justified on the basis of our above reported arguments.

b. Applications to thin films : ITGO as a judicious way to improve the properties of transparent conductive electrodes

Table 1. The choice of the doping elements (IO doped samples).

Ceramic symbolization	Starting materials (99.999%, Alfa)	Doping elements	Examples of formation of conduction band el. (e^-[CB])
IO	In_2O_3	None	"active" oxygen vacancies $In_2O_3 \rightarrow In_2O_{3-x}e^-[CB]_{2x}$
IGO	$xGeO_2+(1-x/2)In_2O_3$ $(100x=2)$	Ge^{4+}	$In^{3+} \rightarrow Ge^{4+}+e^-[CB]$
IZO	$xZrO_2+(1-x/2)In_2O_3$ $(100x=2)$	Zr^{4+}	$In^{3+} \rightarrow Zr^{4+}+e^-[CB]$
ITiO	$xTiO_2+(1-x/2)In_2O_3$ $(100x=2)$	Ti^{4+}	$In^{3+} \rightarrow Ti^{4+}+e^-[CB]$
ITO	$xSnO_2+(1-x/2)In_2O_3$ $(100x=2)$	Sn^{4+}	$In^{3+} \rightarrow Sn^{4+}+e^-[CB]$
ITGO	$xGeO_2+xSnO_2$ $+(1-x)In_2O_3$ $(100x=2)$	Ge^{4+}, Sn^{4+}	$In^{3+} \rightarrow Ge^{4+}+e^-[CB]$ $In^{3+} \rightarrow Sn^{4+}+e^-[CB]$
ITZO	$xZrO_2+xSnO_2$ $+(1-x)In_2O_3$ $(100x=2)$	Zr^{4+}, Sn^{4+}	$In^{3+} \rightarrow Zr^{4+}+e^-[CB]$ $In^{3+} \rightarrow Sn^{4+}+e^-[CB]$
ITTiO	$xTiO_2+xSnO_2$ $+(1-x)In_2O_3$ $(100x=2)$	Ti^{4+}, Sn^{4+}	$In^{3+} \rightarrow Ti^{4+}+e^-[CB]$ $In^{3+} \rightarrow Sn^{4+}+e^-[CB]$

Table 2. Sputtering conditions for ITO (Sn/In=0.1) and ITGO (Sn/In=0.05, Ge/In=0.01) films.

Ambient mbar	Power supply and frequency	Target to substrate distance	Substrate temperature	Film thickness	Morphology [11]
Ar 8×10^{-3}	60 W 13.56 MHz	6 cm	320 °C	1300 Å	average crystallite size = 700 Å

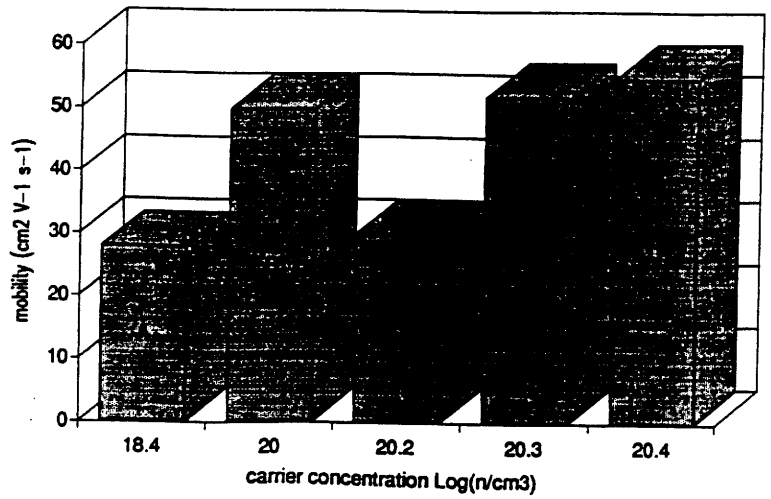

Fig. 1. Evolution of the room temperature carrier mobility and carrier concent ration as a function of the doping elements. A = IO, B = IZO, C = ITiO, D = IGO, E = ITO. For all samples: M/(In+M) = 0.01, and M = Ti, Zr, Ge and Sn.

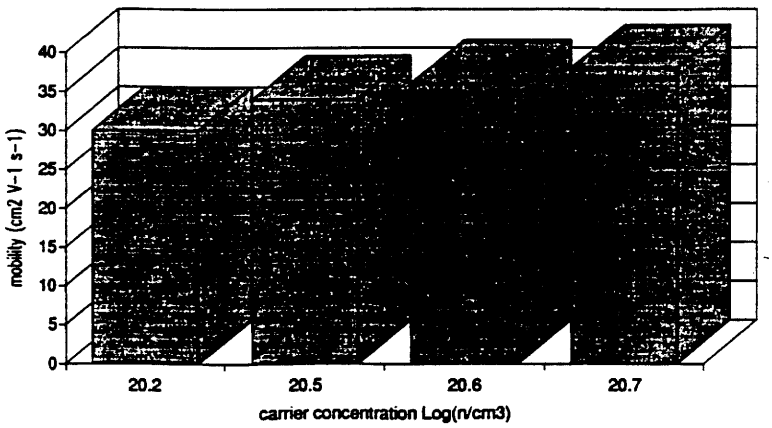

Fig. 2. Evolution of the room temperature mobility and concenturation of carriers as a function of the doping elements. B' = ITZO (starting materials: Sn/(In+Sn+Zr) = 0.01; Zr/(In+Sn+Zr) = 0.01). C' = ITTiO (starting materials; Sn/(In+Sn+Ti) = 0.01; Ti/(In+Sn+Ti) = 0.01. D' = ITGO (starting materials; Sn/(In+Sn+Ge) = 0.01; Ge/(In+Sn+Ge)=0.01). E=ITO which has the same meaning as in Fig. 1. The sample symbolization is chosen to be consistent with that of Fig. 1.

Table 3. Electrical properties of ITO and ITGO films deposited using conditions given in Table 2

	ρ (Ω cm)	n (cm^{-3})	μ ($cm^2 V^{-1} s^{-1}$)	$R_{\square}(\Omega)$
ITO	3.12×10^{-4}	7.25×10^{20}	28	24.0
ITGO	1.66×10^{-4}	1.12×10^{21}	34	12.8

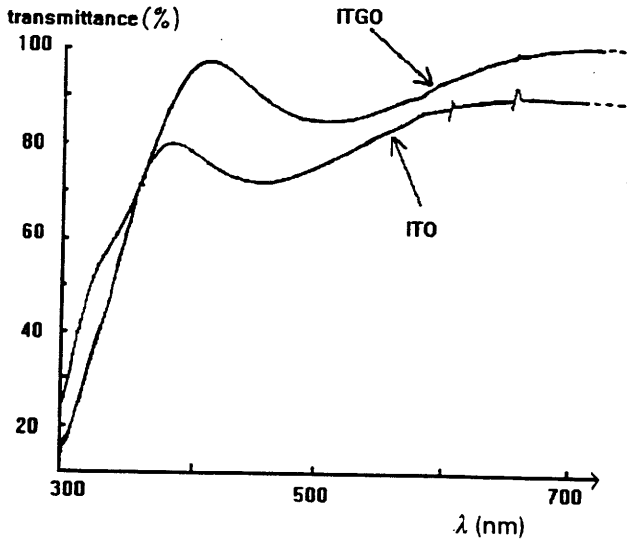

Fig. 3. Transmission spectra for ITO and ITGO films of 130 nm thickness.

It follows that the electronic properties of "conventional ITO" films should be significantly improved by doping with Zr^{4+} or more particularly with Ti^{4+} or Ge^{4+}. As pointed out above we will illustrate our approach merely by comparing the electronic properties of ITGO (i.e., Ge^{4+}- doped ITO) and "conventional" films prepared using similar procedure (Table 3).

Although the average crystallite size is relatively small (~ 700 Å as indicated in Table 2), the related grain boundary effect [9] does not entirely mask the Ge-doping effect: indeed, the ITGO films clearly exhibit higher carrier mobility than ITO (Table 3). Consequently, the "$R_{\square}$" (which is the ratio of the sample resistivity over the thickness) value of 12.8 ohm, occurs: it is about two times lower than that of ITO (table 3). Most interestingly, the carrier mobility observed for ITGO gives the film a higher transparency in the visible region (Fig. 3). Comparing the properties given in Table 3 and shown in Fig. 3, it is clear that an improvement in both electrical and optical properties can be achieved by doping ITO films with Ge^{4+}.

4. Conclusions

The electronic propeties of IO and ITO can be improved by doping with Zr^{4+} and, to a large extent with Ti^{4+} or Ge^{4+}. For instance the charge carrier densities in ITGO based ceramics and films are nearly twice those of ITO, although the electronic mobility in ITGO is higher. We attribute all the results to the higher "Lewis acid strength", for Zr^{4+}, Ti^{4+} and Ge^{4+} compared with Sn^{4+}.

Let us finally point out that higher electronic performances could be expected, for ITGO (ITTiO ...) films, using a different deposition technique, such as reactive evaporation[3].

Acknowledgments

The authors wish to thank Profs. G. Couturier and M. C. R. Shasrtry for helpful assistance.

References

1. K.L. Chopra, S. Major and D.K. Pandya, Thin Solid Films, 102 (1983) 1 and references there in.
2. A. Bharadwaj, B.K. Gupta, A. Rizza, A.K. Sharma and O.P. Agnihotri, Sol. Cells, 5 (1981-1982) 39.
3. I. Hamberg and C.G. Granqvist, J. Appl. Phys., 60 (1986) 123 and references there in.
4. Z. C. Jin, J. Hamberg and C.G. Granqvist, J. Appl. Phys. 64 (1988) 5117.
5. B. Stjerna and C.G. Granqvist, Appl. Phys. Lett., 57 (1980) 1989.
6. S.J. Wen, G. Campet, J. Portier, G. Couturier and J.B. Goodenough, Mat. Sci. and Engg. B, 14 (1992) 115.
7. S.J. Wen, G. Couturier, G; Campet, J. Portier and J. Claverie and P. Hagenmuller, J. Sol. Stat. Chem. (to be published).
8. Y. Zhang, Inog. Chem. 21 (1982) 3886.
9. S.J. Wen, G. Couturier, G. Campet, J. Portier, J. Claverie, Phys. Stat. Sol (a), 130 (1992) 407.
10. Y. Xu, J. Salardenne, G. Campet and J. Portier (under preparation for Active and Passive Elec. Comp.)
11. Y. Xu, J. Salardenne, S.J. Wen, G. Campet, T. Buffeteau and B. Destat (under preparation for Thin Solid Films).

IV. 2. 3. CORRELATION BETWEEN THE THERMOELECTRIC POWER AND HALL EFFECT OF Sn OR Ge DOPED In_2O_3 SEMICONDUCTORS.

(publication)

Materials Science and Engneering, B22 (1994) 274.

Correlations between the thermoelectrtic power and Hall effect of Sn or Ge doped In_2O_3 semiconductors

G. Campet*, S. D. Han, S. J. Wen +, M.C.R. Shastry, B. Chaminade, E. Marquestaut, J. Portier and P. Dordor

Laboratoire de Chimie du Solide du CNRS, Université de Bordeaux I, 351 Cours de la Libération, 33405, Talence cédex, FRANCE

Abstract

The thermoelectric power and Hall effect of Sn or Ge-doped In_2O_3 semiconductors are investigated based on a comparitive study. The metal-type conductivity in both the samples occurs when the carrier concentration exceeds ~10^{19} cm^{-3}. The carrier mobility is found to be higher for Ge-doped samples. The relation between the "Lewis acid strength" of the dopant element and its scattering cross section is also presented.

---

* For correspondence

+ Present address: University of Waterloo, Department of Chemistry, Waterloo, Ontario, Canada N2L 3G1.

1. Introduction

There has been a renewed interest in the last few years to investigate materials which are transparent in the visible region and at the same time possess metal-type electronic conductivity. The simultaneous occurence of optical transparency in the visible region and electronic conductivity requires the creation of electron degeneracy in a wide-band-gap-material by non-stoichiometry and/or appropriate dopants. These conditions can conveniently be obtained for indium oxide (IO) and tin-doped indium oxide (ITO) in thin film form or single crystals. The creation of electrons or metal-type conductivity in these compounds can be accounted for according to the reactions (1) and (2) [1-7] :

(IO)

$$In_2O_3 \text{ ------} > In_2^{3+}O^{2-}_{3-\varepsilon} + 2\varepsilon[e^-(CB)] + \varepsilon/_2\, O_2 \qquad (1)$$

(ITO)

$$x(In_2O_3) + 2\varepsilon(SnO_2) \text{ ---} > In_{2x}^{3+}Sn_{2\varepsilon}^{4+}O^{2-}_{3(x+\varepsilon)} + 2\varepsilon[e^-(CB)] + \varepsilon/_2 O_2 \qquad (2)$$

In the case of ITO, the delocalized electrons in the band can also arise from active oxygen vacancies according to the following process.

$$x(In_2O_3) + 2\varepsilon(SnO_2) \text{ ---} > In_{2x}^{3+}Sn_{2\varepsilon}^{4+}O^{2-}_{3(x+\varepsilon)-p} + 2(\varepsilon+p)[e^-(CB)] + (\varepsilon+p)/_2\, O_2 \qquad (3)$$

The conductivity in heavily doped ITO films is strongly dependent on the concentration of the dopant. The film compactness and the size of the particles can also have a crucial influence on the conductivity [1-8]. The highest conductivity measured in the case of ITO thin films is about 10^4 S/cm [3]. However, with increasing sophistication of active and passive devices based on ITO thin films, there is still a need for improved electrical and optical properties. Therefore an important question arises : "can the conductivity (σ) of ITO be even more improved by doping with other appropriate elements which at the same time do not affect the film transparency?"

Given an upper limit on the charge carrier concentration 'n' which appears to be imposed by an intrinsic reduction limit of the In-O array [6,7], the search for a higher $\sigma = ne\mu$, must turn to search for a higher electronic mobility μ. That has to occur through the use of more appropriate dopants than Sn. In fact we have recently shown [6,9,10] that the ideal doping cation must have a low electronegativity (χ) and a small ionic radius (r)

associated with high effective nuclear charge (Z^*). Indeed, such a cation having high value of $Z^*/_{r2}$ will polarize the electron cloud of oxygen $2p^6$ valence band more strongly thereby screening its charge so as to weaken it as a scattering center. Moreover, a low electronegativity for the dopant cation accounts for a weak interaction between the conduction band electrons and the dopant cation. Zhang [11] established an empirical equation relating the Lewis acid strength of the cation, L, its electronegativity and the $Z^*/_{r2}$ value as

$$L = Z^*/_{r2} - 7.7\,\chi + 8.0 \qquad (4)$$

Under such a circumstance, a high L value of the doping cation necessarily means a reduced scattering effect (and thereby a reduced scattering cross section) of the doping cation with regard to the conduction band electrons. Therefore, when the factor dominating the mobility is the scattering of electrons from the ionized donor centers, higher (lower) mobilities will occur for semiconductors doped with donor elements having higher (lower) L values [6,9,10]. Following this guide line, it appeared that use of Ge^{4+} as a doping element in ITO (partially or totally substituted to Sn^{4+}) could induce an enhancement in the mobility since [11]

$$L_{Ge^{4+}} = 3.06 > L_{Sn^{4+}} = 1.62 \qquad (5)$$

In the present study our main emphasis will be on complementing the choice of geramanium as a dopant using both thermoelectric power and Hall effect measurements performed on a series of In_2O_3 samples either undoped or doped with Sn or Ge. The experiments have been carried out on single crystals and ceramics.

2. Priliminary considerations related to the Thermoelectric power

In this section we shall recaptulate some of the important relations which will be used later in this article. The thermoelectric power (α) which is the temperature gradient of the total emf, is genarally defined as [12,13]

$$\alpha = \Delta E/\Delta T = \Delta(\phi - \mu^* kT/q)/_{\Delta T} \qquad (6)$$

where, ϕ and μ^* designate the electrostatic and reduced electrochemical potentials respectively. In the case of completely non-degenerate semiconductors, Fistul established the following relations [14]

$$\alpha_l = -k/q(2-\mu^*) \quad (7)$$

$$\alpha_i = -k/q(4-\mu^*) \quad (8)$$

α_l and α_i symbolising the thermoelectric powers in a particular case of the carriers whose scattering is mainly limited by phonons and by ions respectively, 'k' being the Boltzmann constant. Let us recall that on one hand, for totally non-degenerate semiconductors the value of the reduced electrochemical potential is less than -2, a value lower than that for the degeneracy limit, $\mu^* = -2$, and under such a circumstance, the dependence of α, as a function of the conduction band carrier concentration, 'n', can be evaluated. Indeed, whatever scattering mechanism intervene (phonon scattering or impurity scattering) 'n' sensibly varies as [15]:

$$n = (\pi)/2 \; N_c \, e^{\mu^*} \quad (9)$$

$N_c = 4\pi(2m^*kT/h2)^{3/2}$ represents the effective density of states in the conduction band. Therefore, expressions (7) and (8) become respectively

$$\alpha_l = -k/q \, [2-Ln(2n/\pi N_c)] \quad (10)$$

$$\alpha_i = -k/q \, [4-Ln(2n/\pi N_c)] \quad (11)$$

On the other hand, in the degenerate semiconductor case ($\mu^* >> 0$), Fistul established the formulae [16]

$$\alpha_l = -k/q \cdot \pi^2/3 \cdot 1/\mu^* \quad (12)$$

$$\alpha_i = -k/q \; (\pi^2 \mu^*)/(\pi^2+\mu^{*2}) \sim -k/q \cdot \pi^2/\mu^* \quad (13)$$

In the case of carrier scattering by phonons or by impurity ions, the conduction band carrier concentrations vary respectively as [17,18]

$$n_l = 2/3N_c \, \mu^{*3/2} \quad (14)$$

$$n_i = N_c/3m^*kT \cdot \mu^{*3/2} \quad (15)$$

Substituting the equations (14) and (15) respectively in (12) and (13), we observe that α_l and α_i vary as $n_l^{-2/3}$ and $n_i^{-2/3}$ respectively.

3. Experimental

(i) Single crystal growth

Either undoped or Sn-doped IO single crystals have been prepared. The doped IO crystals were grown by two methods; (i) by the flux method as described by Remeika [19], (ii) by the vapour phase technique as described by Weiher [20]. These two methods generally yield single crystals with high and low carrier concentration respectively [7]. Inorder to get appropriate high conductivity uniquely the flux method was used to grow the Sn-doped IO single crystals.

(ii) Preparation of ceramics

Either undoped IO ceramics or IO ceramics doped with Sn or Ge, symbolised respectively as ITO and IGO, have been obtained. The undoped ceramics were prepared by heating the pellets (10mm diameter, 1mm thick) to various temperatures (1100°C, 1200°C, 1300°C and 1350°C) employing a heating rate of 100°C/h. The pellets were sintered at those temperatures for 24h. The ITO and IGO ceramics were prepared by intimately mixing the starting material oxides (i.e. $In_2O_3+SnO_2$ or GeO_2). The mixed powders were cold pressed in steel die and then submitted to an isostatic pressure of 5bars. The pellets so obtained were sintered in air for 24h. The heating and cooling rate (100°C) was controlled by an Eurotherm programmer. All electrical measurements were performed using equipments described elsewhere [7, 21].

4. Results and Discussion

(i) Single crystals

Values of the room temperature conductivity, σ, carrier concentration, 'n', and carrier mobility, 'μ', of undoped and of Sn-doped In_2O_3 single crystals are given in table I. The reported values are deduced from Hall effect measurements [7].

The samples 1 and 2, on one hand and samples 3,4 and 5 on the other, were grown from the vapour phase and the flux method respectively (§ III. (i)). Moreover, the differences in the values of the electrical parameters, occuring between samples 1 and 2 or between 3, 4 and 5 (table I) account for different experimental conditions [7, 10]. The decrease in the carrier mobility as 'n' increases, from 1-5, has been reported elsewhere and

accounts for the predominant scattering effect of carriers from the donor centres arising from oxygen vacancies [10]. On the other hand, for some Sn-doped samples (A---C) both 'n' and μ increase with the doping concentration because the carrier effective mass decreases as the impurity band merges with the conduction band [10]. For higher carrier densities (samples D and E) the mobility decreases and the carrier concentration reaches a 'plateau': indeed, in these samples $SnO_{2-\varepsilon}$ appears as a second phase limiting 'n' [10], and causing a decrease in μ related to neutral-impurity scattering phenomenon.

The thermoelectric power of all the samples has been investigated at room temperature. Fig. 1 illustrates the dependence of the thermoelectric power on the carrier concentration. Whereas for the samples with $n < 3.8 \times 10^{19}$ cm^{-3}, α varies proportional to logn (straight line on fig.1) which characterizes a non-degenerated situation. For higher concentrations this proportionality is no longer observed; indeed, for samples B---E, α sensibly varies as $n^{-2/3}$ (relations (13) and (15)) in accordence with the degenarate situation with the predominance of carrier scattering by impurity ions (albeit for sample E the neutral impurity scattering phenomenon reported above also interferes).

(ii) Ceramics

Values of the room temperature conductivity, carrier concentration and mobility, all measured by Hall effect, for undoped and for Sn- or Ge-doped In_2O_3 ceramics are given in table II. The increase (decrease) of n (μ), observed in samples a---c, obviously accounts for an enhancement in the oxygen-vacancy concentration, as mentioned above for undoped single crystals. As the dopant concentration is increased, 'n' increases in the beginning for both Sn-doped (d---g) and Ge-doped (i--l) samples and later reaches a plateau (samples g, h and l, m), correlated to the formation of a second phase ($SnO_{2-\varepsilon}$ or $GeO_{2-\varepsilon}$) as evidenced by X-ray analysis. Moreover, the grain boundary effect inhibits the normally expected increase in the carrier mobility with the Sn ratio (samples d---h), which has been observed for single crystals (see table I, samples A---C). However, grain boundary effects do not entirely hinder the "beneficial" effect of Ge doping on μ. As it is clear from table II despite being ceramics, Ge-doped samples show an increase in μ, which has not been observed for Sn-doped samples. It is important to note that, for similar carrier concentrations, μ is about 50% (or more) higher for IGO than for ITO.

The thermoelectric power, like the mobility can be governed by the scattering mechanisms of the carriers. Therefore, we can expect different values of α for In_2O_3 heavily doped with Sn or Ge impurities. That is illustrated hereafter for samples heavily doped with Sn (e---h) or with Ge (j---m). It is clear from fig. 2 that α values referring to

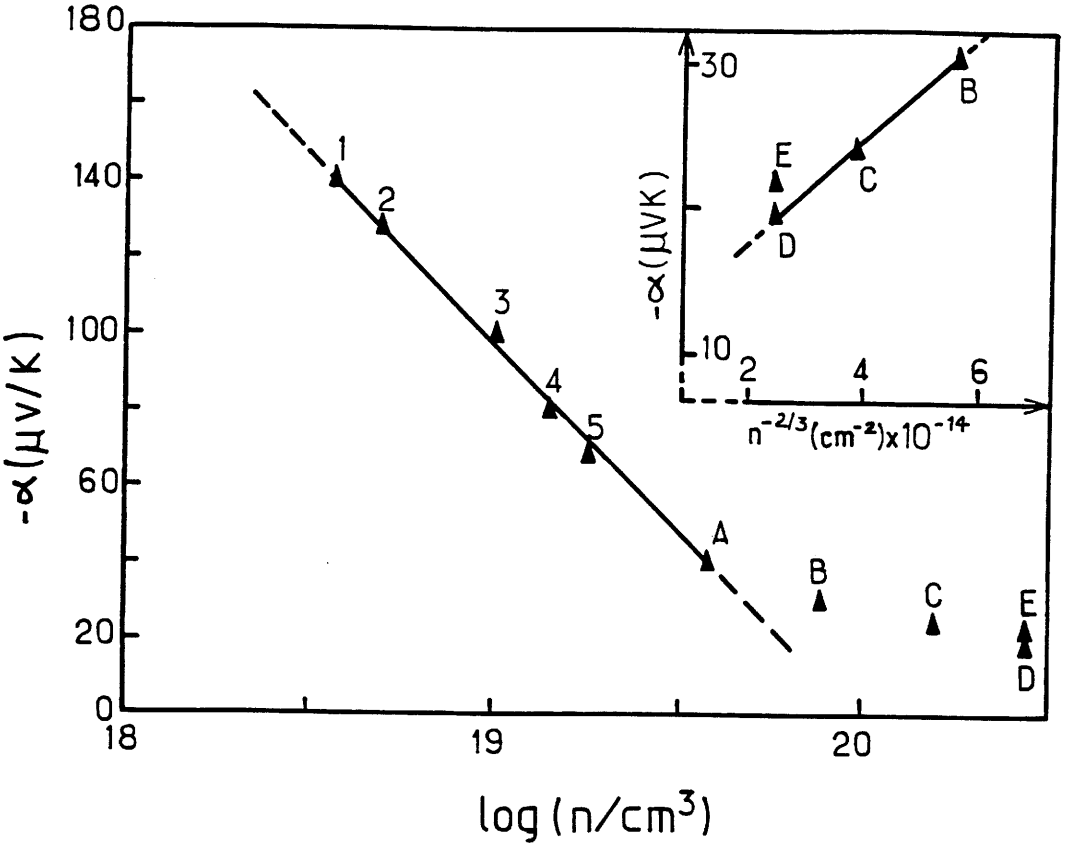

Fig. 1. Dependence of Thermoelectric Power on electron density in undoped and Sn-doped In_2O_3 single crystals at 300K. Numbers and symbols correspond to the same samples as in in Table 1.

Table 1. Values of the carrier mobility, carrier concentration and room temperature conductivity for the undoped (samples 1---5) and Sn-doped In_2O_3 (samples A---E) singlecrystals [10].

$Sn_{/(In+Sn)}$ ratio * (% values)	Sampl symbol	μ_H ($cm^2V^{-1}s^{-1}$)	$n_H \cdot 10^{18}$ (cm^{-3})	$s_H \cdot 10$ (S/cm)
$Sn_{/(In+Sn)}=0$	1	85	2.5 3.40	
$Sn_{/(In+Sn)}=0$	2	70	3.98	4.50
$Sn_{/(In+Sn)}=0$	3	65	10	10.4
$Sn_{/(In+Sn)}=0$	4	58	14	13.0
$Sn_{/(In+Sn)}=0$	5	45	18	13.0
$Sn_{/(In+Sn)}=0.25$	A	48	38	29.2
$Sn_{/(In+Sn)}=0.50$	B	62	78	77.4
$Sn_{/(In+Sn)}=0.80$	C	100	160	256
$Sn_{/(In+Sn)}=1.30$	D	81	280	363
$Sn_{/(In+Sn)}=2.50$	E	75	280	336

* The ratio $Sn_{/(In+Sn)}$ corresponds to 10^2x in $In_{2-2x}Sn_{2x}O_3$.

samples j---m are somewhat higher than those referring to samples e---h. This can be understood, using the equation (13), for the sake of simplicity, which is valid in the degenarate case. Using the expression (13) the basic nature can indeed be foreseen ; one can write

$$\alpha_{IGO}/\alpha_{ITO} \sim \mu^*_{ITO}/\mu^*_{IGO} \quad (16)$$

And also μ^* depends upon the carrier mobility, the carrier effective mass and the scattering cross section Q according to [23]

$$\mu^* = q^2/2m^* n^2 \mu^2 Q^2 \quad (17)$$

Consequently, we can obtain the following expression after simple transformation

$$\alpha_{IGO}/\alpha_{ITO} = [\mu_{IGO}/\mu_{ITO}]^2 [Q_{Ge^{4+}}/Q_{Sn^{4+}}]^2 \quad (18)$$

Using the relation (17), the μ and α values, given respectively in table II and in fig. 2, one gets

$$Q_{Ge^{4+}}/Q_{Sn^{4+}} \sim 0.55$$

It is interesting to note that for similarly heavily doped ITO and IGO (such as f and k) the value obtained above is close to the ratio calculated based on the Lewis acid strengths [11]. Using relation (5) we get,

$$L_{Sn^{4+}}/ L_{Ge^{4+}} \sim 0.53$$

This result confirms the expected close relation between the scattering cross section of the dopant ion and its Lewis acid strength. It appears that when the factor dominating the mobility is the scattering of electrons from the ionized donor centres, L roughly varies inversely as Q.

We note here that the concepts we have put forward also apply for other degenarate oxides having a predominant ionic-bond character as we have recently investigated [9]. Apriori, they may also be conveniently used for semiconductors having covalent-bond character such as Si or Ge heavily doped by As or P ($n >> 10^{19}$ cm^{-3} as it occured here for ITO and IGO) [23]. Matter-of-factly, the "Lewis acid strength" of phosphorous is larger than that of As which is in good agreement with expectation. One apparently has [23]

$$\alpha_{\text{P doped Si}} > \alpha_{\text{As doped Si}}$$

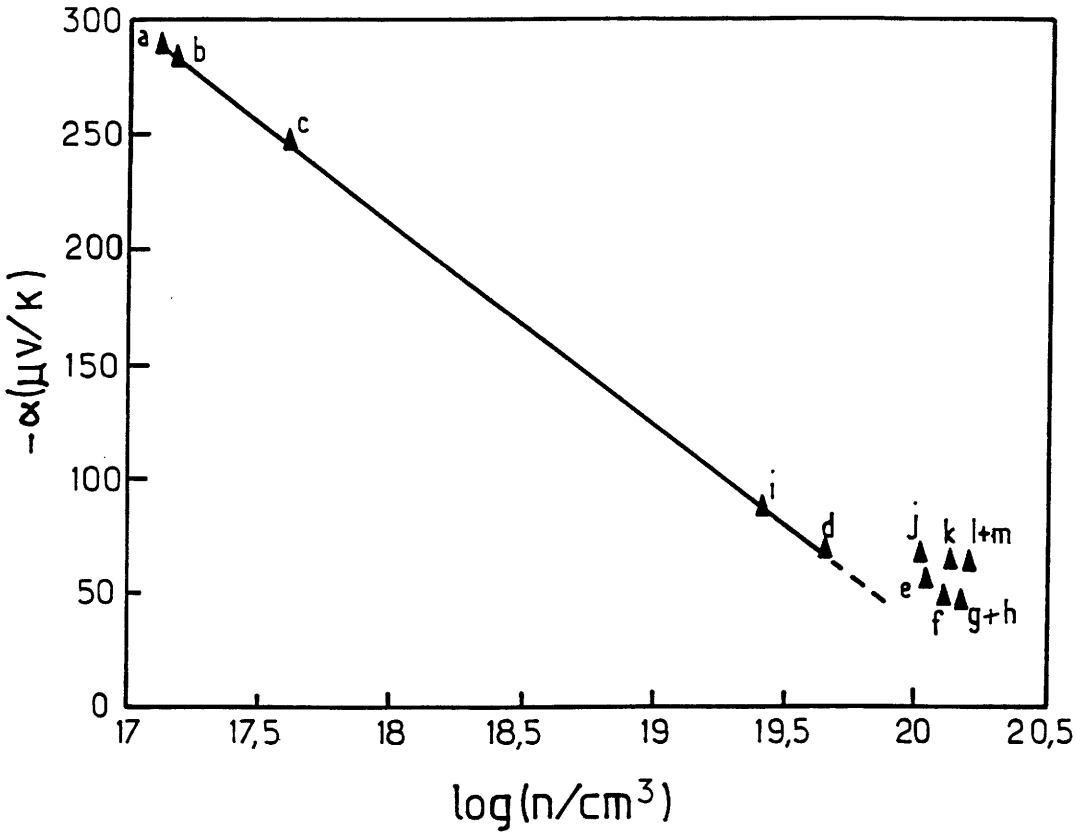

Fig. 2. Dependence of Thermoelectric power on the electron density in undoped or Sn- or Ge-doped In_2O_3 ceramics at 300K. Numbers and symbols correspond to the same samples as in Table 2.

Table 2. Values of the carrier mobility, carrier concentration and room temperature conductivity for the undoped (samples a---c) and Sn or Ge-doped In_2O_3 (samplesd---m)ceramics[3].

$M_{/(In+M)}$ ratio* M=Sn or Ge (% values)	Sample symbol	μ_H ($cm^2v^{-1}s^{-1}$)	$n_H \cdot 10^{18}$ (cm^{-3})	$s_H \cdot 10$ (S/cm)
$Sn_{/(In+Sn)}$ =0 sintered at 1100°C	a	40	0.13	0.083
$Sn_{/(In+Sn)}$ =0 sintered at 1200°C	b	45	0.15	0.108
$Sn_{/(In+Sn)}$ =0 sintered at 1350°C**	c	25	0.40	0.160
$Sn_{/(In+Sn)}$ =0.125	d	35.1	40.0	25.30
$Sn_{/(In+Sn)}$ =0.250	e	30.9	100	49.40
$Sn_{/(In+Sn)}$ =0.500	f	29.0	180	86.30
$Sn_{/(In+Sn)}$ =1.300	g	28.0	190	85.10
$Sn_{/(In+Sn)}$ =2.500	h	25.0	190	76.40
$Sn_{/(In+Ge)}$ =0.125	i	45.0	32.0	23.00
$Sn_{/(In+Ge)}$ =0.250	j	50.0	80.0	64.00
$Sn_{/(In+Ge)}$ =0.500	k	55.0	180	158.0
$Sn_{/(In+Ge)}$ =1.300	l	52.0	190	156.0
$Sn_{/(In+Ge)}$ =2.500	m	50.0	190	152.0

* The ratio $M_{/(In+M)}$ corresponds to 10^2x in $In_{2-2x}Sn_{2x}O_3$ or in $In_{2-2x}Ge_{2x}O_3$.

** No noticeable change in s occurs when the sintering temperature is increased above 1350°C [10], so all the Sn or Ge-doped samples have been sintered at 1350°C (§ III.(i)).

and

$$\alpha_{\text{P doped Ge}} > \alpha_{\text{As doped Ge}}$$

However, further investigation is necessary if one wishes to extend the simple concepts we have proposed here for ITO and IGO, to other semiconductors having, contrarily to ITO and IGO, a strong covalent-bond character.

4. Conclusions

An attempt has been made to compare the properties of Sn-doped and Ge-doped In_2O_3 in single crystal and ceramic forms. Thermoelectric power and Hall effect measurements have been carried out on all samples. It is evidenced that the Ge-doped samples possess higher mobility compared to the Sn-doped sample with the same carrier concentration. An empirical correlation of the Lewis acid strengths of the two ions to their scattering cross sections which can be used as a means to choose the doping cation has also been suggested.

Acknowledgements

The authors wish to thank prof. G. Couturier for useful discussions and technical assistance and Mrs. Radhika Shastry for her help in the preparation of the manuscript.

REFERENCES

1. K. L.Chopra, S. Majorand D. K. Pandya, Thin Solid Films, **102**, (1983), 1 and references therein.
2. A. Bharadwaj, B.K. Gupta, A. Rizza, A.K. Sharma and O.P. Agnihotri Solar Cells, **5**, (1981/1982), 39.
3. I. Hamberg and C.G. Granqvist, J. Appl. Phys. **60**, (1986), 123 and references therein.
4. Z. C. Jin, I. Hamberg and C.G. Granqvist, J. Appl. Phys. **64**, (1988), 5117 and references therein.
5. B. Stjerna and C.G. Granqvist, Appl. Phys. Lett. **57**, (1980), 1989 and references threin.
6. S.J. Wen, G. Campet, J. Portier, G. Couturier and J. B. Goodenough, Mat. Sci. and Eng. B, **14**, (1992), 115.
7. S.J. Wen, G. Coutirier, J.P. Chaminade, E. Marquestaut, J. Claverie and P. Hagenmuller, J. Solid State Chem. **101**(2), (1993), 203.
8. S.J. Wen, G. Couturier, G. Campet, J. Portier and J. Claverie, Phys. Status Solidi (a), **130**, (1992), 407 and references therein.
9. G. Campet, S.D. Han, S.J. Wen, J.P. Manaud, J. Portier , Y. Xu and J. Salardenne, Mat. Sci. and Eng. B (accepted for publication (1993)).
10. S.J. Wen, Doctoral Thesis, University of Bordeaux, (1992).
11. Y. Zhang, Inorganic Chem. **21**, (1982), 3886.
12. V. I. Fistul, "Heavily doped Semiconductors" Plenum Press, New York , (1969).
13. Reference 12, pp 47, 48 and 140.
14. Reference 12, pp 48.
15. Reference 12 pp 53 and 104-106.
16. Reference 12 pp 143.
17. Y. Marfaing, "Interface Semiconducteur Electrolyte", CNRS , Ecole d'Hiver, Aussois, 9-15, December, (1984), pp 10.
18. Reference 12 pp 53 and 104-106.
19. J.P. Remeika and E.G. Spencer, J. Appl. Phys. **35**, (1964), 2803.
20. R.L. Weiher, J. Appl. Phys. 33, (1962), 2834.
21. P. Dordor, E. Marquestaut, Rev. Phys. Appl., **15**, (1980), 1607.
22. Reference 12, pp 146.
23. Reference 12, pp 144 and 145.

V. CONCLUSION GENERALE

Notre premier objectif était la réalisation et l'étude de matériaux d'électrodes pour générateurs secondaires au lithium: Li_XSnO_2, Li_XWO_3 et Li_XTiO_2.

Les matériaux de départ (SnO_2, WO_3 et TiO_2), préparés sous forme de poudre, présentent une texture nanocristalline associée à une grande surface spécifique. Ils ont été obtenus soit par voie sol-gel classique, soit par une voie originale (voie polymère): pyrolyse du polymère POE-MCl_X-n(H_2O), (M = Sn, W et Ti).

Les propriétés physiques (surface spécifique, taille des cristallites, ...) des poudres de SnO_2 préparées par voie sol-gel, sont fortement influencées par les traces de NH_4Cl provenant de la calcination du gel.

Les matériaux présentant une texture nanocristalline et une grande surface spécifique ont une capacité d'insertion en ions Li^+ accure.

A l'interface entre cristallites existent une zone de charge d'espace et une zone d'accumulation. Cette dernière, très riche en électrons, favorise les processus d'insertion (faible énergie d'activation).

Remarquons que les valeurs relativement faibles des potentiels mesurés pour Li_XTiO_2 permettent d'envisager son utilisation en tant qu'électrode négative dans des dispositif << rocking - chair >>.

Un problème majeur que nous essayé de résoudre était d' empécher l'agglomération des nanocristallites en particules de taille trop importante, nuisant aux cinétiques des réactions électrochimiques. Ce problème a été en partie résolu en << encapsulant>> les cristallites dans des groupements organiques (POE). C'est ainsi que des électrodes hybrides, de caractère organique-inorganique ont été élaborées et étudiées. Ces derniers materiaux présentent un intérét évident sur les plans pratique (fabrication de générateurs électrochimiques tout solide

à électrolyte polymère, qui soient souples et peu encombrants) et fondamental. Leur étude sera poursuivie; il faudra en particulier étudier ces << longues fibres de TiO_2>> présentes dans le POE (§III. 2).

Nous avons finalement complété les études antérieures sur les dispositifs électrochromes (contre-électrodes et électrodes transparentes). Nous avons notamment montré que:

(i) l' oxyde de fer préparé en couches minces par voie sol-gel pouvait être avantageusement utilisé comme contre-électrode.

(ii) la conductivité des électrodes transparentes à base d' ITO était améliorée par dopage avec Ti^{4+} ou Zr^{4+}.